



Universidade do Estado do Rio de Janeiro

Centro de Tecnologia e Ciências

Faculdade de Engenharia

Thiago Franco Leal

**Stochastic mathematical-computational simulations of actin provision and
polymerization in filopodia**

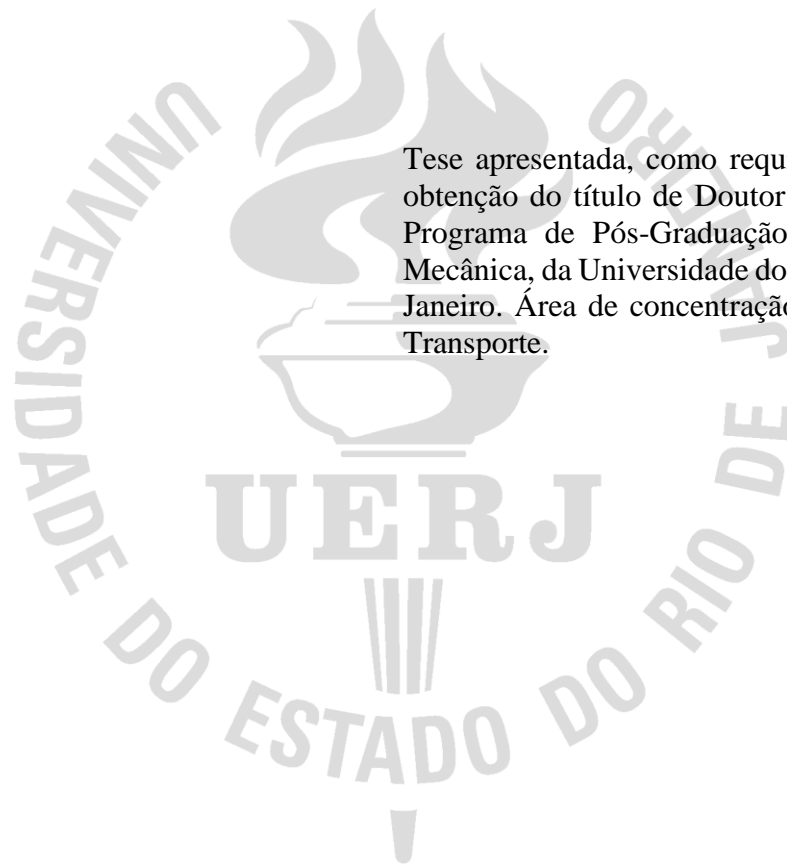
Rio de Janeiro

2020

Thiago Franco Leal

**Stochastic mathematical-computational simulations of actin provision and
polymerization in filopodia**

Tese apresentada, como requisito parcial para
obtenção do título de Doutor em Ciências, ao
Programa de Pós-Graduação em Engenharia
Mecânica, da Universidade do Estado do Rio de
Janeiro. Área de concentração: Fenômenos de
Transporte.



Orientadores:

Carlos Antônio de Moura

Maurício Vieira Kritz

Andreas Prokop

Rio de Janeiro

2020

CATALOGAÇÃO NA FONTE
UERJ / REDE SIRIUS / BIBLIOTECA CTC/B

L435 Leal, Thiago Franco.
Stochastic mathematical-computational simulations of actin
provision and polymerization in filopodia / Thiago Franco Leal. – 2020.
141f.

Orientadores: Carlos Antônio de Moura, Maurício Vieira Kritz,
Andreas Prokop.

Tese (Doutorado) – Universidade do Estado do Rio de Janeiro,
Faculdade de Engenharia.

1. Engenharia mecânica - Teses. 2. Teoria do transporte - Teses. 3.
Processo estocástico - Teses. 4. Actina - Teses. I. Moura, Carlos
Antônio de. II. Kritz, Maurício Vieira. III. Prokop, Andreas. IV.
Universidade do Estado do Rio de Janeiro, Faculdade de Engenharia. V.
Título.

CDU 66.02/.04

Bibliotecária: Júlia Vieira – CRB7/6022

Autorizo, apenas para fins acadêmicos e científicos, a reprodução total ou parcial desta tese,
desde que citada a fonte.

Assinatura

Data


Thiago Franco Leal

**Stochastic mathematical-computational simulations of actin provision
and polymerization in filopodia**

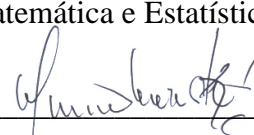
Tese apresentada, como requisito parcial para obtenção do título de Doutor em Ciências, ao Programa de Pós-Graduação em Engenharia Mecânica, da Universidade do Estado do Rio de Janeiro. Área de concentração: Fenômenos de Transporte.

Aprovada em: 28 de dezembro de 2020.

Banca examinadora:



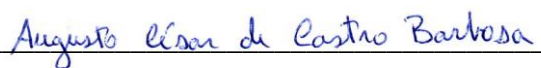
Prof. Dr. Carlos Antônio de Moura (Orientador)
Instituto de Matemática e Estatística – UERJ




Prof. Dr. Maurício Vieira Kritz (Orientador)
Laboratório Nacional de Computação Científica – LNCC and School of
Biological Sciences, FBMH, University of Manchester




Prof. Dr. Andreas Prokop (Orientador)
School of Biological Sciences, FBMH, University of Manchester



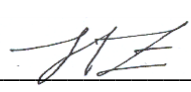
Prof. Dr. Augusto César de Castro Barbosa
Instituto de Matemática e Estatística – UERJ



Prof. Dra. Aruquia Barbosa Matos Peixoto
Centro Federal de Educação Tecnológica Celso Suckow da Fonseca –
CEFET/RJ



Prof. Dr. Alberto Franco de Sá Santoro
Instituto de Física – UERJ



Prof. Dr. Jorge Passamani Zubelli
Instituto de Matemática Pura e Aplicada – IMPA
Rio de Janeiro

DEDICATÓRIA

To my family, the foundation of everything I am.

ACKNOWLEDGEMENT

Many people impact our lives in several ways. Some do it purposefully, others do not. But an important gesture in return on our journey is never to fail in showing our acknowledgment and gratitude. Encouragement, kindness, and affection are gifts that mark our hearts. Wisdom, knowledge, and share of life experiences are gifts that expand our minds. All of this makes us greater and that is what we take forward with us.

I am deeply grateful to my family, especially my mother Rosemary. A true warrior to whom I owe every successful step I take in my personal and professional life. My whole family gives me all support I need, all love, and I couldn't feel more protected. Thanks a lot for everything, yesterday, today, tomorrow, and ever.

I would like to express the deepest appreciation to my supervisors Carlos Moura, Maurício Kritz, and Andreas Prokop. With Moura, I have a long partnership, always very attentive, and sharing his experiences with me, and that is why any thanks will still not be enough. From every discussion or meeting I have had with Mauricio, I learned countless ways of thinking, which had a fundamental role in my research and professional qualification.

Andreas, you are an inspiration in professional and leadership terms. I greatly appreciate the opportunity to have worked in your lab. I use today with my students approaches and quotes ("*Just jump!*") that I kept from you in the two months that we worked together almost daily. And I want to thank also Andreas' lab group, which received me so incredibly well that I couldn't have felt more comfortable and part of the lab. Ines, Andre, Cristina, Yuting, you are amazing friends. Thanks for all the memories.

Friends make life more colorful. I would like to thank all the friends who supported me to conclude this project. In particular, Rycharda placed herself as one more advisor, always giving essential support, advice, and affection during the most difficult times. Viviane, more than a therapist, she fits perfectly in my mentions of greatest friends. Since the beginning, she listened to me, supported me, pushed me forward. Each step had her incentive words. So, thank you all for sharing the burden of this whole process. Alexsandra rose in my life bringing a healing and heartwarming smile, and certainly should receive my greatest gratefulness.

I would like to express my gratitude to all teachers who went through each stage of my formation, either as citizen or professional. There is no Science at all without teachers. At each step, we must revere their importance, because when we look back, we will see that they paved

the beginning of the road we are taking now. They are mirrors and deserve all possible admiration.

I would like to offer my special thanks to Rio de Janeiro Federal Institute, where I work as a full-time professor, for granting me the requested leaves, first to visit the University of Manchester, and then to conclude this thesis project. I am very proud to work at this institution and now I feel even more prepared and motivated to give back to society the investment made in my Ph.D. qualification.

Special thanks also to UK Biotechnology and Biological Sciences Research Council (BBSRC) for sponsoring project BB/L026724/1, to FAPERJ for project APQ-5 E-26/110.931/2014, UERJ-SR2 Visiting Researcher 2014-2016 grant, and a CNPq/DTI grant. These agencies' support made possible an enriching collaboration between researchers of Faculty of Life Sciences (FLS - University of Manchester), Brazilian National Laboratory of Scientific Computing (LNCC), and Rio de Janeiro State University (UERJ), where my Ph.D. program is held. This project encompasses the results of that whole agreement.

My deepest heartfelt appreciation goes to every here mentioned person or institution for having a quite decisive contribution to my research or life during this period. Thank you so much for that!

Essentially, all models are wrong,
but some models are useful.

George Box

RESUMO

LEAL, T. F. *Stochastic mathematical-computational simulations to unravel mechanical relations of fluid flow and influence of actin regulators on filopodial dynamics*. 2020. 141 f. Tese (Doutorado em Engenharia Mecânica) - Faculdade de Engenharia, Universidade do Estado do Rio de Janeiro, Rio de Janeiro, 2020.

A actina é a proteína mais abundante nas células eucarióticas, onde formam polímeros filamentosos (actina-F) e se organizam em redes que fornecem o esqueleto das células e desempenham papéis vitais em muitas funções celulares. Por exemplo, feixes paralelos proeminentes de actina-F mediam a formação e a dinâmica dos filopódios, que são longas protrusões de membrana, semelhantes a dedos, em células ou neurônios em crescimento. Os filopódios têm funções importantes na migração e comunicação celular, relevantes para o desenvolvimento neural, envelhecimento, degeneração e regeneração. No filopódio, a actina-F exibe um padrão de “esteira” constante, isto é, refluxo de todo o feixe de actina-F impulsionado por sua polimerização na ponta distal do filopódio e sua desmontagem concomitante na base do filopódio. Sabe-se que várias proteínas reguladoras da actina mediam e regulam esses processos. Além disso, grandes quantidades de actinas monoméricas são necessárias como blocos de construção na ponta dos filopódios e precisam percorrer todo o estreito espaço interno ao longo do comprimento dos filopódios. Para entender as bases mecânicas da esteira de actinas no filopódio, este trabalho apresenta uma formulação alternativa de modelo estocástico que simula os deslocamentos de moléculas. Ele considera não apenas difusão como fenômeno de transporte essencial, mas inclui fluxo citoplasmático na direção do topo (a fim de repor o volume removido pelo fluxo retrógrado dos filamentos de actina), mas também as propriedades e afinidades específicas dos reguladores de actina, em particular profilina e Ena/VASP. Uma implementação que integra parâmetros físicos e bioquímicos em um modelo computacional foi possível por meio de simulações centradas em partículas, uma abordagem que se mostra sem precedente em modelagem na biologia. Quando aplicado, o modelo centrado em partículas desenvolvido gerou filopódios de até 40 μm de comprimento, a dinâmica do fluxo interno no filopódio pôde ser deduzida e nos permitiu testar como os diferentes parâmetros contribuem para esta dinâmica. Além disso, tem a capacidade de ser refinado ao adicionar gradualmente mais ou melhores parâmetros obtidos por estudos biológicos ou físicos, servindo assim como um meio interativo de previsão e validação. O modelo centrado nas partículas desenvolvido aqui demonstra claramente o potencial desta estratégia para uma ampla aplicação em problemas biológicos.

Palavras-chave: Biologia; Modelagem matemática e computacional; Citoesqueleto; Filopódios; Dinâmica de actinas; *Drosófila*; Fluxo de citoplasma; Modelo Estocástico; Conservação de massa; Fenômenos de Transporte.

ABSTRACT

LEAL, T. F. *Stochastic mathematical-computational simulations to unravel mechanical relations of fluid flow and influence of actin regulators on filopodial dynamics*. 2020. 141 f. Tese (Doutorado em Engenharia Mecânica) - Faculdade de Engenharia, Universidade do Estado do Rio de Janeiro, Rio de Janeiro, 2020.

Actin is the most abundant protein in eukaryotic cells which forms filamentous polymers (F-actin) that get arranged into networks providing the skeleton of cells and play vital roles in many cellular functions. For example, prominent parallel bundles of F-actin mediate the formation and dynamics of filopodia, which are long, finger-like membrane protrusions of cells or growing nerve cells. Filopodia have important functions in cell migration and communication relevant for neural development, aging, degeneration, and regeneration. In filopodia, F-actin undergoes constant "treadmilling", i.e. backflow of the entire F-actin bundle driven by their polymerization at the distal tip of filopodia and their concomitant disassembly at the base of filopodia. An amount of actin-regulating proteins is known to mediate and regulate these processes. In addition, large amounts of monomeric G-actins are required as building blocks at the very tip of filopodia and need to travel through the entire length of the confined, narrow lumen of filopodia. To understand the mechanic basis of actin treadmilling in filopodia, this work presents an alternative stochastic model formulation to simulate molecule displacement. Unlike previous attempts, it considers not only diffusion as the essential transport mode, but adds cytoplasmic flow towards the tip (occurring to replace volume taken out by the back-flowing actin filaments), but also the specific properties and affinities of actin regulators, in particular, profilin and Ena/VASP. Integrated implementation of these physical and biochemical parameters into one computational model was possible by using particle-centered simulations, an approach that seems to be unprecedented in biological modeling. When applying this particle-centered model, filopodia grow up to about 40 μm in length, sub-filopodial flow dynamics can be deduced, and it allows to test how the different parameters contribute to filopodial dynamics. Also, it has the capacity to be refined by gradually adding more or improved parameters obtained from biological or physical studies, thus serving as an iterative medium of prediction and validation. The particle-centered model developed here clearly demonstrates the potential of this strategy for the wider application to biological problems.

Keywords: Biology; Mathematical - computational modeling; Cytoskeleton; Filopodia; Actin dynamics; Drosophila; Cytoplasmic flow; Stochastic model; Mass conservation; Transport phenomena.

LIST OF FIGURES

Figure 1.1: Microscopy image of cytoskeleton components.....	22
Figure 1.2: Microscopy image of a cell cytoskeleton	23
Figure 1.3: Microscopy image of microfilaments	24
Figure 1.4: Microscopy image of intermediate filaments	24
Figure 1.5: Microscopy image of microtubules	25
Figure 1.6: Different arrangements of actin filaments	26
Figure 1.7: Treadmilling generated by polymerization and disassembly.....	27
Figure 1.8: Cartoon model of actin regulation	28
Figure 1.9: Schematic representation of ABPs involved in treadmilling	29
Figure 1.10: Parallel arrangement of actin filaments inside filopodium	30
Figure 1.11: Filopodia on a neuron growth cone	31
Figure 1.12: Filopodial dynamics as an ideal system to model.....	32
Figure 1.13: Filopodia emerging from cancer cell	33
Figure 1.14: Microscopy image of plasma membrane lipid bilayer	34
Figure 1.15: The fluid-mosaic-model of the cell membrane	35
Figure 2.1: Representation of Peskin's Brownian ratchet model	38
Figure 2.2: Scheme of simple compartmental-based simulation in Erban's	39
Figure 2.3: Examples of investigations presented at Mogilner and Rubinstein's	39
Figure 2.4: Active transport by motor molecules	44
Figure 3.1: Polymerization inducing inflow of matter into filopodium	45
Figure 3.2: Two-phase model scheme	47
Figure 3.3: Cartoon models of filopodial dynamics	48
Figure 3.4: Planar random walk	49
Figure 3.5: Variable random fluctuations on economics application of BM	50
Figure 3.6: Molecules moving in Brownian motion in a two-dimensional domain	52
Figure 3.7: Cross-section picture of actin filament bundle	53
Figure 3.8: Hexagonal packing of actin filament bundle in microvilli	54
Figure 3.9: Hydration shell around actin filaments	55
Figure 3.10: Hexagonal packing of actin filaments in the presence of hydration	56
Figure 3.11: Hexagonal packing of actin filaments in the absence of hydration	57
Figure 3.12: Bundle edge of an actin filaments hexagonal packing	58

Figure 3.13: Interactions in filopodial dynamics are driven by distances	64
Figure 3.14: Filopodial compartmentalized model	65
Figure 4.1: Molecules, bindings, and filaments as computational objects	70
Figure 4.2: OOP scheme of actin dynamics in filopodia	74
Figure 4.3: A geometric representation of the modeled domain.....	75
Figure 4.4: Boundary condition for membranes in filopodial tip	76
Figure 4.5: Region of attraction to polymerization	77
Figure 5.1: Reachable filopodial final lengths.....	80
Figure 5.2: Standard simulation scheme	81
Figure 5.3: Roadmap of the particle-based computational model	82
Figure 5.4: G-actins distribution for $N = 20$ and 1500 particles	84
Figure 5.5: G-actins distribution for $N = 30$ and 1500 particles	85
Figure 5.6: G-actins distribution for $N = 50$ and 1500 particles	85
Figure 5.7: G-actins distribution for $N = 20$ and 3000 particles	86
Figure 5.8: G-actins distribution for $N = 30$ and 3000 particles	86
Figure 5.9: G-actins distribution for $N = 50$ and 3000 particles	86
Figure 5.10: G-actins distribution combining values of N , s , and N_P	87
Figure 5.11: Hetero-dimers AP distribution for $N = 20$ and 1500 particles	88
Figure 5.12: Hetero-dimers AP distribution for $N = 30$ and 1500 particles	89
Figure 5.13: Hetero-dimers AP distribution for $N = 50$ and 1500 particles	89
Figure 5.14: Hetero-dimers AP distribution for $N = 20$ and 3000 particles	90
Figure 5.15: Hetero-dimers AP distribution for $N = 30$ and 3000 particles	90
Figure 5.16: Hetero-dimers AP distribution for $N = 50$ and 3000 particles	91
Figure 5.17: Hetero-dimers AP distribution combining values of N , s , and N_P	92
Figure 5.18: Velocity profile driven by each transport phenomena, $N=20$ and $s=0$	99
Figure 5.19: Velocity profile driven by each transport phenomenon, $N=30$ and $s=0$	100
Figure 5.20: Velocity profile driven by each transport phenomenon, $N=50$ and $s=0$	101
Figure 5.21: Diffusion contribution to flow velocity with only G-actins.....	102
Figure 5.22: Drift contribution to flow velocity with only G-actins.....	102
Figure 5.23: Total velocity of inflow cytoplasm in a filopodium with only G-actins.....	103
Figure 5.24: Velocity profile driven by each transport phenomenon, $N=20$ and $s=12$	104
Figure 5.25: Velocity profile driven by each transport phenomenon, $N=30$ and $s=12$	105
Figure 5.26: Velocity profile driven by each transport phenomenon, $N=50$ and $s=12$	106
Figure 5.27: Physical transport phenomena contributions, $s = 12$	107

Figure 5.28: Velocity profiles of the cytoplasm flux mediated by ABPs.....	108
Figure 5.29: Filopodial length for $t_s = [0, 200]$	116
Figure 5.30: Filopodial length for $t_s = [0, 2000]$	117
Figure 5.31: Filopodial length with mediation of profilin and Ena/VASP.....	118
Figure 5.32: Influence of profilin.....	118
Figure 5.33: Influence of profilin and filopodial extinction.....	119
Figure 5.34: Ena/VASP regulating bundle tip with no profilin in the system.....	120
Figure 5.35: Ena/VASP regulating bundle tip with profilin in the system.....	120
Figure 5.36: Influence of active transport for $t_s = [0, 200]$ and $t_s = [0, 2000]$	121
Figure 5.37: Actin regulators and active transport influence in filopodial length	123
Figure 6.1: <i>Drosophila</i> as a versatile biological model to study filopodial dynamics.....	127
Figure A1.1: Concentration as function of the length	136
Figure A1.2: Concentration as function of the number of filaments	137
Figure A1.3: Influence of k_{on} in $C(L)$, for different N	138
Figure A1.4: Influence of k_{on} in $C(N)$, for different L	139
Figure A2.1: Surface representing function $L = L(N, C)$; $N = [20, 50]$, $C = [0, 10]$	140
Figure A2.2: Set of points representing function $L = L(N)$, when $C = 2 \mu\text{M}$	141

LIST OF TABLES

Table 1: Parameter values	40
Table 2: Variation of L in G-actin distributions as function of s	87
Table 3: Variation of L in hetero-dimers AP distributions as function of s	91
Table 4: Variance between the lengths after 10 runs for each considered case.....	93
Table 5: Comparison of cases with different N_P and just G-actins in the system	94
Table 6: Comparison of cases with different N_P and ABPs in the system	94
Table 7: Comparing filopodial length for $N_P = 6000$ and $N_P = 10000$ G-actins.....	95
Table 8: Comparing filopodial length, $N_P = 6000$ and $N_P = 10000$, with ABPs.....	96
Table 9: Simulation of filopodia with 10000 particles and 500 time steps	97
Table 10: Contribution of active transport in filopodial elongation	122
Table 11: Concentration estimative as function of polymerization rate	137

LIST OF ABBREVIATIONS

ABP – Actin binding protein

ADP – Adenosine diphosphate

ATP – Adenosine triphosphate

BM – Brownian motion

DNA – Deoxyribonucleic acid

OOP – Object-oriented programming

VASP – Vasodilator-stimulated phosphoprotein

LIST OF SYMBOLS

C	Concentration of G-actin
C_o	Concentration of G-actin at filopodial base
D	G-actin diffusion coefficient
D_p	Diffusion coefficient of particle p
N	Number of filaments in the bundle
N_o	Number of filaments to support membrane
N_{ret}	Number of actins to supply retrograde flow
N_{step}	Set of actin filaments with depolymerized subunits at a certain time step
N_p	Number of actins polymerized
δ	Half-size of G-actin monomer
L	Length of filopodia
L_c	Length of F-actin bundle
L_{final}	Length of filopodia at the end of simulation
L_{crit}	Length of filopodia on which the G-actin concentration is critical
n_c	Number of compartments
h_c	Length of each compartment
R	Filopodial radius
r	Actin filament radius
x	Distance from filopodial base
s	Inter-filament spacing
$r_{[reaction]}$	Affinity distance for reaction to occur
Ω_p	Region with attraction to polymerization
j	Inter-filament density
k_{on}	G-actin polymerization rate
ℓ	Hexagon packing area out of bundle
t	Time
t_s	Time of simulation
t_{final}	Maximum time of simulation
Δt	Time step

S_C	Cross-section area of microfilaments
S_H	Cross-section area of hexagonal packing
S_{in}	Area where cytosol flows into filopodia
S_{out}	Area where cytosol flows out of filopodia
S_{empty}	Empty space inside actin filament bundle
S_{filop}	Total cross-sectional area of the filopodium
S_{bundle}	Total cross-sectional of N -filament hexagonal packing
Q_{in}	Filopodial inflow volume rate
Q_{out}	Filopodial outflow volume rate
v_{in}	Incoming flux speed
v_{out}	Outcoming flux speed
v_{ret}	Retrograde flux speed
v_{dif}	Velocity contribution by diffusion
v_{drift}	Velocity contribution by drift
v_{mol}	Outflow molecules velocity
$v_{cytosol}$	Outflow cytosol velocity
$v_x _p$	Velocity of particle p in x -direction
$v_y _p$	Velocity of particle p in y -direction
$\vec{v} _p$	Velocity vector of particle p
AA	Reaction of G-actin polymerization
AP	Reaction of dimerization Actin-Profilin
EP	Reaction Ena/VASP-Profilin to promote G-actin polymerization catalytically
EF	Reaction of Ena/VASP association with bundle tip

CONTENTS

INTRODUCTION.....	17
1 BASIC BIOLOGICAL CONCEPTS.....	22
1.1 Cytoskeleton.....	22
1.2 Actin dynamics.....	26
1.3 Properties of filopodia.....	30
1.4 Properties of plasma membrane.....	34
2 THE CURRENT STATE OF ACTIN AND FILOPODIA MODELING.....	37
2.1 Models based on actin diffusion and binding kinetics.....	37
2.2 Diffusion alone cannot explain G-actin delivery to the filopodial tip.....	40
2.3 Motor transport of G-actin is not sufficient to the filopodial tip.....	40
3 A NOVEL STOCHASTIC MODEL OF FILOPODIAL DYNAMICS:	
MATHEMATICAL ASPECTS.....	45
3.1 A filopodial pump: advection as a potential transport mechanism	45
3.2 Towards an integrated approach combining different mechanisms and properties	47
3.3 Brownian motion to simulate diffusion	49
3.4 Properties of back-flowing F-actin bundles	53
3.5 Specific molecular affinities and interactions	62
3.6 Filopodial elongation	64
3.7 Advection and its coupling with diffusion	66
4 A NOVEL STOCHASTIC MODEL OF FILOPODIAL DYNAMICS:	
COMPUTATIONAL ASPECTS	70
4.1 Computational Objects: defining the classes	70
4.2 Modeling filopodial geometry	75
4.3 Computational model for stochastic filopodial dynamics	78
5 RESULTS AND DISCUSSION	80
5.1 Filopodial growth and bundle configuration	83
5.1.1 Inter-filament spacing slightly enhances filopodial growth	84
5.1.1.1 Statistical evaluation of model stability	93
5.1.2 Amount of particles enormously enhances filopodial growth	94
5.1.3 More time of experimentation greatly improves filopodial growth	97
5.2 Predominance of each transport phenomenon	98
5.3 Testing original hypotheses about inter-filament spaces	109
5.3.1 Inflow cytoplasm within bundle spaces stops compensatory mechanisms	110
5.3.2 Encapsulated outflow cytosol is a viable possibility	112
5.4 Influence of ABPs and active transport in filopodial growth	115
5.4.1 Basic filopodial model (Ena/VASP = 'off' and Profilin = 'off')	116
5.4.2 Filopodial growth is improved (Ena/VASP = 'on' and Profilin = 'on')	117
5.4.3 G-actin is sequestered (Ena/VASP = 'off' and Profilin = 'on')	118
5.4.4 Decrease in polymerization rate (Ena/VASP = 'on' and Profilin = 'off')	119
5.4.5 Motors have relevant contribution (Active transport = 'on', others = 'off')	121
5.4.6 All modeled filopodia aspects leads to consistent elongation (Active transport = 'on', Ena/VASP = 'on', and Profilin = on')	122
CONCLUSION AND FUTURE WORK	124
REFERENCES	129
APPENDIX 1	136
APPENDIX 2	140

INTRODUCTION

Biological phenomena rely on physical and chemical interactions. As elements of a physical phenomenon, their components interact freely with one another: exchanging energy and momenta whenever in contact. The chemical interactions of components are not as free since they depend on biochemical compatibilities and chemical affinities of the interacting elements. This makes biological interactions highly complex. The elements giving cause to biological phenomena are dynamic, self-regulatory, resilient, and often interact through the exchange of information (signals), without being necessarily in contact or even close together.

In addition to interactions and reactions that regulate biological systems, physical transport phenomena play a key role. At most scales, these processes encompass momentum, mass, and/or energy transfer [84]. As an example, molecules' movements within the cell can be influenced by diffusion and advection. Other mechanisms not merely physical may also occurs, such as active transport, when a specific molecule can transport another through a noncovalent chemical bond [50]. Several models of these processes in biological systems might be found in literature, like hemorheology [17], nutrition [24, 48], cellular motility [20, 61], and the understanding of some diseases and their treatments [22, 31, 58].

To understand biological systems at the sub-cellular scale, we need to disentangle the organizational (or functional) status of biological elements, the regulatory elements, physical and chemical interactions, and rules that underlie their dynamics. All biological processes are grounded on physical and chemical interactions but some of them only have sense within cells or other organisms and are unlikely to occur spontaneously elsewhere.

A way to gain an understanding on this complexity is to have the physicochemical dynamics well described and documented as a working and consensual mathematical/computational model amenable to manipulations at higher levels, to unveil regulatory mechanisms induced by signaling and other stimuli. This can be achieved through modeling strategies with purpose of representing the behavior of complex systems occurring in life-phenomena [8, 14, 38, 39, 60].

There are basically two fundamental approaches to the mathematical modeling of systems involving chemical reactions and transport phenomena: deterministic and stochastic. Deterministic models are based on differential equations, usually suited to display a proper continuum description of the system's behavior. On the other hand, stochastic simulations provide a more detailed understanding of the particle-centered point of view, describing with

good approximation interactions and individual displacement of molecules, which is useful in modeling on biological contexts [28].

As an example, the outstanding complexity of the web of interactions supporting cell motility makes invaluable their theoretical and computational representation. Computational models can help us to better understand experimental results, test hypotheses, and settle theoretical foundations for meaningful interpretations [104]. Thus, both types of observation, experimental data and virtual simulation results complement each other providing a better understanding of biological phenomena.

Computational and mathematical modeling depends on data, observations, insights, and concepts derived from real phenomena (in this case, biological systems). On the other hand, mathematical and/or computational models, used as virtual laboratories, offer several advantages to advance the understanding of biological systems, since they allow: (a) to test wider ranges of parameters far beyond the capacity of the human mind, (b) to operate at space and time scales that cannot be experimentally addressed, (c) to change variables and geometries to study their impacts on the system, (d) to make predictions or to suggest the existence of particular interactions and structures that can then be investigated experimentally, (e) to provide opportunities to test assumptions and theoretical knowledge in order to refine hypotheses, (f) to determine which experimental variables are most important in a system, and (g) to synthesize experimental data and test data interpretation methods.

As said in [100], computational modeling ought to gain the same status as theoretical analyses and laboratory experiments. This methodology enlarges the possibilities inherent in the scientific hypothesis-deduction-observation cycle and relaxes the constraints imposed by the impossibility of performing certain experiments. Thereby, mathematical models, computational simulations, and laboratory experiments constitute a set of complementary tools when analyzing systems that usually involve a large number of parameters, variables, and interactions, in particular, biological systems.

A sub-cellular biological system that has an intricate machinery is the cytoskeleton [1]. The cytoskeleton is mechano-resistant complex and yet highly dynamic. It is a collection of networks composed of filamentous protein polymers that support cell architecture and dynamics [32]. Virtually all cell functions depend on the cytoskeleton and on the essential binding proteins that regulate its dynamics [23, 87]. Accordingly, genetic defects of cytoskeleton components will have multiple effects that causes many human diseases which are complex systemic phenomena [87]. Furthermore, there is a great interest in clearly understanding cytoskeleton functionalities to investigate tumor cell migration and metastasis

[31, 102], as well in the study of neural disorders [22]. Since cytoskeletal dynamics is the cause and the consequence of both chemical interactions and physical forces, their analysis requires thinking at the interface of biology, biochemistry, and biomechanics [9, 96].

Start studying such complex system requires a choice of cytoskeleton-driven biological phenomena that are sufficiently simple to translate into a computational model before addressing higher complex systems [23]. A promising context to address is filopodia. Filopodia are long, finger-like membrane protrusions of cells, with important functions in cell migration and environment sensing relevant for development, aging, degeneration, and regeneration [1, 85]. Filopodia contain prominent parallel filament bundles of F-actin that essentially mediate their formation and dynamics. These bundles consist of a fundamentally linear structure whose elongation/retraction directly translates into a mono-dimensional increase/decrease of the entire filopodium.

However, even this apparent simplicity of filopodia still poses a major challenge due to the complex interdependence of the mechanical, physical, chemical, and biological processes. It justifies the usefulness of developing computational models as an effective way to gain additional new insights [104]. For example, the F-actin in filopodial bundles undergoes constant "treadmilling", i.e. backflow of the entire F-actin bundle driven by their polymerization at the distal tip of filopodia and their concomitant disassembly at the base of filopodia. The quantity of polymerization versus disassembly at any point in time will determine the flow rate and the elongation behavior of filopodia.

As it will be explained in Chapter 1, this requires uninterrupted delivery of large amounts of new actin building blocks (G-actins) to the tip of filopodia [30, 35, 57, 62], and some actin-regulating proteins are known to mediate and regulate these polymerization/disassembly processes. As will be explained in Chapter 2, current mathematical or computational models of filopodial dynamics are mainly based on the diffusion of actin building blocks towards the tip [28, 51, 64, 75, 104, 105], achieving only very short filopodia that are far from representative of the biological structure observed. Therefore, new models are required.

On this project, I developed a new mathematical-computational model simulating filopodial dynamics. I propose a stochastic and integrative two-phase model that considers catalyzed actin polymerization dynamics, molecule displacement by Brownian motion, reactions occurring due to molecules proximity, as well as cytoplasmic flow dynamics within filopodia. To integrate all these parameters, I applied similar concepts of particle methods [29] to this biological context, which seems not to have been done before, thus paving the way for

potential future applications of stochastic particle-centered simulations to biological problems. By using this strategy to couple all of the above-mentioned phenomena, I am able to investigate actin delivery to filopodial tips and polymerization undergoing a drift effect from the inflow cytosol besides diffusion, and its relations with filament bundle geometric configuration. Also, in this work, I analyze the influence of some relevant proteins that regulate actin dynamics and filopodial growth and maintenance itself.

Essentially, this work intends to answer questions as:

- Is diffusion a sufficient transport phenomenon to supply actin polymerization?
- What are the physical mechanisms that mediate G-actin transport along filopodia?
- Does the inflow triggered by outflowing actin bundles and the assumption of proper mass conservation generate enough transport capacity for G-actins to sustain polymerization?
- Are there mechanical relations between F-actin bundle geometric constitution and physical mechanisms of molecules transport?
- What are the effects on G-actin dynamics caused by the absence of a particular regulatory molecule?

To guide the reader through the underlying thought processes, implementations, and experimental simulations, this thesis is subdivided into the following chapters:

Chapter 1 brings to light basic biological concepts of the underlying biological problem, explaining the wider role of the cytoskeleton, filopodial architecture, G-actin dynamics, roles of the main actin-regulating proteins, and the structure and mechanical properties of the plasmatic membrane.

Chapter 2 describes existing modeling approaches and addresses the phenomenon of diffusion as the main transport mechanism applied in these models so far. It explores as to whether diffusion can be considered a process that is sufficient to explain the displacement of actin molecules in filopodia in order to supply polymerization processes at the tip. It also discusses expected minor roles of motor protein-driven actin transport.

Chapter 3 addresses further properties, parameters, and transport modes that I considered to be sensible to include in a filopodial model. It describes the idea of cytoplasm flowing into the filopodium as a physical transport mechanism, Brownian motion as a way to model diffusion, properties of the back-flowing actin filament bundle, the involvement of

enzymes and specific molecular affinities in the polymerization process, and the interaction between inflow actin monomers and the membrane.

Chapter 4 describes the implementation of the model where object-oriented programming was used as a modeling strategy to integrate the various parameters and ideas described in Chapter 3. Methods and attribute definitions are briefly explained, followed by a presentation of the filopodial geometry and its computational representation.

Finally, Chapter 5 describes the properties of our model as observed in a series of simulations in which parameters were systematically changed to assess their influence on the overall behavior of filopodia. We describe what information can be extracted and what conclusions can be drawn about the mechanisms that regulate filopodial behavior. One of the major achievements of the model is to develop filopodial dynamics reaching up to 40 μm length, although limited by the available computational resources.

1 BASIC BIOLOGICAL CONCEPTS

1.1 Cytoskeleton

In order to work properly, cells must be organized in space and interact mechanically with their surroundings. Cells should be duly shaped, physically robust, and well-structured internally. Many cells may need to change their shape and migrate to other locations. Also, every cell must be able to rearrange its internal components as a result of processes of growth, division, or adaptation to changes in the environment. All these structural and mechanical functions are highly developed in eukaryotic cells and dependent on an intricate protein filament system called cytoskeleton [1].

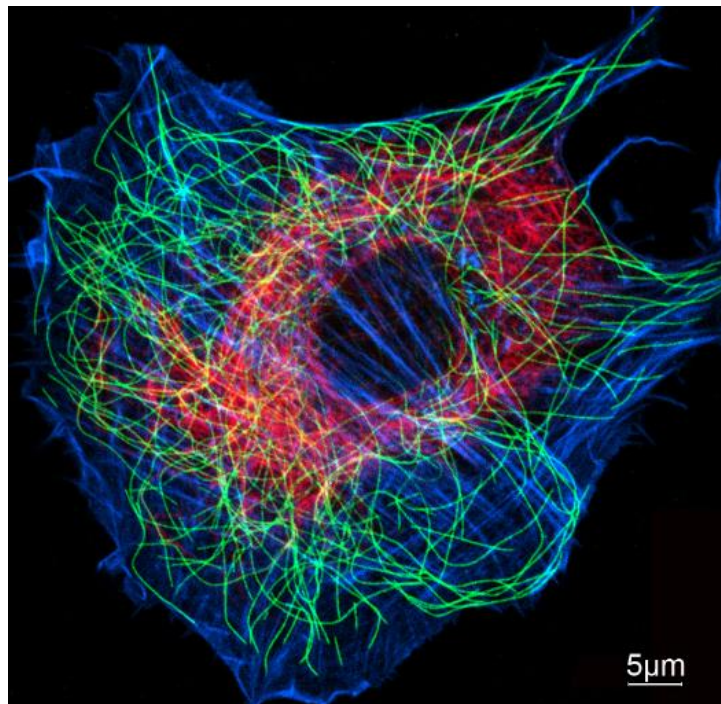


Figure 1.1: Microscopy image of cytoskeleton components labeled with fluorescent proteins. Microfilaments are shown in blue, microtubules are in green, and intermediate filaments are in red. This image is a courtesy provided by Harald Herrmann (University of Heidelberg, Germany) and it was published in [82].

The cytoskeleton is a complex and highly dynamic network of protein fibers and their associated regulatory proteins. The cytoskeleton determines the shape of cells and has fundamental roles in virtually all functions of cells [85], including cell division, motility, adhesion, signaling, endocytic trafficking and transport, and organelle shapes [1]. For example,

the cytoskeleton supports the plasma membrane providing shape and stress resistance, allows the mobility of specific cells like sperm and leukocytes, mediates the contraction of muscle cells, and implements the guided growth of axons and dendrites to form neuronal networks [83].

The main components of the cytoskeleton are microfilaments, intermediate filaments, and microtubules, each one of them with distinct architectures, functions, and mechanical properties. The dynamics of their assembly, their polarity, and the type of molecules that can associate with them differ considerably. Figures 1.1 and 1.2 show examples of cytoskeleton images distinguishing all its components. The networks they form constantly reorganize themselves in response to chemical signals from the environment or externally applied forces, performing important roles in maintaining the dynamic integrity of cells.

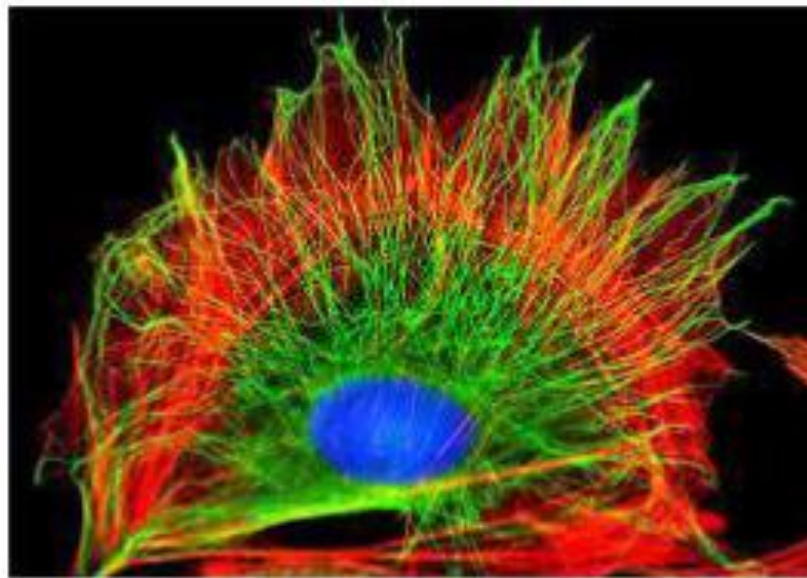


Figure 1.2: Microscopy image of a cell cytoskeleton. Notice that the cytoskeleton spreads through the cell interior, spanning from the nucleus surface to the plasma membrane. The single cytoskeletal elements are explained in greater detail in the following three images. Image taken from [60].

Microfilaments (from now on called actin filaments or F-actin) are polymers arranged in a helical-chain, formed by attached actin monomers and have around 8 nm of diameter. Actin filaments form a cortical network that lines the inner surface of the plasma membrane of animal cells, granting its strength and shape. They can also be organized into lattice-like (e.g. in veil-like lamellipodia important for cell motility), antiparallel bundles (e.g. stress fibers that can contract cells), or parallel bundles (e.g. in finger-like microvilli increasing the surface of cells

lining the gut or in dynamic filopodia exploring the immediate environment of migrating or developing cells) [1]. Figure 1.3 shows microfilaments at different resolutions.

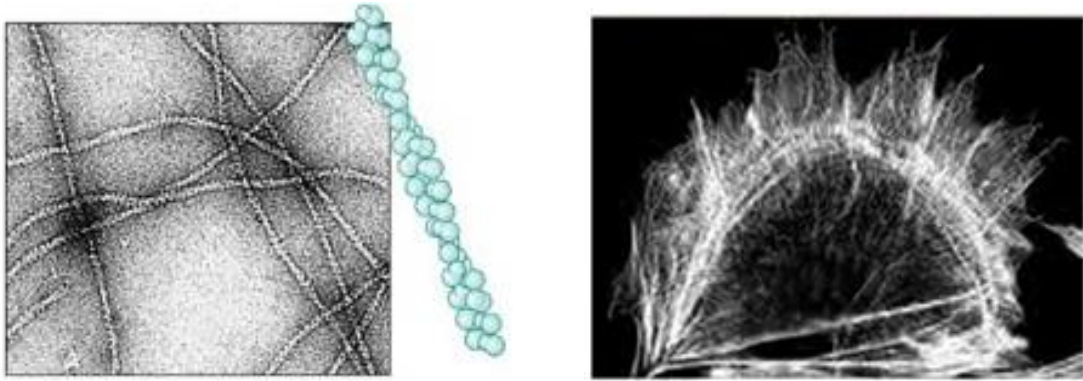


Figure 1.3: Microscopy image of microfilaments with a schematic drawing in the left; actin fraction of the cell cytoskeleton depicted in Figure 1.1. Image taken from [98].

Intermediate filaments are strong rope-like polymers around 10 nm in diameter that provide mechanical stability to cells and tissues. These structures are the most stable component of the cytoskeleton. They are composed as a chain of antiparallel building blocks composed of 8 hetero-tetramers¹ which are resistant to stretch and play a structural role in the cell, maintaining its integrity, providing nuclear membrane support, and protecting the cell's DNA. Because of its high tensile strength, intermediate filaments are therefore found in particularly durable body structures such as the upper skin layer (epidermis), hair, and fingernails, but also the long processes of nerve cells [1, 42]. Figure 1.4 shows images of intermediate filaments at different resolutions.

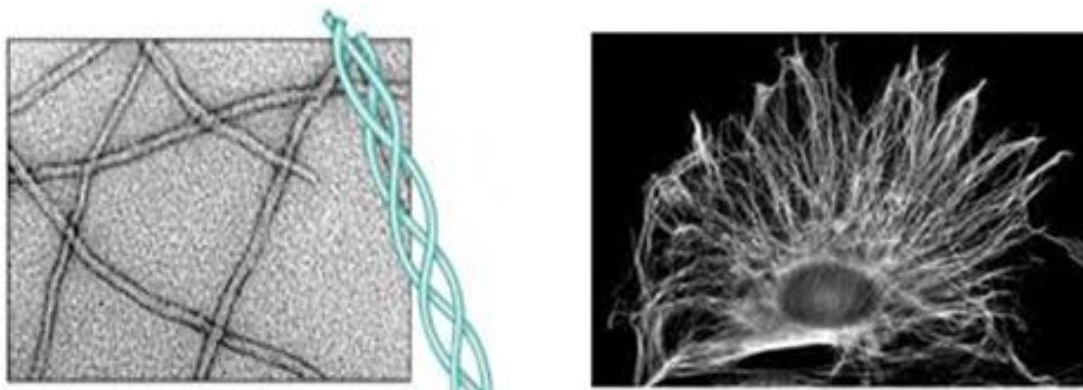


Figure 1.4: Microscopy image of intermediate filaments with a representative drawing in the left; cytoskeleton part made of intermediate filaments. Image taken from [98].

¹ A hetero-tetramer is protein containing four non-covalently bound subunits, wherein the subunits are not all identical [1].

Microtubules are long, hollow, cylindrical filaments composed of tubulin heterodimers²; they usually have an outer diameter of 25 nm and are much stiffer than actin filaments [40]. This said, they are highly dynamic structures that can increase or decrease in length by the addition or loss of tubulin subunits. They are generally anchored at one end (usually the minus end) via specific end-binding proteins, e.g. to the centrosome, the Golgi apparatus, or the cell membrane. Microtubules provide major highways for motor protein-mediated intracellular transport, responsible for the placement of organelles within cells, and establish the mitotic spindle required for chromosome transport in cell division [1]. Figure 1.5 shows microtubules at different resolutions.

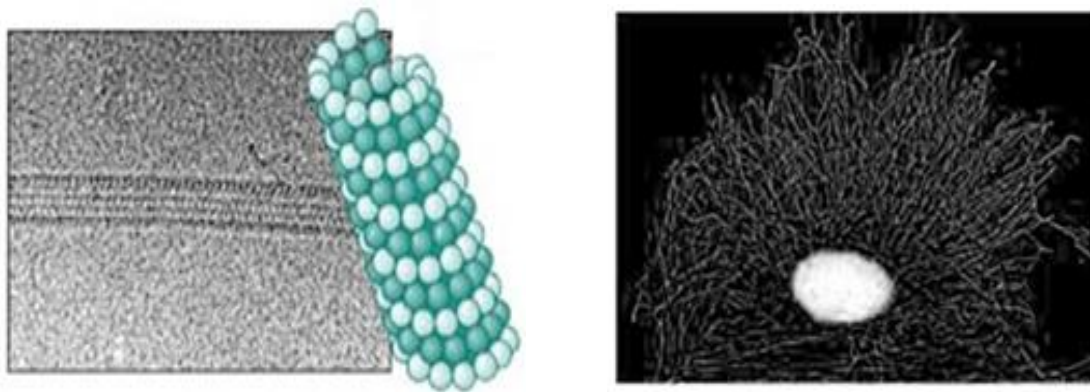


Figure 1.5: Microscopy image of microtubules with a representative drawing in the left; cytoskeleton part made of microtubules. Image taken from [98].

G-actin or tubulin are polymerized into filaments (F-actin or microtubules, respectively), through depolymerization, severing processes, or damage they are removed again. The polymerization of actin is an exothermal reaction that generates energy and allows to produce directed forces which change cell shape. Together with the acting of motor proteins that move along actin filaments and microtubules, they generate the forces required to form and maintain the architecture of cells.

F-actin is regulated through the action of different actin binding proteins (ABPs) and can organize into different types of networks which perform distinct roles in cells. The number of ABPs is surprisingly low [23, 87], but they can be employed in different contexts, contributing to very distinct cytoskeletal networks and dynamics. Different actin regulators perform different functions: nucleation (the seeding of new filaments) [95], cross-linkage

² A hetero-dimer is a protein composed of two polypeptide that are not identical [1].

between actin filaments, polymerization (adding new actin monomers), depolymerization (disassembly of F-actin into single actins), severing (cutting actin filaments), capping (protecting the ends of actin filaments), active transport (myosin motor proteins walk along actin filaments) or sequestering (storing actin monomers) [85]. These regulatory proteins may respond to chemical stimuli or mechanical forces from inside or outside the cell, by changing their activity status and, hence, the local organization of actin networks.

Several studies relate certain pathologies to changes in cytoskeleton formation. For example, in the nervous system, temporal lobe epilepsy, cortical dysplasias, and schizophrenia show some involvement with alterations that occur in aspects of cytoskeleton dynamics [22, 58]. In addition to neuron-related pathologies, the relationship of the cytoskeleton in tumor cell development and cancer metastasis can also be mentioned [31, 102].

1.2 Actin dynamics

Actin is the most abundant protein in eukaryotic cells [1]. Actin exists as globular actin monomers called G-actin and polar actin filaments called F-actin. Actin filaments are head-to-tail polymers of G-actin subunits. The minus (or pointed) end of actin filaments is relatively inert displaying slow growth *in vitro*. The opposite plus (or barbed) end grows much faster through exothermic polymerization both *in vitro* and *in vivo* [11, 68].

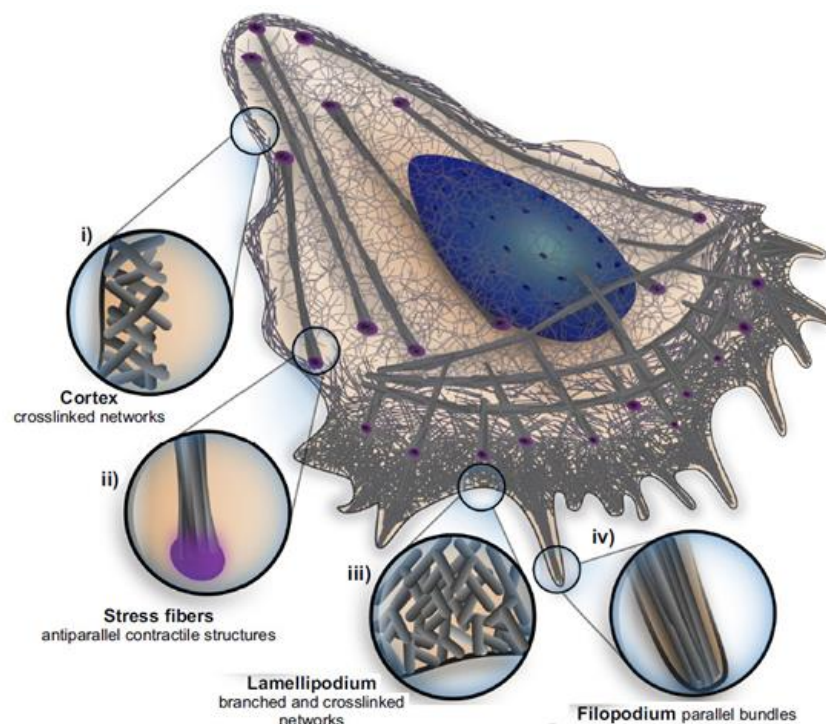


Figure 1.6: Different arrangements of actin filaments. Image taken from [9].

The actin cytoskeleton is continuously assembled and disassembled in response to the local activity of signaling events. Actin networks are present at the nucleus and on certain intracellular compartments, but the highest concentration is found at the membrane leading edge of motile cells driving the migratory processes, or at specialized surfaces such as the luminal surface of gut-lining cells where actin forms finger-like microvilli to increase the cell surface for increased nutrient absorption [54].

In the cytoskeleton, actin filaments can be arranged into parallel bundles (e.g., in finger-like membrane protrusions called filopodia), into anti-parallel bundles (e.g., in stress fibers stretching across cells and acting as their contractile “muscle”), lattice-like networks of long filaments (e.g., in lamellar cell protrusions called lamellipodia), carpet-like networks of short filaments (e.g., in cortical actin underlying and structurally supporting the cell membrane), or as networks surrounding intracellular organelles, as shown in Figure 1.6 [9, 49]. The investigation of these different actin networks, in particular the flows and mechanical effects underlying plasma membrane protrusions, is an active field of experimentation and modeling, as is reviewed elsewhere [9, 23, 32, 67, 74].

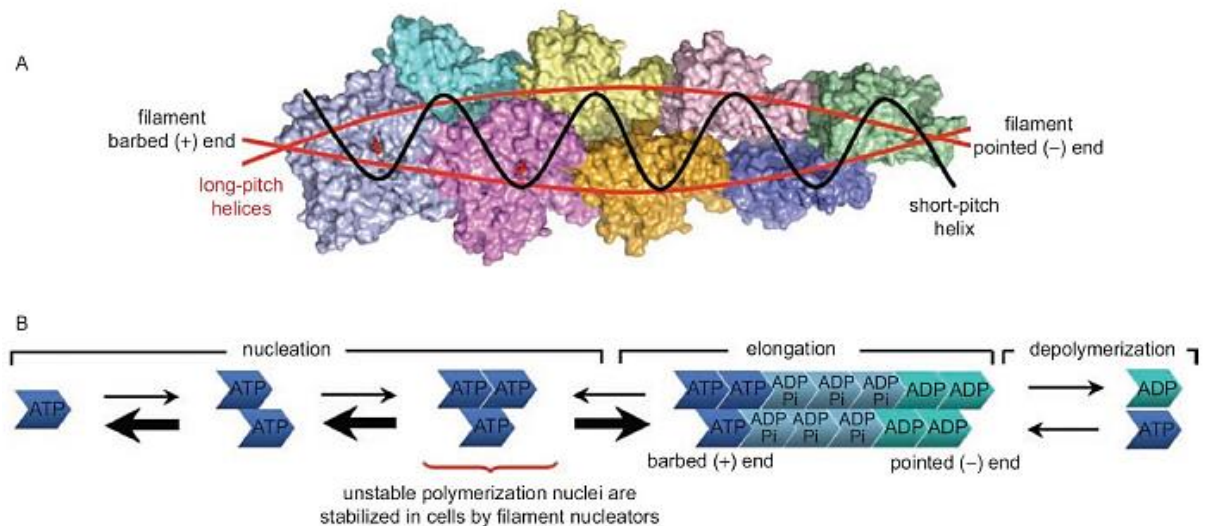


Figure 1.7: Treadmilling generated by plus-end polymerization and minus-end disassembly. Image taken from [26].

Nucleation is the first step in actin polymerization, which is the formation of a small aggregate consisting of three actin monomers, catalyzed by actin-binding proteins called nucleation factors [13] (Figure 1.8). From this, actin filaments are able to start elongating efficiently through energy-favored polymerization by the reversible addition of monomers to

both ends, especially the plus-end which elongates five to ten times faster than the minus-end. The actin monomers bind ATP, which is hydrolyzed to ADP after monomer's assembly to the filament. Although ATP is not required for polymerization, actin monomers to which ATP is bound to polymerize more readily than those to which ADP is bound [16].

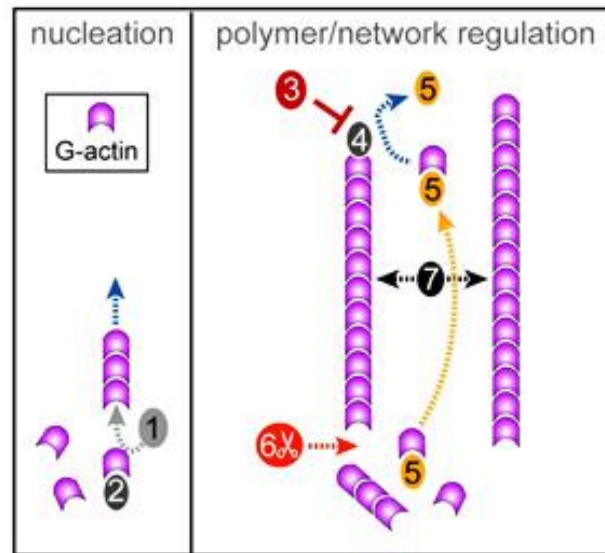


Figure 1.8: Cartoon model of actin regulation. During nucleation, nucleation factors (1) cooperate with support factors (2) to generate linear actin oligomers which can then undergo exothermic polymerization. Polymerization site is negatively regulated by capping proteins (3) which are competitively displaced by Ena/VASP proteins (4) which cooperates with a profilin-actin dimer (5) in actin polymerization. Filament disassembling factors (6) act at the other end. Cross-linking factors (7) assemble microfilaments into networks or bundles and/or exert pulling forces. Image taken from [83].

Continued plus-end polymerization accompanied by concomitant minus-end disassembly generates so-called "treadmilling" (Figure 1.7), one of the key processes in the dynamics of actin-based cellular structures [80]. When polymerizing against membrane resistance, treadmilling translates into the retrograde flow of whole actin networks; if these back-flowing networks become anchored to a rigid surface via transmembrane receptors, their treadmilling translates into a forward-pushing force able to push out membrane protrusions [79, 81, 99].

Actin treadmilling in cells is regulated by a number of ABPs that bind G-actin and/or plus-ends of the actin filaments; of particular importance in this context are Ena/VASP, profilin, formins, fascin, cofilin, and capping proteins [5, 7, 26, 53, 59, 67, 81, 86]. An illustration of these ABPs is shown in Figure 1.9.

Capping proteins bind and stabilize the F-actin plus-end, i.e., suppress polymerization and protect from depolymerization [3, 26] (pink half-circular crown in Figure 1.9). Profilin binds and sequesters G-actin (green square in Figure 1.9) and is, therefore, by default, an inhibitor of nucleation and enhancer of depolymerization [7]. However, this role changes dramatically if Ena/VASP is present, expelling capping proteins from the plus-end (green cross, Figure 1.9). These proteins bind actin-profilin hetero-dimers with high affinity and utilize it as a G-actin source to catalyze and actively promote plus-end polymerization [5].

In contrast, cofilin binds to the minus-end half of actin filaments where actin has undergone ATP hydrolysis (light blue Actin-ADP, Figure 1.9) and promotes filament disassembly. Fascin ('7' in Figure 1.8) acts as a cross-linker between parallel microfilaments [53] and formin can act as a nucleation factor ('1' in Figure 1.9) [10, 82] but also as an elongation factor acting similar to Ena/VASP (yellow star in Figure 1.9 and '4' in Figure 1.8). Therefore, apart from the physical properties of actin and its polymerization processes, the biochemical and biophysical contributions of these actin regulators need to be considered in any models aiming to describe actin dynamics (summarized in Figures 1.8 and 1.9).

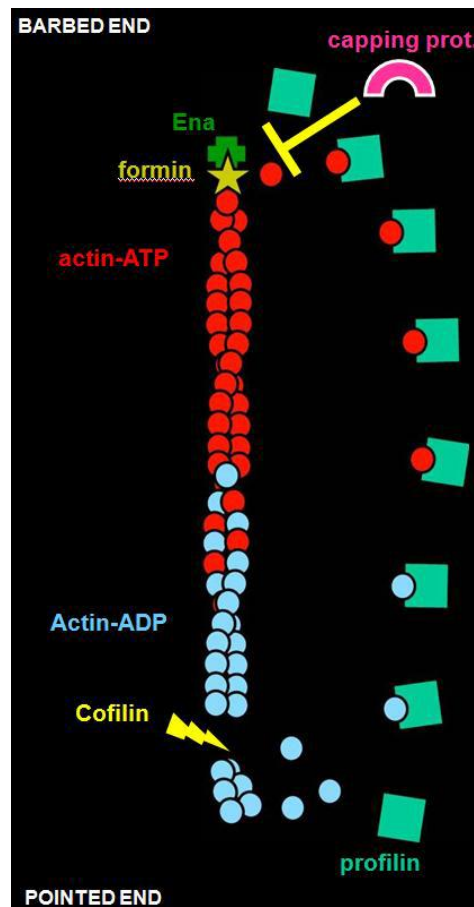


Figure 1.9: Schematic representation of ABPs involved in treadmilling. Image kindly provided by A. Prokop.

1.3 Properties of filopodia

In motile cells, thin ($0.1 - 0.3 \mu\text{m}$) sheet-like protrusive structures called lamellipodia emerge from the leading edge filled with a branched network of actin. This network can be locally reorganized into tightly cross-linked parallel bundles of F-actin, pushing the membrane to create elongated filopodia (Figure 1.10) [13, 56].

Filopodia are long, finger-like membrane protrusions with numerous roles in signaling and cell navigation [30, 36, 57, 62]. Filopodia can grow or retract at a range of speeds, or maintain a steady-state equilibrium, switching between these different dynamics due to an internal regulation and in response to chemical or mechanical changes in the environment. These dynamic regimes allow a filopodium to probe cell surroundings, perform its role as a mechanochemical³ receptive structure to guide cell motility [104], or contribute to processes such as endocytosis, phagocytosis, morphogenesis, and neuronal growth (Figure 1.11) [56].

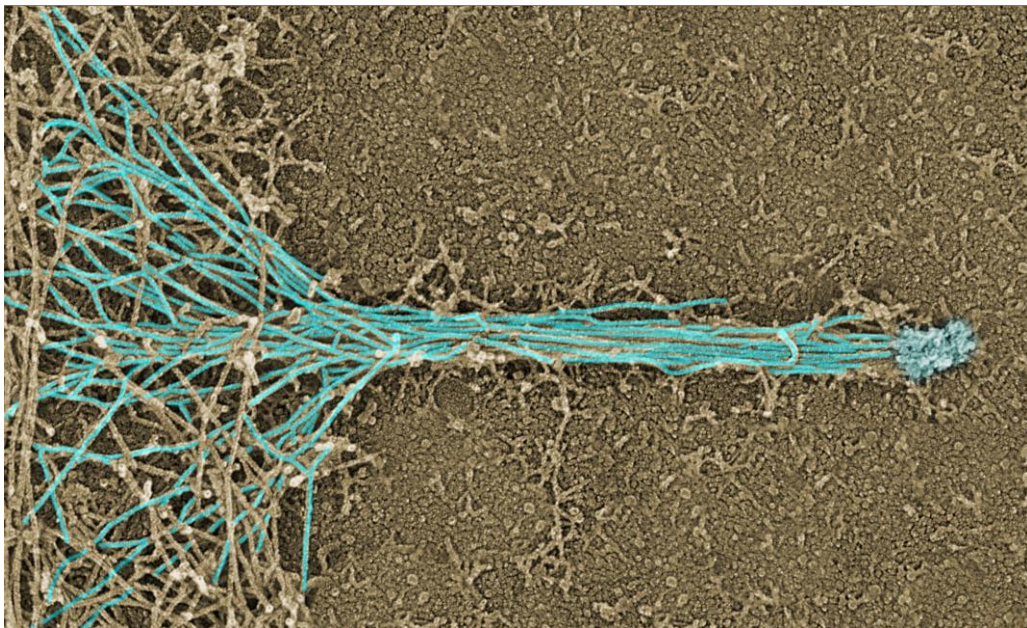


Figure 1.10: Parallel arrangement of actin filaments inside filopodium. This image is a courtesy provided by Tatyana Svitkina (University of Pennsylvania).

The filopodial diameter measures $50 - 250 \text{ nm}$ [1], depending on the elastic properties of the membrane. Fibroblasts and nerve growths cone harbor filopodia which rarely exceeds $10 \mu\text{m}$, but in sea-urchin embryos filopodia can reach up to $40 \mu\text{m}$, featuring a variety of lengths

³ Mechanochemical enzymes converts chemical energy into mechanical energy [55, 72].

that must be taken into account [4, 63, 77, 88, 90]. The parallel bundles of actin filaments at the core of filopodia generate the positive or negative forces that elongate or retract the tips of filopodia. Those bundles typically consist of 10 – 50 filaments cross-linked by specific molecules, providing mechanical rigidity to the bundle, such as fascin ('7' in Fig. 1.9) [15, 56].

Although rooted in lamellipodia, filopodia can protrude independently of their lamellipodium, driven by a balance between plus-end polymerization and minus-end destabilization as mediated by the ABPs (Section 1.2) [103].

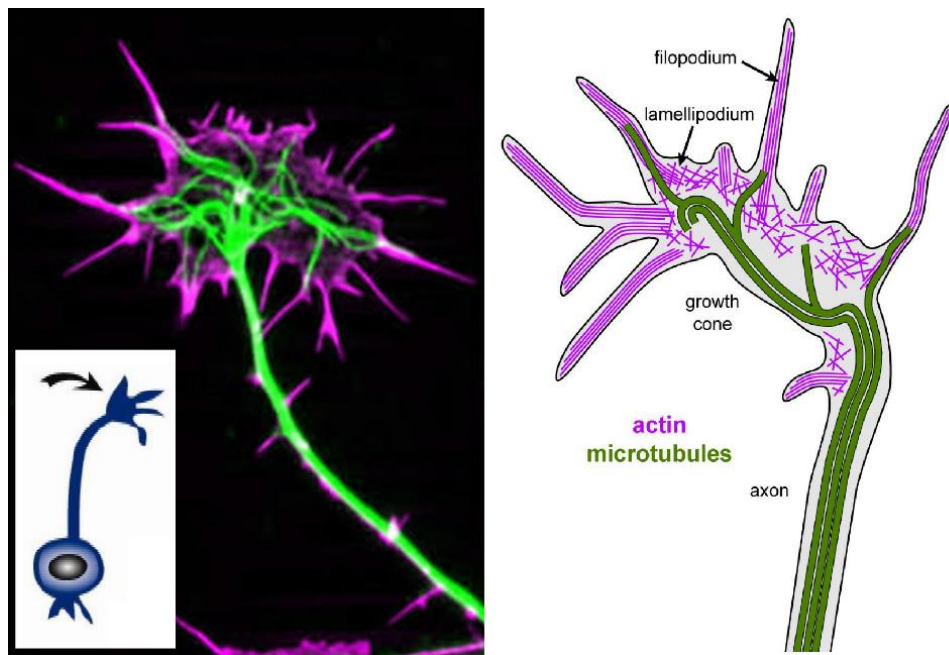


Figure 1.11: Filopodia on a neuronal growth cone. On the left, growth cone of fly neurons in culture, with actin shown in magenta and microtubules in green. On the right, a growth cone showing bundles of F-actin in filopodia and lattices in lamellipodium. Image kindly provided by A. Prokop.

Unlike the enormous complexity of most cellular regions with dynamically interchanging actin networks, the comparatively simple organization of filopodia offers great advantages: (1) they contain only one form of prevailing actin network consisting of parallel F-actin bundles; (2) accordingly, the number of molecular players is limited; (3) filopodial dynamics are predominantly one-dimensional, and (4) length changes of filopodial actin filament bundles directly translate into length changes of the entire filopodium, thus providing simple and efficient readouts for functional studies that can be carried out iteratively with modeling approaches [69]. Therefore, filopodia provide a promising context in which to start the modeling of actin network regulation in cells.

However, a key challenge to understand filopodial dynamics is the high rate of polymerization that occurs at the very tip, thus requiring constant delivery of actin monomers through the entire length of these slender and long structures. This poses the intriguing question as to what transport mechanisms may be at play that can deliver G-actin under these conditions in sufficient amounts. Answering this question harbors key explanations for filopodial behavior.

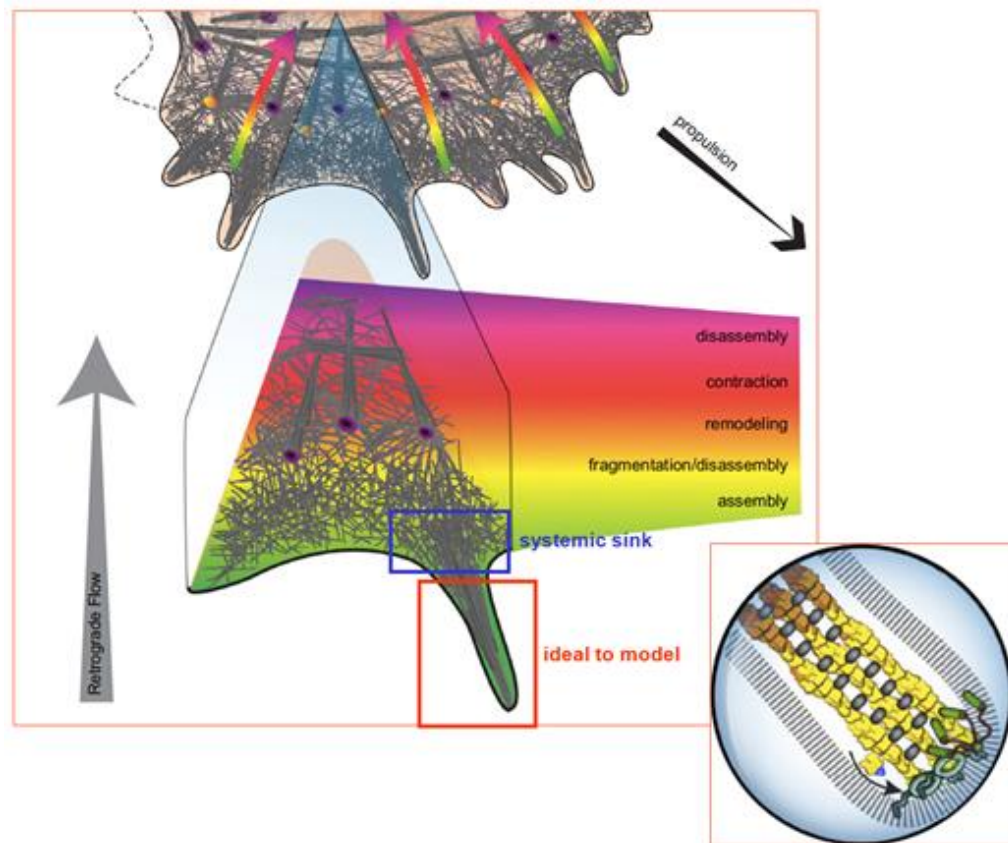


Figure 1.12: Filopodial dynamics as an ideal system to model most basic cytoskeleton interactions. Image adapted from [9].

Any models of this process have to consider that most G-actin is likely bound to profilin which will possibly have a negative impact on its diffusion properties but, on the other hand, increase their affinity for F-actin plus ends (through the high affine binding of profilin to Ena/VASP [5]), thus enabling polymerization even at very low concentrations of G-actin [5]. In support of this assumption, Ena/VASP as active polymerizers and interactors of profilin are concentrated at filopodial tips, and deficiencies of profilin or Ena/VASP cause dramatic shortening of filopodia [79].

Therefore, several studies relate some involvement of certain pathologies to changes in aspects of cytoskeleton formation, in particular, filopodia. So, actin regulation by those proteins is quite relevant to understand their roles in filopodial dynamics, which is essential to comprehend, for example, disorders related to neuronal growth as temporal lobe epilepsy or Alzheimer's, cortical dysplasias, and schizophrenia [22, 58]. In addition to neuron-related pathologies, wound healing, embryonic development, and tumor cell development, and cancer metastasis can also be mentioned [31, 102]. Figure 1.13 shows a microscopic image of a cancer cell.

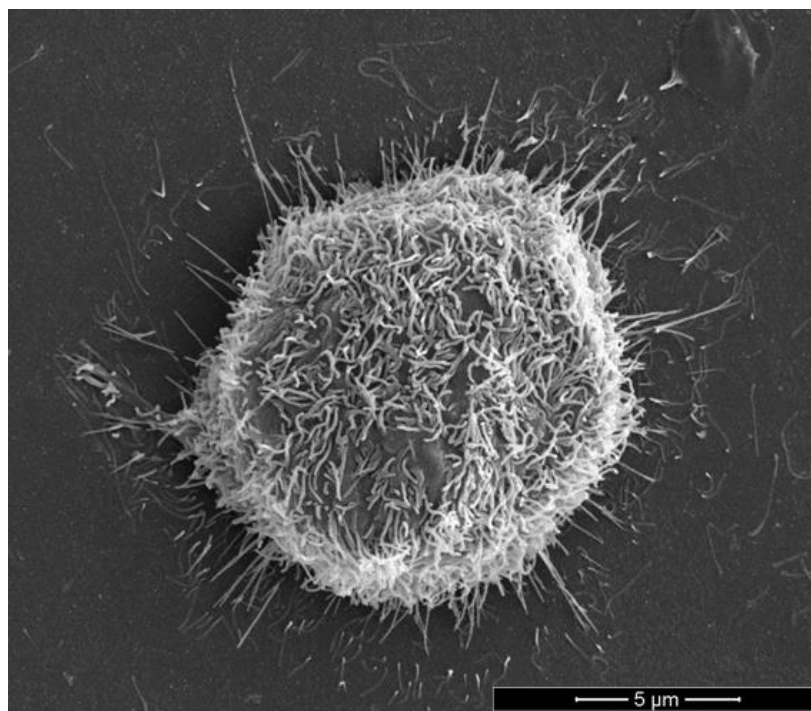


Figure 1.13: Filopodia emerging from a cancer cell⁴.

Morphologically similar to filopodia, other specialized cellular protrusions that can be mentioned here are microvilli, stereocilia, and the bristles of insects best studied in *Drosophila melanogaster* [87, 89]. Despite extensive studies over decades, the biological functions, assembly and regulation mechanisms of filopodia and the other related structures mentioned above are not yet fully understood. Research and findings, some apparently contradictory and other complementary, are often reported, and information about possible new actors in filopodial formation is constantly being uncovered [30, 32].

⁴ Image with copy rights due to Pierson Klein. Available for non-commercial publications at <https://www.flickr.com/photos/nderc/9264760446/>

1.4 Properties of plasma membrane

Another important factor to be considered when thinking about filopodia or other actin-driven protrusions is the cell or plasma membrane. The plasma membrane is a structure that delimits all living cells, both prokaryotic and eukaryotic. It establishes the boundary between the intracellular and extracellular environment, thus containing the cytoplasm and all inner cell components. The plasma membrane is a thin (5 to 10 nm), highly structured lipid bilayer with different classes of proteins embedded in or associated with it (Figure 1.14).

The configuration of the plasma membrane is not static, but dynamic and may be seen as a fluid with its molecules moving within. The cell membrane fluid mosaic model describing the membrane as a bi-dimensional fluid was first proposed by Singer and Nicholson in 1972 [94].

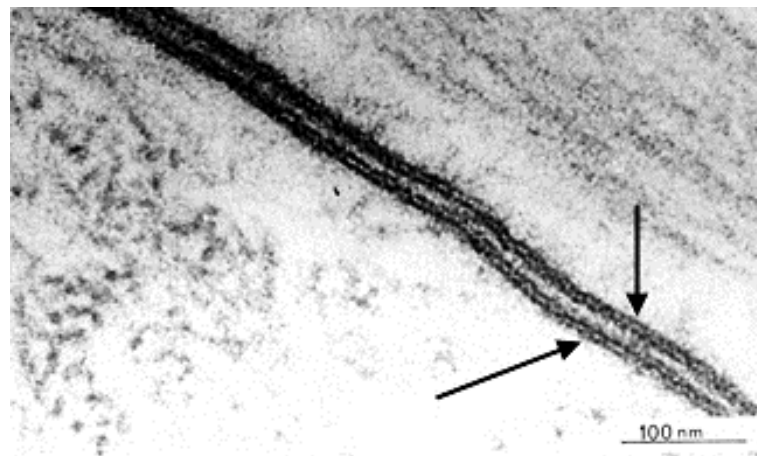


Figure 1.14: Microscopy image of plasma membrane lipid bilayer⁵.

There is a wide variety of proteins associated with the plasma membrane. Half of the membrane mass is estimated to be constituted by proteins, and 30% of all proteins encoded by an animal cell genome is located in the membrane (Figure 1.15). These proteins mediate virtually all essential membrane functions, such as nutrient entry in the cell and removal of metabolic waste products, vital reactions as ATP synthesis, cytoplasm communication with the extracellular medium, endocytosis, exocytosis, signal sensing, osmotic control, cell adhesion, shaping and motility [1]. In addition, some of these proteins connect to an actin microfilament

⁵ Available at https://www.histology.leeds.ac.uk/cell/plasma_membrane.php

network attached just below the membrane called cellular cortex, exerting forces and responding to mechanical stress, supporting the membrane, and preventing disruption [44].

Transport of vital substances across the plasma membrane is carried out by proteins through different transport systems: active or passive. Some proteins are open channels, allowing ions to diffuse directly into the cell body, but others use the concentration gradient of the solute to aid diffusion or use ATP as an energy source to pump materials against a gradient. In the first case, the transport is passive (where diffusion occurs spontaneously) and, in the second, active (where the transport occurs with energy expenditure to the cell).

Moreover, lipid-soluble molecules can permeate the membrane, but its phospholipid structure forms a nearly impermeable double layer to water-soluble molecules, due to the polarity of lipid molecules: they consist of a hydrophilic end facing out of the layer (small balls in Figure 1.15), and a hydrophobic property facing inwards (zigzagged lines in Figure 1.15) [25].

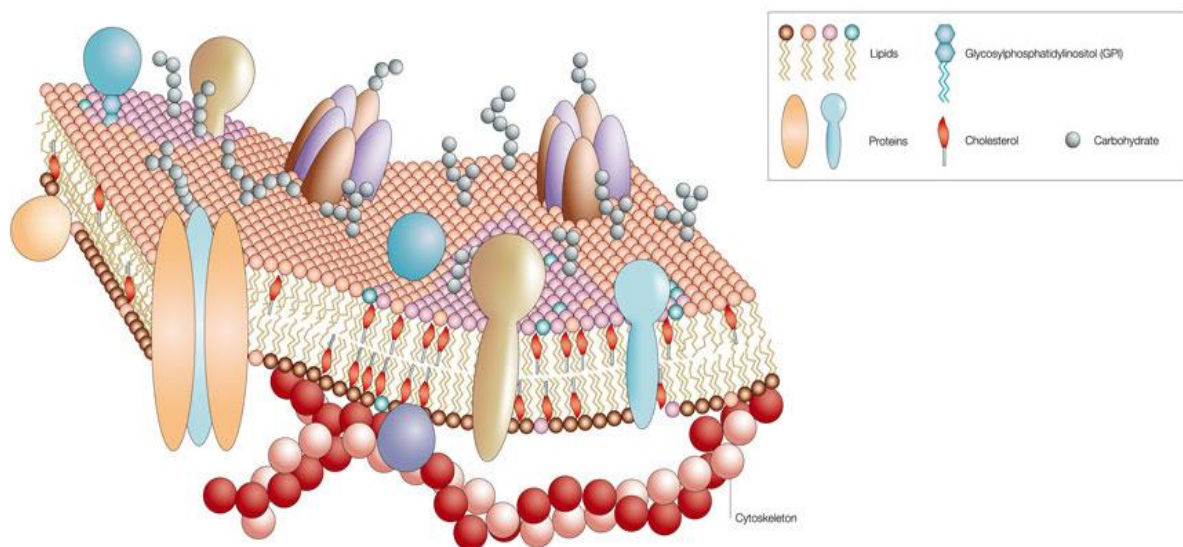


Figure 1.15: The fluid-mosaic model of the cell membrane⁶. Cell membrane is a complex structure made up of many different molecules, such as proteins, phospholipids, and cholesterol.

The cell membrane is remarkably flexible due to its chemical structure and presents physical properties that make it the ideal boundary for rapidly growing and dividing cells [25]. The elastic properties of the cell membrane, especially its bending modulus κ ($= 20 \text{ K}_B T$) and

⁶ Available in Nature Education website at www.nature.com/scitable

surface tension at rupture ς ($= 0.06$ N/m) [3] are basic mechanical parameters fundamental to the dynamics of all processes that may depend on these characteristics.

The relationship between the cell membrane and cytoskeleton, and its dynamics, are subject to these parameters, optimized to provide cell maintenance and structural integrity. It can be correlated to specialized cell functions associated with shape deformation and/or force production. Mathematical and computational modeling provides powerful tools also to investigate those correlations, as can be seen in recent publications [2, 19, 52, 64, 104].

2 THE CURRENT STATE OF ACTIN AND FILOPODIA MODELING

2.1 Models based on actin diffusion and binding kinetics

The cytoskeleton drives many cellular processes including structural support within cells, cell migration, endocytosis, and cytokinesis [3]. In that complex scenario, modeling approaches arise as useful strategies for evaluating problems. Here I will briefly describe approaches that have been used to this end so far.

Since the end of the 1950s, researchers have been developing models to quantitatively validate experimental results concerning actin dynamics from laboratory experiments [23]. Very early on, Oosawa and colleagues found that actin polymerization processes were dependent on G-actin concentration [70]. In another early seminal study, Wegner mathematically described actin treadmilling [99]. A further good example is the ordinary differential equation model developed by Bindschadler and colleagues which explicitly accounts for nucleotide-dependent actin polymerization and depolymerization [6].

At about the same time, taking advantage of technological advance and detailed experimentally measured data, Vavylonis and colleagues built a quantitative discrete model of actin polymerization [97]. This model could be validated by new *in vitro* experiments using reflection fluorescence microscopy [33]. Mechanisms of actin polymerization have been studied including the interactions between actins and ABPs and the rate constants for each step leading to quantitative models of polymerization [81].

Another important model that elucidated thinking about how actin polymerization can dynamically control cell shape and motility was the Brownian ratchet model by Peskin and colleagues [77] which aims to explain how chemical reactions generate protrusive forces by rectifying Brownian motion. The ratchet mechanism is the intercalation of monomers between the barrier (i.e. membrane) and the polymer tip, as shown in Figure 2.1. A particle diffuses in one dimension ahead of a growing microfilament, executing a continuous random walk in a constant force field. As a result, it describes polymerization velocity as a function of the membrane load force.

Actin dynamics in motile cells have also been subject of many modeling approaches. For example, the model by Mogilner and Keshet showed how lamellipodial protrusion velocity depends on actin monomer concentration, reactions with ABPs, barbed end polymerization, and using diffusion as a transport mechanism [62]. Others used a reaction-drift-diffusion equation

to combine active transport, diffusion, and advection to describe G-actin delivery in lamellipodia [69]. Others investigated the mechanisms of pushing and pulling driven by actin polymerization [18], and anterograde flow of cytoplasm to provide sufficient material for the extension of protrusions at the front of the lamellipodium [63]. As these examples illustrate, the modeling of actin in biological contexts has to include different levels of resolution, such as structural, physical, and chemical properties of actin filaments and protein complexes that govern actin dynamics.

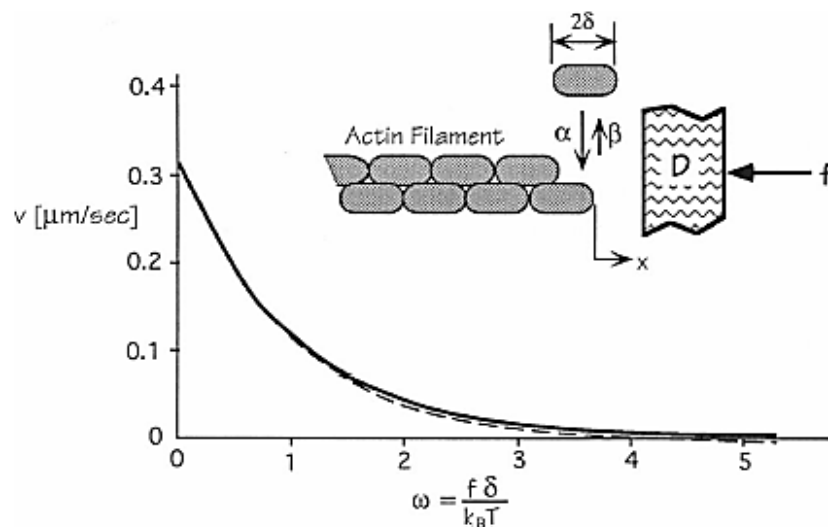


Figure 2.1: Representation of Peskin's *Brownian ratchet* model. Polymerization in a single actin filament occurring against a barrier to open gaps for adding new monomers. The curve shows the speed of polymerization ratchet (v) as function of the barrier load force (ω). Polymerization and depolymerization rates at filament barbed end are given by α and β , respectively. Image reproduced from [77].

With regard to modeling filopodia, several previous attempts should be mentioned. For example, Dawes and colleagues investigated the spatial distribution of actin filaments and their barbed ends in filopodia, the interplay between filament branching, growth, and decay at the leading edge [18]. Lan and Papoian used stochastic simulations of filopodial dynamics, discretizing space into compartments, and simulating protein motion by diffusion along filopodia as a random walk [51]. Erban and colleagues approached the problem of G-actin delivery to the filopodial tip through multiscale stochastic reaction-diffusion models, comparing the efficiency of compartmental-based and molecular-based algorithms as strategies to simulate actin dynamics. Modeling filopodia by subdividing them into compartmentalized domains proved to be an interesting technique in these last cited works. An example of a compartmentalized domain is in Figure 2.2 [28].

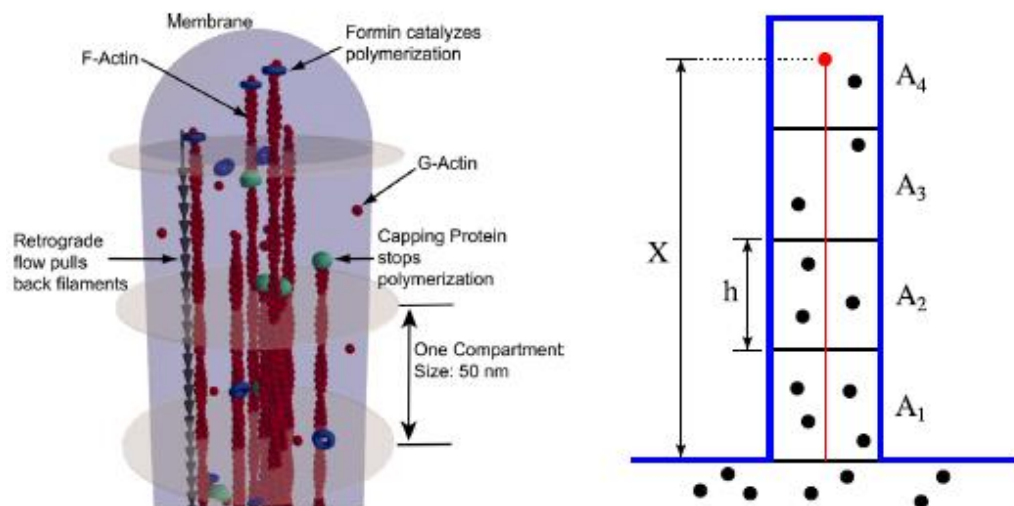


Figure 2.2: Scheme of simple compartmental-based simulation in Erban's. In the left, a 3D representation of a filopodium divided into compartments; in the right, a 2D simplified model of a filopodium with four compartments and moving particles (G-actins) stochastically distributed within the domain. Image reproduced from [28].

Also, the relations between filopodial protrusions and monomer concentration are discussed in Mogilner and Rubinstein's work [64]. This model uses essentially diffusion as a physical mechanism of molecule transport to analyze aspects such as physical properties of filopodia. In their study, the stiffness of the F-actin bundle as a function of the cross-linkage and the number of filaments in the bundle are approached to understand how the filopodial length can be limited by buckling when the bundle is forced against membrane resistance. More presented results are in respect to cross-linkers distribution in the F-actin bundle, as well as calculations about G-actin concentration distribution in filopodial protrusions formation. These results from [64] are shown in Figure 2.3.

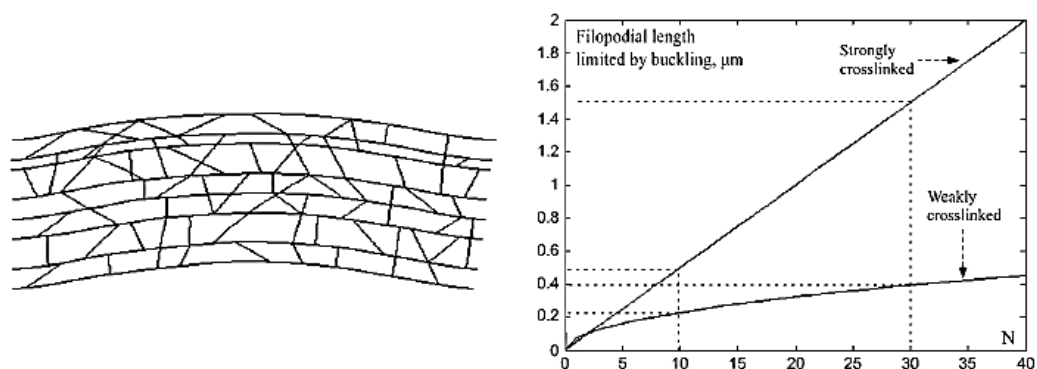


Figure 2.3: Examples of investigations presented at Mogilner and Rubinstein's. In the left, a computed distribution of cross-linkers in the bundle; in the right, filopodial lengths as function of the number of filaments in the bundle, and the strength of the cross-linkage. Images reproduced from [64].

2.2 Diffusion alone cannot explain G-actin delivery to the filopodial tip

Diffusion is the most basic approximation to explain the motion of G-actins [52]. As it turns out, diffusion is insufficient to generate long filopodia. Here, this finding was put further to the test by carrying out my own calculations to explore whether, and under which conditions, diffusion might be sufficient to supply barbed end actin polymerization processes in filopodia, also considering the work by others mentioned in Section 2.1. For simplicity, my calculations in this section do not consider filopodial elongation but analyze conditions where retrograde flow and polymerization are in balance, thus maintaining filopodial shape, length, and retrograde flow in a steady state. For all calculations and simulations from here, we used the parameter values indicated in bold text in Table 1. The results I obtained are described in the following and were published elsewhere [67].

Table 1: Parameter values

Notation	Meaning	Values	References
L	Filopodial length	24 – 55 μm	[4]
		0.03 – 0.15 μm	[63]
		1 – 10 μm	[77]
		10 – 20 μm	[88]
		3 – 10 μm	[90]
		Here: 1 – 30 μm	
N	Number of filaments in the filopodial bundle	10 – 30	References in [64]
		≤ 40	[4]
		60	[75]
		Here: 10 – 50	
k_{on}	Polymerization rate	10 $\mu\text{M}^{-1}\text{s}^{-1}$	[64]
		11.6 $\mu\text{M}^{-1}\text{s}^{-1}$	[104]
		Here: 10.8 $\mu\text{M}^{-1}\text{s}^{-1}$	Appendix 1
C_o	G-actin concentration at filopodial base	10 μM	[64]
N_o	Number of filaments to support protrusion	13	[64]
δ	Half-size of actin monomer	2.7 nm	[64], [75], [77]
η	Unit conversion factor	20	[64]
D	G-actin diffusion coefficient	4 $\mu\text{m}^2/\text{s}$	[62]
		5 $\mu\text{m}^2/\text{s}$	[56]
		5.65 – 6 $\mu\text{m}^2/\text{s}$	[105]
v_{ret}	F-actin retrograde flow velocity	70 nm/s	[65]
		30 – 80 nm/s	[89]

In protrusions or short filopodia with less than 2 μm , the concentration of free actin at the filopodial base is still sufficient to supply enough polymerization for F-actins extension to occur [64]. This is in agreement with equation (2.1) for estimating the approximate time required for a particle to diffuse over a given distance x , in an environment where its diffusion coefficient is D ,

$$t \approx \frac{x^2}{q_i D}. \quad (2.1)$$

In (2.1), q_i is 2, 4, or 6 depending on the number of dimensions ($i = 1, 2$ or 3) [43]. Considering a linear displacement ($q_1 = 2$) and a diffusion coefficient $D = 5 \mu\text{m}^2/\text{s}$, a G-actin can travel up to 3.16 μm at the first second. Considering $v_{ret} = 70 \text{ nm/s}$ and elongation reaching 1.2 $\mu\text{m/min}$ in protrusions [91], G-actin delivery to polymerization seems to be effective just by diffusion.

For filaments longer than a few micrometers, we can analyze the concentration of free actin according to function (2.2) mentioned in [64], derived from a diffusion equation

$$C(x, t) = C_o - \frac{C_o x}{L(t) + (D\eta e^{N_o/N}) / (k_{on} N)}. \quad (2.2)$$

In expression (2.2), $L(t)$ indicates filopodial length as a function of time, (i.e., considering filopodial elongation or shrinkage). This investigation does not consider elongation, so we assume $L(t) = L$ constant, removing time dependency at this first moment. Furthermore, the filopodial length interval was chosen to cover for a wide range of natural filopodia (see in Table 1), although values between 10 and 20 μm are more frequently observed [9].

Function C provides G-actin concentration at a given distance between the filopodial base ($x = 0$) and the filopodial tip ($x = L$). Therefore, the free actin concentration at the tip of the filopodia is given by the function expressed in

$$C = C(L, N, k_{on}) = C_o - \frac{C_o L}{L + (D\eta e^{N_o/N}) / (k_{on} N)}. \quad (2.3)$$

The key question is whether diffusion is sufficient to sustain polymerization in order to balance the actin-bundle retrograde flow ($v_{ret} = 70 \text{ nm/s}$ in Table 1). To achieve this velocity, a

polymerization frequency of 26 actins/s per filament in the bundle is required when considering that every new actin elongates a filament by 2.7 nm (Table 1). Therefore, in a bundle with N filaments, $N_{ret} = 26N$ actins should be polymerized per second. This will be compared with the number of actins that can reach filaments plus-ends to check if diffusion is enough to sustain F-actin retrograde flow.

During a stabilization phase, the growth rate of the filopodial bundle was reported to be 0.3 $\mu\text{m/s}$, which means that about 110 actins should be polymerized per filament each second [79]. For a bundle with N filaments, the number of polymerizing actins N_p would be 110N/s. But, considering that G-actin concentration varies with length, we can use function (2.3) to better describe N_p , and then

$$N_p = 11NC \quad (2.4)$$

is the number of actins polymerized at a given concentration $C = C(L, N, k_{on})$.

Here, $N_p = 11NC$ because the number of polymerized actins is directly proportional to the concentration of monomers. At a concentration of 10 μM , 110 actins are polymerized per second on each filament, providing 11 actins/s per filament at 1 μM . The expression (2.3) yields $C \rightarrow C_o$ when $L \rightarrow 0$, ensuring that $N_p = 110N$ for a concentration close to that at the base of filopodia.

Thereby, it allows for calculating how many actins reach the polymerization point in scenarios generated by varying L , N , and k_{on} . The calculations were performed by the following routine:

```

for L in range(min = 0.5, max = 30, step = 0.5):
    for N in range(min = 10, max = 50, step = 1):
        for k_on in range(min = 10, max = 11.6, step = 1.6):
            Calculate C = C(L, N, k_on), following function (3.3)
            N_ret = 26N
            N_p = 11NC
            If N_p < N_ret
                Add one in the number of cases where N_p < N_ret
            else
                Add one in the number of cases where N_p ≥ N_ret
print 'Number of cases where N_p < N_ret (in %)'

```

Using this algorithm in combination with the values given in Table 1, we obtain that of all cases the polymerization does not supply retrograde flow in 91.52%. In comparison, when setting the filopodial length interval to $L \in [0.5, 2] \mu\text{m}$ and $k_{on} = 11.6 \mu\text{M}^{-1}\text{s}^{-1}$ diffusion is ineffective in 7.14% of cases for $N_{max} = 30$, or 33.23% when $N_{max} = 50$. This result suggests that diffusion alone is not sufficient in many scenarios, especially when reaching filopodial lengths beyond $1.5 \mu\text{m}$ and with N greater than 25.

This is consistent with the results of [64], which uses diffusion as the main transport mechanism in protrusions. In our calculations, since we use $N = N_o$ and $k_{on} = 10 \mu\text{M}^{-1}\text{s}^{-1}$ for $L \leq 2 \mu\text{m}$, we have $N_p > N_{ret}$ for all cases. However, as filopodia grow and these parameters change, diffusion becomes fragile or even unfeasible, justifying our analysis and the hypotheses that G-actin diffusion should be combined with other physical transport phenomena.

Further reports agree with these results. For example, in [103] Monte Carlo simulations were used to investigate G-actin translocation during protrusion within a lamellipodium and its conclusions show that elongation is too rapid to be explained just by passive diffusion. The use of compartmental and molecular stochastic models to study actin motion by diffusion concluded that filopodia would reach a steady-state length of as little as $1 \mu\text{m}$ because of the transport flux of G-actin monomers continuously diminishes as the tube becomes longer [28]. Also work on filopodia-like acrosomal processes of sperm found that the kinetics of diffusion-limited actin polymerization were not sufficiently rapid to account for the observed acrosomal elongation dynamics [75].

Going in the same direction, Zhuravlev and colleagues used deterministic and stochastic models to show that diffusional flux of G-actin to the polymerizing end is a limiting factor to filopodial growth when in the absence of other chemical or mechanical regulation [104]. Their work suggests that molecular motors may be a candidate for supplementing the passive diffusion of G-actin during filopodial elongation and highlights a complex coupling of active transport by molecular motors, passive diffusional transport, and polymerization, and retrograde flow fluxes as essential to dynamically regulate filopodial growth. According to these authors, filopodial lengths of tens of micrometers can only be achieved if the G-actin flux forward is much greater because diffusion is too slow to explain G-actin delivery [103].

This analysis shows that diffusion is an appropriate first approximation to model the physical mechanisms of G-actin transport in protrusions but needs to be combined with other phenomena to explain the actual length of filopodia observed in nature.

2.3 Motor transport of G-actin is not sufficient

A further mode that might contribute to G-actin movement is the so-called active transport by motor molecules. These mechanochemical molecules, called myosins (a protein family with 18 members [72]), can walk over actin filaments through chemical bonds and ATP break-down. In a simplified way, the molecule has two ends, head and tail. The tail has two binding sites that can connect to F-actin. When one of those sites is released, the other remains strongly connected, until the first exerts mechanical force to connect further ahead, making a "step" along the filament. The motor head is free for G-actin sequestration to perform its transport. A schematic illustration of motor transport is shown in Figure 2.4.

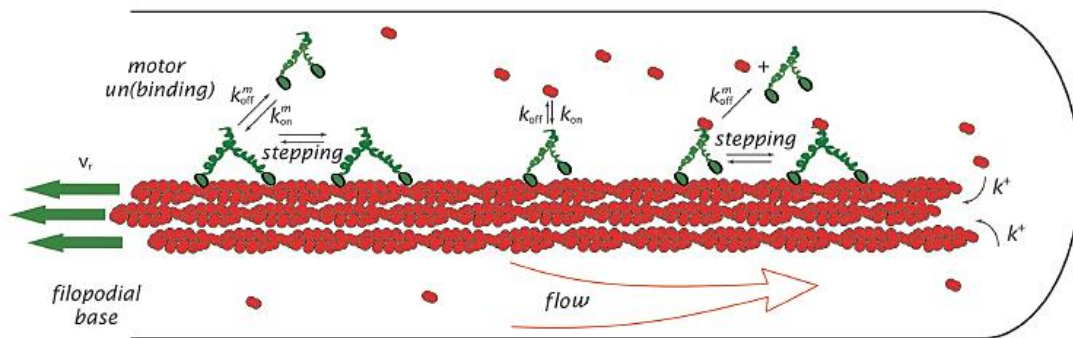


Figure 2.4: Active transport by motor molecules. Image adapted from [104].

G-actin active transport by molecular motors is considered in the model presented by Zhuravlev and colleagues. They proposed that diffusional transport of G-actin monomers to the polymerizing barbed ends is a key limiting factor for filopodial elongation and investigated potential roles of active motor-driven transport of G-actin [103]. They concluded that “a naive design of molecular-motor-based active transport would almost always be inefficient; an intricately organized kinetic scheme, with finely tuned rate constants, is required to achieve high-flux transport”. According to Zhuravlev and Papoian [103], motors like myosin have a contribution of about 30% or less in the delivery of G-actins. A possible cause is due to the sequestering of G-actin by freely diffusing profilin. Therefore, they suggested the possibility that other processes need to be considered to fully understand G-actin transport in filopodia.

As the above calculations and previous work show, diffusion and motor active transport alone appear not sufficient to supply the amount of G-actin needed to sustain the observed rates of polymerization and F-actin backflow. An additional mechanism proposed here could be the advective effect caused by the flow of cytoplasm towards the filopodial tip.

3 A NOVEL STOCHASTIC MODEL OF FILOPODIAL DYNAMICS: MATHEMATICAL ASPECTS

3.1 A filopodial pump: advection as a potential transport mechanism

As the above calculations and previous work reporting show, diffusion and motor transport alone appear not sufficient to supply the amount of G-actin needed to sustain the observed rates of polymerization and F-actin backflow. I propose therefore an additional mechanism provided by the advective effect caused by the flow of cytoplasm towards the filopodial tip.

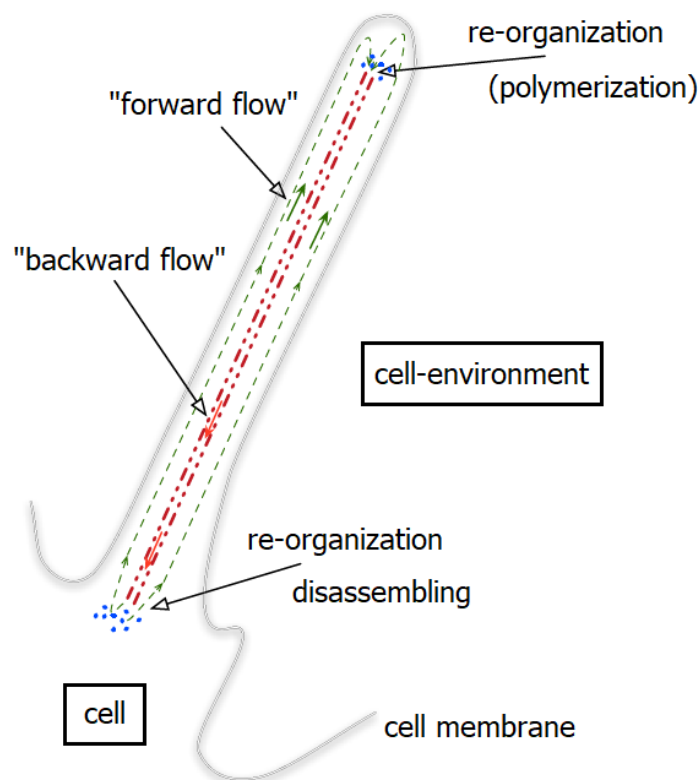


Figure 3.1: Polymerization inducing inflow of matter into filopodium. The inflowing suspended molecules rearrange into filaments as long as polymerization occurs and the retrograde flow consumes the reorganized volume at filaments plus-ends, inducing a compensatory inflow of cytoplasm due to a drop of pressure in the filopodial tip, which generates a volume flux within filopodia. Image kindly provided by M.V. Kritz.

The idea is as follows: F-actin filaments at the core of filopodia are constantly flowing backward from the tip towards the cell body, driven by disassembly processes occurring at the

filopodial base; the back-flowing volume comprises the actin filaments and their hydration coat, other attached molecules such as cross-linkers, and perhaps even cytoplasm trapped in between the tightly packed actin filaments; the back-flow, therefore, extracts substantial volume which takes effect at the filopodial tip; if this volume loss is combined with a sufficiently rigid membrane structure to prevent membrane collapse, this would generate a negative pressure based on the mass conservation principle, thus triggering a compensatory incoming flow of cytoplasm to prevent cavitation. Figure 3.1 shows a representative image of this process.

In this way, the “backflow” of volume can be expected to drive a compensatory influx in the space between the actin bundle and cell membrane towards the tip of the filopodium. The inflow volume should be a mixture of cytosol, which is essentially colloidal water, and molecules dissolved within, which are G-actin molecules or G-actin/profilin complexes. Then, combining both advection and diffusion may therefore be a legitimate strategy to develop models and testable hypotheses. For simplicity, every moving molecule (free G-actin or its combination with profilin) will be mentioned as a *particle*, highlighting its properties when needed.

Since polymerization is a chemically reactive process, beyond the affinities of G-actins and ABPs, it suggests a reaction-diffusion-advection system to be modeled. In this context, molecules may move and react, simultaneously or not, depending on their motions, and it may be influenced by several factors due to the high complexity of filopodial dynamics. Notice that different processes may be predominant in very distinct regions of the filopodia. Hence, a stochastic approach seems feasible and potentially more promising to describe a chaotic system, with a large amount of interactions and mechanisms occurring almost simultaneously.

In vivo, cells may undergo osmotic control through aquaporin water channels in the plasma membrane [72], allowing water to cross the membrane. Such channels would impact on the amount of compensatory cytoplasmic flow. However, since it is unclear as to whether such channels exist in filopodia, we will not consider such complications and the filopodial inner volume will be regarded as following conservation laws.

In [67], we have presented a comprehensive description of this proposed coupling of physical mechanisms and biological regulations to unravel G-actins transport within filopodia. Calculations that shown the inefficiency of diffusion to explain such process for longer filopodia in Section 2.2 were the starting point of this investigation. Although, advection as a physical consequence of volume removal from filopodial tip can be mathematically modeled as long as this matter consumption is quantified and, as it is shown in this chapter, it has straight connection with structural configuration of the filopodium.

3.2 Towards an integrated approach combining different mechanisms and properties

As should have become clear, filopodial dynamics depends on an intricate web of chemical affinities, physical properties, and mechanical outcomes, with biological agents interacting stochastically [104]. As detailed above, existing models have incorporated affinities at the F-actin plus end, diffusion, and I have proposed the idea of a filopodial pump contributing to G-actin transport through advection. Also, active motor transport of G-actin might contribute to a certain degree ($< 30\%$ as said in [103]) but will not yet be incorporated in our model, although these data will be used as an input for simulations in Section 5.4 to observe their potential effects.

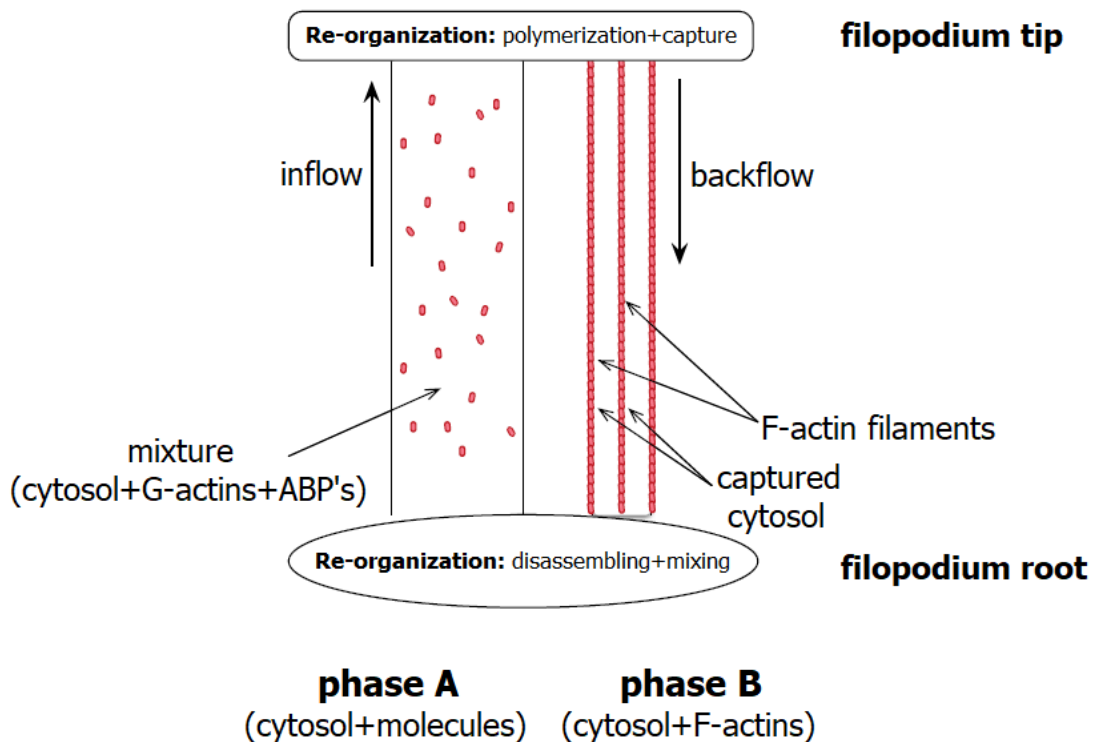


Figure 3.2: Two-phase model scheme of polymerization inducing inflow of matter into filopodium. In so-called phase A, the cytoplasm, essentially a mixture of cytosol and suspended molecules (G-actins and ABPs), inflows into filopodia towards the tip, where polymerization induces a reorganization of this fluid. In that stage, G-actins are captured by filaments plus-ends through polymerization, which backflows to the body cell, also consuming a volume of cytosol trapped within bundle filaments. It promotes a reorganization of the cytoplasmic fluid, which consists of the model phase B. The reorganization of fluid and its consequent removal of volume in the filopodial tip in phase B induces a compensatory inflow of cytoplasm, back to the phase A. Image kindly provided by M.V. Kritz.

In addition, it is reasonable to assume that regulatory molecules are also subjected to the same phenomenon to move. However, the flow of cytoplasm cannot be modeled considering it to be a mere fluid, but one must consider also the larger amount of particles it contains, their trajectories, interactions, and mechanical effects of their movement. Therefore, we will incorporate processes of molecular diffusion, chemical reactions, cytoplasmic flow, conservation of mass, and a two-phase fluid reorganization (described in Figure 3.2), which together represent a remarkable quantity of information.

Integrating such data load across physical and biochemical phenomena occurring at different scales in one computational model will require an adequate choice of tools and strategies. The challenge of this task is illustrated in Figure 3.3 which compares cartoon representations of the biological layout (A), the mathematical-computational model (B), a physical description of the cytoplasmic flow (C), and a composite model (D).

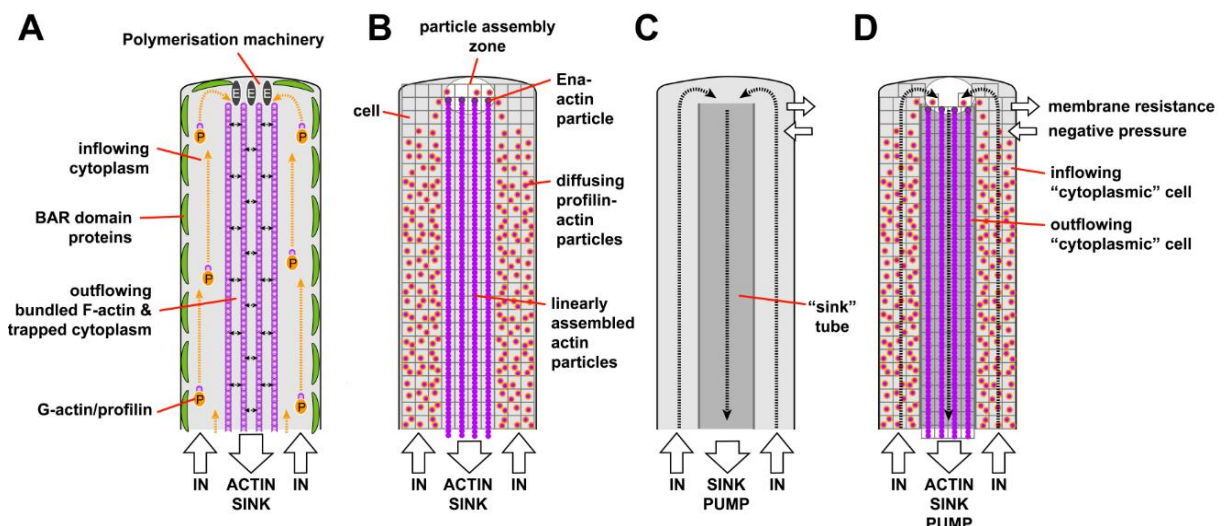


Figure 3.3: Cartoon models of filopodial dynamics. (A) Biological model: F-actin bundles retrograde flow compensated through Ena/VASP-mediated plus-end polymerization requiring supply (yellow arrows) with profilin bound with G-actin. Filopodial membranes are stabilized by BAR domain proteins. (B) Mathematical/computational model: filopodia is subdivided into a coordinate system within which G-actin (magenta dots) undergo Brownian motion, diffusion, and assembly processes. (C) Flow model: filopodia are represented by a tube-in-tube scheme where volume (actin filaments with potentially trapped cytoplasm) flows out of filopodia, driven by a pump at the base of the inner tube, causing a compensatory inflow of cytoplasm. (D) Combinatorial model: on circulating cytoplasm flow from (C), G-actin with different properties (as in B) can diffuse and/or react within this dynamic context, thus possibly combining cytoplasmic flow dragging, diffusion, and regulator-mediated polymerization. Image kindly provided by A. Prokop.

As will be detailed in Chapter 4, a promising strategy to achieve the required integration could be to use Object Oriented Programming (OOP). However, before explaining the

implementation of such a model, I will explain the detailed considerations for each of the implemented processes, starting with diffusive motions (Section 3.3), the properties of back-flowing actin bundles (Section 3.4), specific molecular interactions (Section 3.5), mathematical statements about filopodial elongation (Section 3.6), and the coupling of advection with diffusion in this context (Section 3.7).

3.3 Brownian motion to simulate diffusion

The most basic phenomenon of particles' movement is diffusion, although it contributes in this context only to a limited degree [77, 103], as was discussed in Section 2.1 and verified in Section 2.2. Brownian motion (BM) is generally a suitable tool for simulating diffusive particles, based on their erratic motion in a chaotic system whose displacements are influenced by several factors [84]. Its discovery dates back to the year 1827 when the Scottish botanist Robert Brown observed pollen grains moving randomly when suspended in water. He described this motion but was not able to explain the phenomenon. Brown wasn't, in fact, who first observed erratic motion of particles. Lucretius had already used the chaotic motion of dust particles as evidence of atoms' existence in 60 B.C.

After Brown, others approached his experimentation trying to fill its understanding. In 1905, Albert Einstein confirmed Lucretius' conclusions in a publication which explained that the pollen was being moved by collisions with water molecules. But the existence of those essential units of the matter was only theoretical until 1908, when Jean Perrin experimentally verified Einstein's hypothesis, earning him the 1926 Nobel Prize in Physics for his work “on the discontinuous structure of matter” [76].

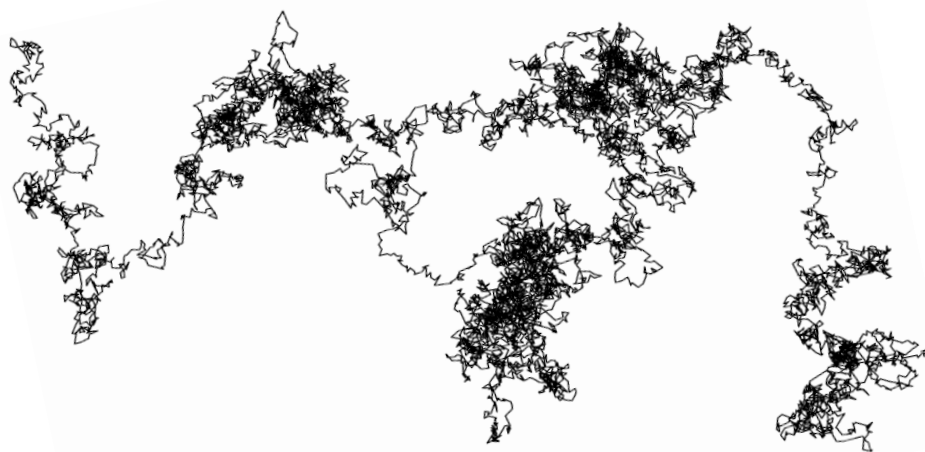


Figure 3.4: Planar random walk. Image taken from [66].

From a physical point of view, BM is a random movement of particles in a fluid due to their collisions with atoms or molecules in the surrounding medium. Even when the considered particle is much larger than the other atoms or molecules involved, as in the example of a pollen grain suspended in water, it still can be moved by the impact of smaller fast-moving masses.

BM can be seen as a visible chaotic path through a particle that is randomly affected by several microscopic effects, over a time interval. Since diffusion can be defined as the movement of particles from a region of higher to lower concentration, it has on BM a simplified model to represent the movement of particles in an eventual fluid throughout these regions. Figure 3.4 above shows an example of particle random walk over a plane.

Stochastic processes are practical situations that can be simulated using BM. Such examples occur frequently in pure and applied mathematics, economics, engineering, physics, biology, chemistry, and other knowledge areas. In most of the cases, these models may involve approximations and simplifications, but in general, BM is proper frameworks for creating mathematical models to observe random procedures or statistical analysis of variable fluctuations, like the illustrative example in Figure 3.5.

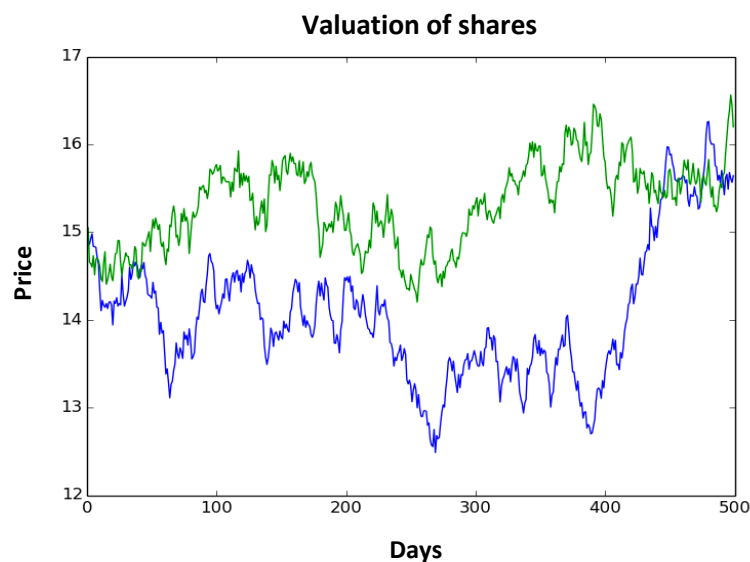


Figure 3.5: Variable random fluctuations in an economics application of BM. Prices of shares in financial markets present a quite dynamic variation with respect to a certain period. These values are subjected to countless random factors, whose behavior can be represented by a chaotic path over time. Image adapted from *Arte dos fatos* website⁷.

⁷ Available at www.artedosdados.blogspot.com

The mathematical description of BM is based on concepts of probability and is usually modeled by the Wiener process, a continuous-time stochastic process named in honor of Norbert Wiener⁸ [66, 84]. Let's say that during a small time interval $[t_1, t_2]$, particle positions are measured at times t_1 and t_2 , but not in between, where a particle will have its motion affected by other particles randomly. The path that matches the positions at each step of time is influenced by this time interval, not the quantity of collisions among the interacting particles.

Then, considering X a path that describes the BM of such particle, we write $X(t) = X_t$ to denote particle position X_t at time t . From this, it makes sense that $X_{t_2} - X_{t_1}$ should be a random value that increases as long as $t_2 - t_1$ does too. Thus, we can mathematically define a (linear) BM. Generalizations for two or three dimensions are analogous.

Definition. Let $X = X(t)$ be a random variable continuously dependent on time t in $[0, T]$. Brownian motion (or Wiener process) is a real-valued stochastic process $\{X(t) : t \geq 0\}$ if the following holds:

- i. $X(0) = X_0 = 0$;
- ii. $X(t)$ has independent increments, i.e. if $0 \leq t_1 < t_2 < \dots < t_n = T$ then the difference $X(t_{i+1}) - X(t_i)$ for $i = 0, 1, 2, \dots, n$ is also independent;
- iii. For each $0 \leq a \leq b \leq T$, $X(b) - X(a) \sim N(0, s^2(b - a))$ is normally distributed, where $N(0, s^2(b - a))$ is a Gaussian variable with mean zero and a time-scaled variance s^2 .

From these properties, we can make the following comments:

- a) In (i), we suppose the initial point of movement in $X_0 = 0$. Depending on the context, this data should be adapted;
- b) X satisfies the Strong Markov Property, which means that determining the future position $X(t)$ does not depend on previous positions (for $t < t$);

⁸ American mathematician noted for important contributions in computation and cybernetics. In probabilistic physics, his research focused on a statistical study of the motion of elementary particles in a liquid; a mathematical description for Brownian motion.

- c) In a linear case, the distance traveled over a time t by a Brownian particle satisfies the relation $\langle g^2(t) \rangle = 2Dt$, with a mean displacement $\langle g(t) \rangle$ and diffusion coefficient D . It derives from Einstein's kinetic theory for particles displacement. A proof for that is not relevant for the development of this work but can be seen in [41].

Computationally, we can use the following algorithm to simulate the Brownian movement of a particle in a two-dimensional domain and show its path over the interval $[0, T]$:

Define final instant T

Create a partition of $[0, T]$, such as $0 < t_1 < t_2 < \dots < t_n = T$, with $\Delta t = t_{i+1} - t_i$

Make $X(0) = 0$

For i in range($\min = 1$, $\max = N$, $\text{step} = 1$):

Calculate $N \sim N(0, \sigma^2 \Delta t)$

$X(t_i) = X(t_{i-1}) + N$

Plot segment $\overline{X(t_{i-1})X(t_i)}$

The application of particle random walks for our purposes can be exemplified by Figure 3.6. In our very preliminary simulations, with filopodial geometry not properly set yet, particles move in Brownian motion through a two-dimensional domain, where it is possible to observe G-actin concentration depletion in the area around the filament's barbed end (red dot in Figure 3.6). This is an expected behavior since G-actins are quickly consumed by the barbed end, slowing down polymerization speed and the motion of other particles was not efficient or fast enough to fill the vacant spaces (yellow circle in Figure 3.6).

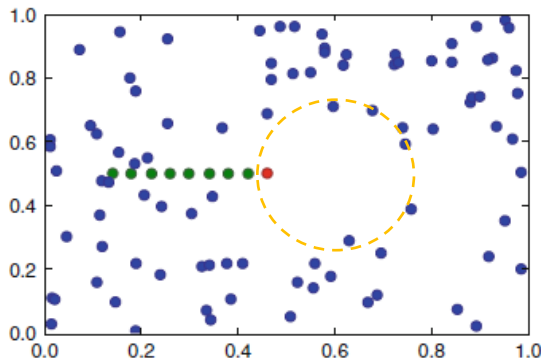


Figure 3.6: Molecules moving in Brownian motion in a two-dimensional domain. A preliminary simulation, with G-actin monomers in blue, F-actin in green, and the polymerization point (red dot) from where filament backflows. Note decreasing G-actin concentration around the microfilament plus-end (yellow circle). Simulation by the author.

3.4 Properties of back-flowing F-actin bundles

The development of a diffusion-advection model should consider the inflow and outflow volumes in the filopodium and their respective velocities. The inflowing fluid is essentially cytosol containing a number of G-actins or profilin-actin complexes. The outflow actin filament bundle is hexagonally packed (Figure 3.7 and Figure 3.8) [37, 46] and the filaments are cross-linked by specific proteins, such as fascin [87].

Cross-linkers are located every 25 - 60 actin subunits and bring mechanical cohesion and stiffness to the bundle [9, 37, 64], also suppressing any lateral movement of these actin filaments. Several authors have analyzed the relation between the length and/or binding strength of cross-linkers and the resistance of bundles to buckling [64, 104]. Then, based on those works, there is a theoretical foundation to argue that inter-filament spacing is narrow, fairly constant, and varies in the range of few nanometers.

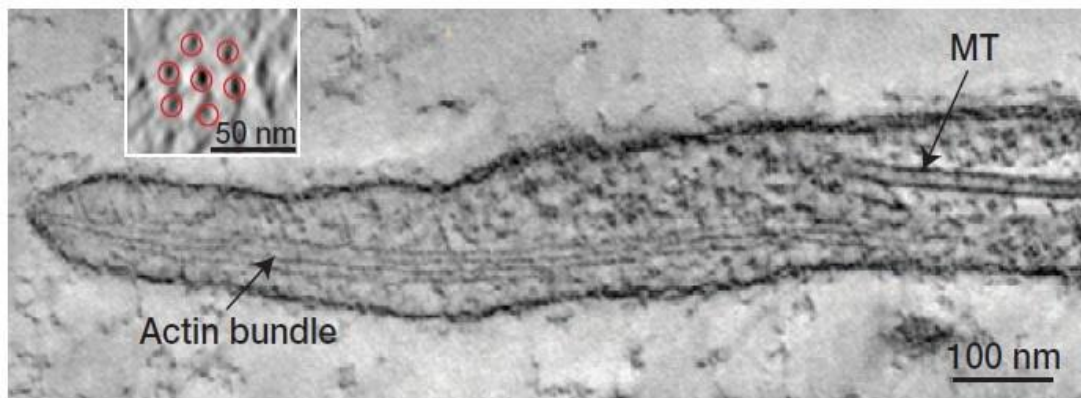


Figure 3.7: Cross-section picture of actin filament bundle. In detail, its hexagonally packed configuration. Image taken from [27].

The most accepted values for inter-filament spacing was mentioned to range from 7 to 12 nm [41]. However, filaments can be expected to be hydrated; actin molecules are polar and their charges can attract water molecules [47]. This is a chemical property of both G-actin⁹ and F-actin. In the case of actin filaments, hydration is a cellular self-regulatory process in order to compensate high osmotic stress. Once intracellular osmotic control is reestablished, filaments'

⁹ Just to mention, hydration of G-actin is also possible and plays an important role in occupying intramolecular spaces and in relation to the associated ATP (or ADP) molecule. Because hydrated G-actins are not the focus of this work, more details may be consulted at [34, 71, 93, 101], if appropriate.

hydration layers become less thick [55, 93]. This directly impacts on the structure of the filament bundles. The hydration layer increases filaments diameters, thus increasing the outflowing volume and reducing the unoccupied inter-filament spaces to likely negligible values [34, 47, 55, 72] (Figure 3.9). Depending on values of cross-linker lengths and the presence of hydration shells (or not), bundle mechanical properties may change in consequence, as bundle resistance to stress and buckling, as shown in [64].

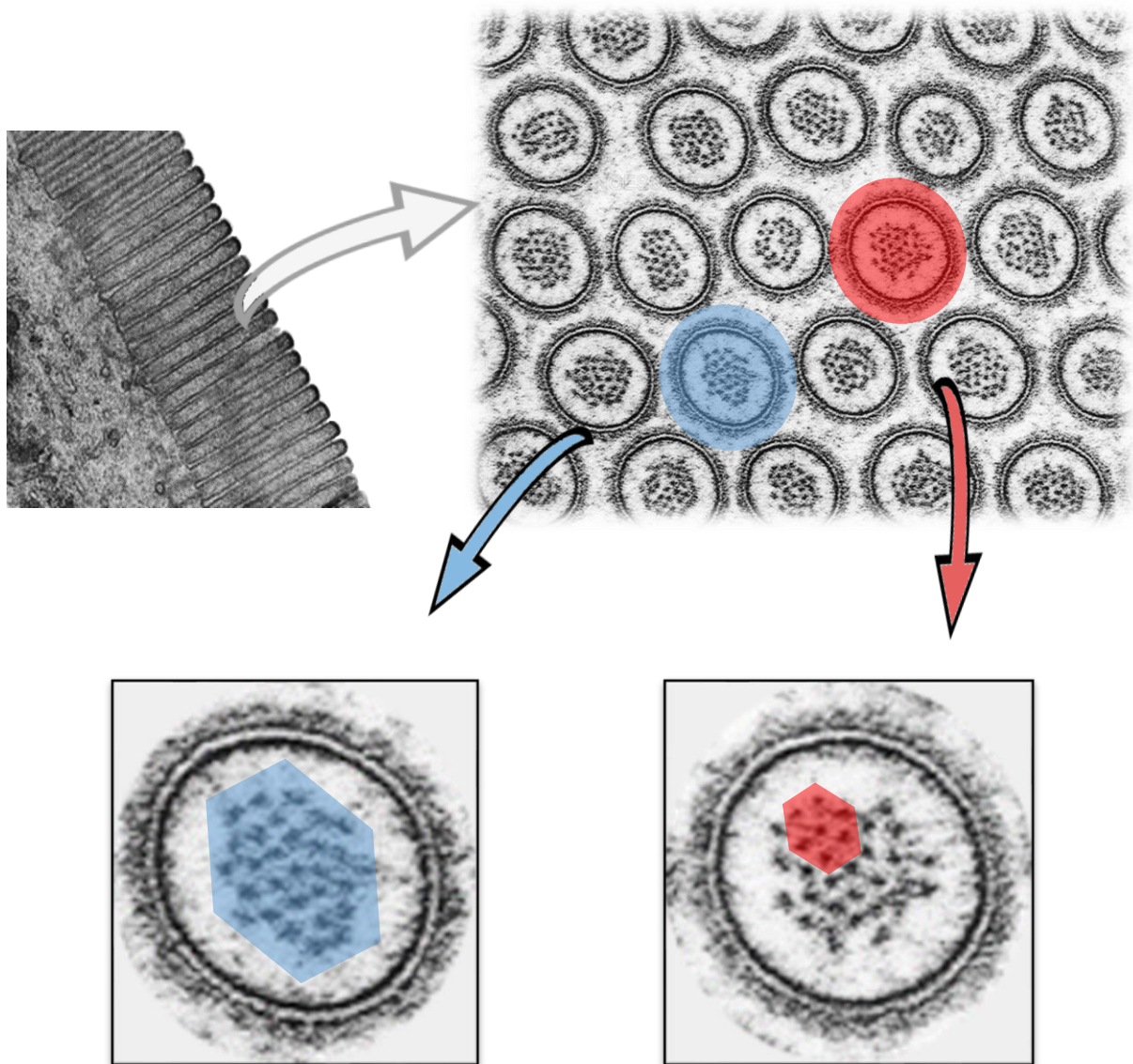


Figure 3.8: Hexagonal packing of actin filament bundle in microvilli. It is possible to observe a tendency of a global hexagon pattern formation, which is, in the entire bundle (follow the blue marks), or locally, in a part of it (follow the red marks). Image adapted from Biophoto Associates / Science Source.

Potentially free inter-filament spaces will be filled with part of the fluid contained within the filopodium. One hypothesis of this work is that such cytosol trapped in these inter-filament spaces might be taken together with the whole bundle back to the cell body. This would further contribute to the outflow volume, thus triggering a correspondingly larger compensatory inflow of matter (cytoplasm) to satisfy the mass conservation law.

To test this hypothesis, we need to calculate the flow rate of cytoplasmic fluid entering and leaving filopodium as a function of the inter-filament spaces in the possible configurations that may occur (i.e. with and without hydration). By these configurations, we mean bundles with a different number of filaments and length of cross-linkers. At this first moment, because of hexagonal filament packing in the bundle, a filopodial cross-section area is essential to identify (and quantify) spaces through the fluid can pass by, in- or outcoming from filopodium.

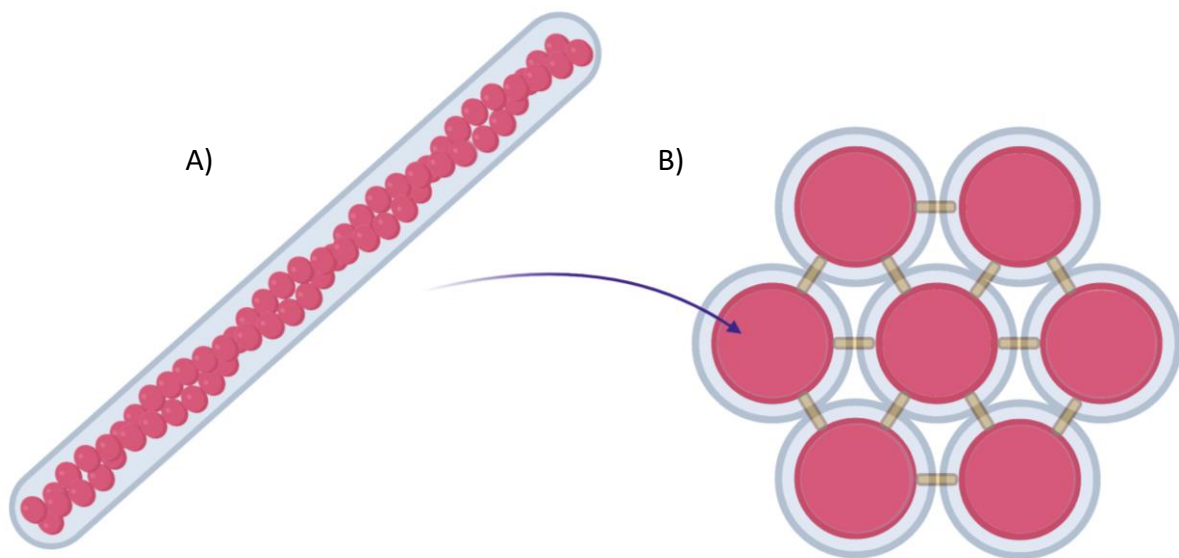


Figure 3.9: Hydration shell around actin filaments. A) Schematic representation of a single microfilament with its hydration coat, which is composed of water molecules attracted to the polar actins. B) Schematic example of a cross-linked bundle, where every microfilament and cross-linkers are surrounded by shells of hydration, filling a fraction of inter-filament spaces and increasing the filaments diameters. Notice that this may leave some spaces unfilled. Image created by the author with BioRender¹⁰.

Let us name S_{empty} the fraction of filopodial cross-section area corresponding to inter-filament spaces. Obviously, that depends on the number of filaments N and crosslinks with

¹⁰ Available at www.biorender.com

length s . Considering the data and arguments presented, we can obtain the packing density j covered by the filaments. To do this, we treat two cases for the length of the links: $s = 0$ in case of hydrated filaments, and $s > 0$ in intermediate scenarios or absence of hydration.

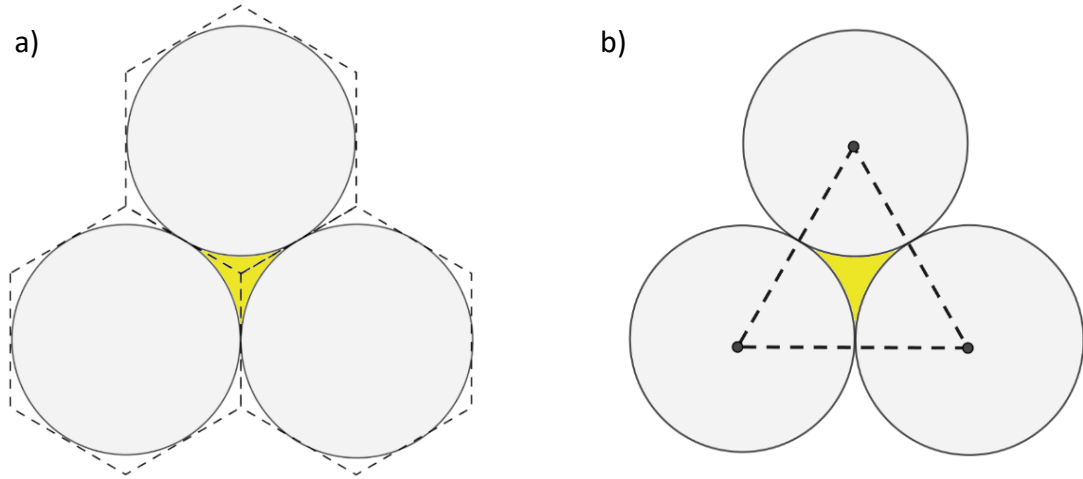


Figure 3.10: Hexagonal packing of actin filaments in presence of hydration. In a), a cross-section representation of packed hexagons surrounding filaments, and in b), approach to calculate corresponding inter-filament space. Image created by the author with Geogebra¹¹.

For $s = 0$, being S_C the total area corresponding to the circles in Figure 3.10 and S_H the total area of packed hexagons, we have:

$$S_C = 3\pi r^2 \quad (3.1)$$

$$S_H = 6r^2 \sqrt{3} \quad (3.2)$$

$$j = \frac{S_C}{S_H} = \frac{3\pi r^2}{6r^2 \sqrt{3}} = \frac{\pi}{2\sqrt{3}} \sim 0.9069 \quad (3.3)$$

In this case, density j does not depend on filament radius r or any other parameter, providing 90.69% occupancy of the packing space. It means that we have 9.31% of “empty area”, where hypothetically the fluid could flow through it.

¹¹ Available at www.geogebra.org

Since this is a very small area and our analysis is done on a molecular scale, we may wonder if it would be a feasible space where cytosol can flow. In fact, the diameter of a water molecule is 0.28 nm and it can be modeled as a massive sphere that has a cross-sectional area of 0.062 nm². Using 8 nm for actin filament diameter, this is perfectly compatible with an illustrative scenario where S_{empty} would be divided into several regions with area 7.74 nm².

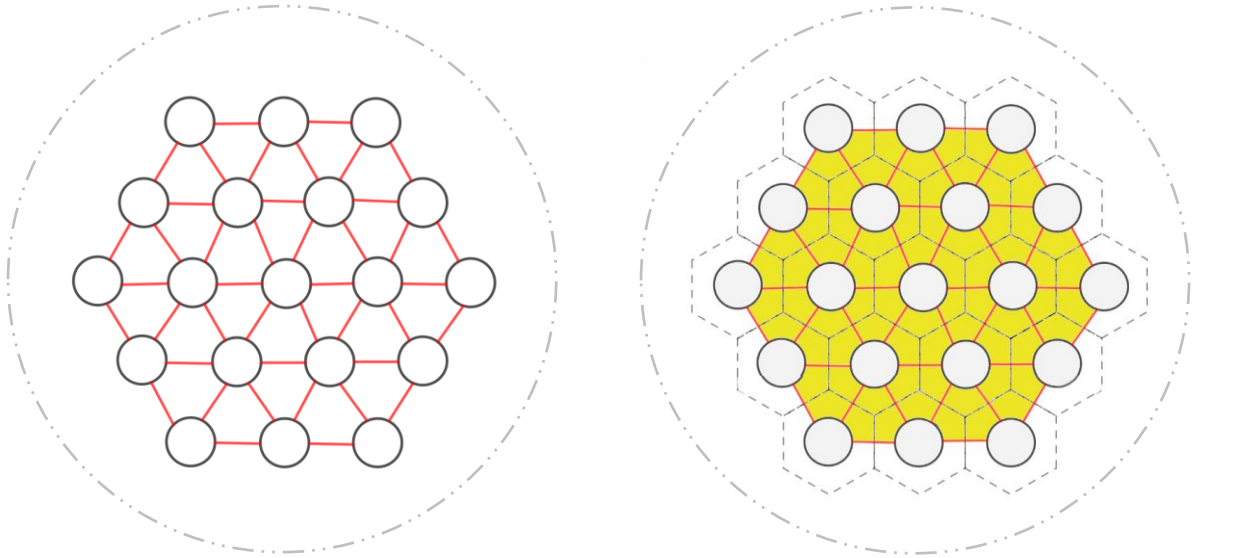


Figure 3.11: Hexagonal packing of actin filaments in absence of hydration. In a), a cross-section representation of a filopodium, with the dashed circle illustrating the plasma membrane and a centered linked filament bundle, as a geometric model for the hexagonal pattern exhibited in Figure 3.7. In b), the assumed hexagons in the packing are represented to make feasible the calculation of the total cross-sectional area considered in the model as inter-filament spaces, which is highlighted in yellow. The fraction of the packed hexagons' areas discarded is considered filled by inflow cytoplasm since it is sheltered between the most external hexagons of the packing and the membrane. Proportions are out of scale. Image created by the author with Geogebra.

For $s > 0$, that is, in intermediate hydration stages or in its absence, the parameters r and s itself must be carefully observed because their variation will directly impact all other data (Figure 3.11). So, we can say that $j = j(r, s)$ and write:

$$S_C = pr^2 \quad (3.4)$$

$$S_H = \frac{(2r + s)^2 \sqrt{3}}{2} \quad (3.5)$$

$$j = j(r, s) = \frac{S_C}{S_H} = \frac{2\sqrt{3}pr^2}{3(2r + s)^2} \quad (3.6)$$

From there, we have the percentage of regions in the hexagonal packing occupied by filaments in each case. The area of empty regions is easily obtained by doing $(1 - j)$. Then, the total cross-sectional area that represents the inter-filament spaces in a bundle of actin filaments is:

$$S_{empty} = (1 - j) \times S_H \times N - e. \quad (3.7)$$

Here we are using e to represent the fraction of this calculation regarding “free inter-filament spaces” in the bundle. These regions have their areas calculated but do not correspond to what we want. We consider that cytosol can outflow of filopodia just through the inner of the actin filaments bundle. To make it clear, let define a “bundle edge” to delimitate the region that we can consider within the bundle. That boundary joins the centers of most external assumed hexagons in the pack and it is represented by a blue line in Figure 3.12. With this said, to estimate e we observed some optimal cases of hexagonal packing of circles and the areas out of the packing edge in each case, to better fit in the biological context.

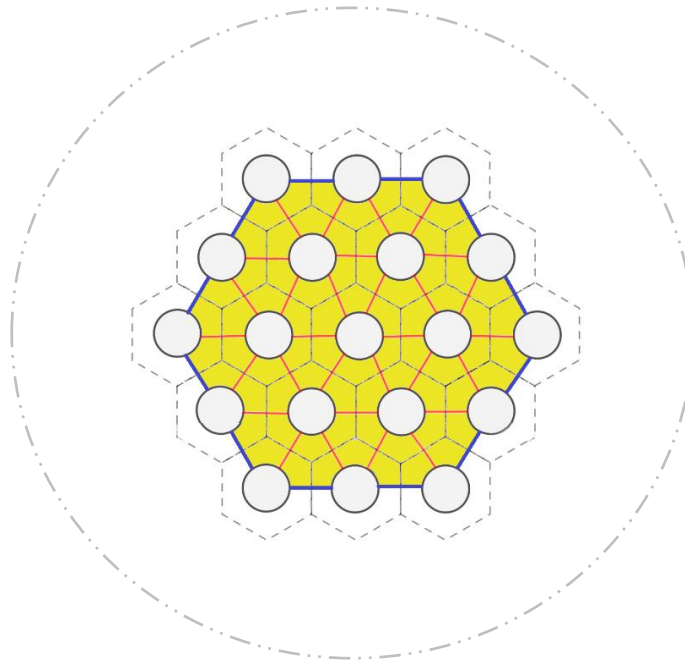


Figure 3.12: Bundle edge of an actin filaments hexagonal packing. In blue, we define a boundary which encloses the total inter-filament spacing area in a F-actin bundle, on which the cytosol is supposed to outflow. The dashed gray circle represents a cross-section of the filopodium (out of scale). The areas of hexagons out of this blue line is supposed to be part of cytosol inflowing path and it should be subtracted from total bundle inner spaces. The space between dashed circle and the blue boundary comprises the inflowing cytoplasm area. Image created by the author with Geogebra.

Since N is the number of packed hexagons, we can quote some optimal configuration:

$$\begin{aligned} N = 10 & \quad \textcircled{R} \quad e_{10} = 40\% \\ N = 19 & \quad \textcircled{R} \quad e_{19} = 30\% \\ N = 29 & \quad \textcircled{R} \quad e_{29} = 27\% \\ N = 51 & \quad \textcircled{R} \quad e_{51} = 20\% \end{aligned}$$

A weighted average between these cases can give us a good hint to obtain e . We see that, as N increases, e decreases. But in the biological scenario in question, the number of filaments in a bundle will not much exceed the greater N considered above. In effect, *in vivo*, they rarely reach such values. Then, it follows:

$$e = \frac{\sum N \times e_N}{\sum N} = 0.2544 \sim 0.25.$$

From this point onward, we will estimate that about 25% is a disposable area in the calculation of S_{empty} . In practice, we rewrite:

$$S_{empty} = 0.75 \times (1 - j) \times S_H \times N. \quad (3.8)$$

With these estimates taking place, we begin to determine areas and flow rates that correspond to incoming and outgoing of matter in the filopodium. This is fundamental to quantify the volume flux within filopodium, which causes a drop of pressure due to the volume removal in filopodial tip, thus inducing a compensatory inflow of cytoplasm as a response.

Naming S_{filop} the whole cross-sectional area of the filopodium and S_{bundle} the total area of the N -filament hexagonal packing, we can calculate the area S_{in} through cytosol can flow in direction of the tip and write:

$$S_{in} = S_{filop} - S_{bundle}, \quad (3.9)$$

or:

$$S_{in} = pR^2 - S_H N. \quad (3.10)$$

From expression (3.7), we have the following:

$$S_H N - j S_H N - e = S_{empty} . \quad (3.11)$$

Noting that $j = \frac{S_C}{S_H}$:

$$S_H N - \frac{S_C}{S_H} S_H N - e = S_{empty} . \quad (3.12)$$

Then:

$$(S_H - S_C) N - e = S_{empty} . \quad (3.13)$$

If we compute $(S_H - S_C) N - e$, we will get the empty spaces inside the “bundle edge”, as we agreed previously. That will be exactly the way through the fluid would outflow of filopodium, according to our hypothesis.

So, calling that as S_{out} , we finally have:

$$S_{out} = S_{empty} , \quad (3.14)$$

which we are able to calculate already.

Let us now make some more considerations about the fluid itself. As it was said above, the fluid we are dealing with here is a mixture composed of molecules suspended on colloidal water on a certain percentage of each part. Eventually, quantities of “solid” (molecules) and “liquid” (cytosol) substances of inflow mixture may not be the same of outflowing ones. That depends on several parameters as polymerization rate, configuration of F-actin bundle, action of ABPs, and specially velocities involved due each transport phenomena, that is, diffusion and advection, or, if it is desired, active transport by motor proteins like myosins.

Due to the principle of mass conservation, we have continuity equation for fluids, which gives that in a confined system and at a time interval Δt holds:

$$Q_{in} = Q_{out}, \quad (3.15)$$

where Q_{in} and Q_{out} are filopodial inflow and outflow rates, respectively. Then, using physical parameter collected from literature or some described in this work (Table 1), we expect to analyze the impact of fluid advection on particles motion, fluid velocities, and outflow of matter through inter-filament spacing. From this point onward, we may mention advection process as *drift* to reinforce the idea of matter dragged by the fluid. It occurs as consequence of a hydrodynamic pressure on filopodial tip or elongation, when a certain inner volume has to be filled due to the consumption of matter in the filaments plus-ends.

Since we are interested in join diffusion and advection (or drift) effects, we chose to decompose the flow speed into parts related to the contribution of each phenomenon. And it is worth noting that each kind of transport mechanism will affect each part of the mixture in a specific way. Thus, on the incoming flow velocity v_{in} there is contribution of diffusion and drift processes, with v_{dif} velocity due diffusion and v_{drift} velocity due fluid dragging.

So, inflow rate may be described as:

$$Q_{in} = S_{in} \times v_{in}, \text{ where } v_{in} = v_{dif} + v_{drift}. \quad (3.16)$$

Similarly, outflow rate will be:

$$Q_{out} = S_{out} \times v_{out}, \text{ where } v_{out} = v_{mol} + v_{cytosol}. \quad (3.17)$$

In this case, outcoming flow velocity v_{out} combines velocities of molecules v_{mol} (actins and ABPs) and $v_{cytosol}$ velocity on which the cytosol, by our hypothesis, outflow through inter-filament spaces, or trapped into hydration coats, or both. Molecules will be subjected to actin dynamics and polymerization, and because of this we make $v_{mol} = v_{ret}$ for G-actins, since its polymerization maintain F-actin retrograde flow. More accurate comments and specific assumptions about how to treat liquid part of mixture and other molecules will be addressed in following sections, which will also include calculations related to the proposed investigations.

Moreover, in simulations it was established a linear relation between r and s . Every hydration shell in F-actin polymers increases their radius in 0.3 nm, which is approximately the diameter of a water molecule. It reduces inter-filament spaces. Considering 12 nm as the

maximum value for s , and $r = 4$, we set $s = -2r + 20$. Thus, we have extreme cases $s = 0 \text{ } r = 10$ and $s = 12 \text{ } r = 4$. Even if some configuration between these is not feasible or realistic *in vivo*, it is still important to observe patterns in varying those parameters.

It should be highlighted that we only mentioned fascin molecule and used data from the literature regarding to its performance as a crosslink. It is needed to make it clear that fascin is an example of linker and this is not the only one that acts on the cytoskeleton, or particularly on filopodia context. Molecules like α -actinin, fimbrin, espin and filamin are also present in this system [45, 54, 87]. However, according to [45], fascin is emerging as a major target for cancer treatment research because of its significant role in filopodia, specifically in cell migration. In the future, if there is interest in refining the analysis of this section, the same arguments and methods can be applied in relation to data referring to other linkers.

These calculations of spatial parameters in filopodia allow us to perceive the paths by where the cytoplasm can inflow within the filopodium. This flux is induced by the generation of a negative pressure in filopodial tip as long as the fluid reorganization occurs through polymerization, where molecules and cytosol are consumed through specific dynamics. The total outflow volume (molecules and trapped cytosol) is precisely computed from the assumptions that it had just been done to provide an overview of the cytoplasmic flux within the filopodium through volumes and velocities in each model phase. Further, the model description must take into account molecular interactions and how filopodia grow as decisive information about how diffusion and drift can be associated in guiding filopodial dynamics. These topics are approached in the following sections.

3.5 Specific molecular affinities and interactions

As cited before, actin dynamics in the formation and maintenance of filopodia is regulated by physical mechanisms of transport, but also affinities and interactions between specific molecules. In this proposed model, we will therefore consider interactions displayed by profilin (P), Ena/VASP (E), actin in globular (A) or filamentous (F) states, although we must be aware that more players will have to be considered in future.

It is worth noting that the total number of molecules of each interacting species does not change. In this context, interaction does not mean that any reactant agents X and Y that have chemical affinity can generate a new product Z. This means that there is only a temporary combination of molecules, which can (and will) be undone after certain period of time.

A number of rules need to be defined:

- i.* $A + A \rightarrow AA$, actin polymerization. Actins cannot interact with each other, except during polymerization at the filament tip, when G-actin becomes F-actin in a reaction that we will denote as AA. Each new polymerized monomer causes a reorganization of the cytosolic mixture in that one monomer is discounted from the percentage of free ones, but there is no change in terms of the filopodial internal volume.
- ii.* $A + P \rightarrow AP$, G-actin sequestration reaction. Hetero-dimer AP formation holds diffusion coefficient linearly proportional to the sum of actin and profilin molecular weights.
- iii.* $E + F \rightarrow EF$, plus tip-binding of Ena/VASP. Ena/VASP binds the F-actin tip to prevent filament capping. In this position, EF reaction can occur while hetero-dimers AP are attracted to Ena/VASP enhancing actin polymerization through a catalytic process, described in reaction *iv*.
- iv.* $AP + EF \rightarrow EF + P$, Ena interaction with actin-profilin. Profilin becomes highly attracted to Ena/VASP but only if it is bound to F-actin tips. This interaction catalyzes actin polymerization. After actin polymerization, filament length increases by one subunit (represented by F), with Ena/VASP still bound to the tip, whereas profilin is released to perform new G-actin sequestration.

In the literature, some studies use rates to determine the probability of reactions to occur. For example, expressions like $P_{[XY]} = \int X(t)Y(t)k_{XY}dt$ calculate the probability $P_{[XY]}$ of a particle X react with Y, on a simulation with time step dt , with $X(t)$ and $Y(t)$ representing the amounts of particles of each type in the system, and k_{XY} is the occurrence rate between them [28]. These probabilistic expressions are called propensity functions [43, 51].

In this present work, reactions will not be done as function of a random time or defined rate. It will be subjected to proximity among particles, simulating what seems to be reasonable to happen *in vivo*; two particles with mutual chemical affinities react when they are close

enough, as in Figure 3.13. The probability of occurring such reactions will depend on the molecules' own random movement once they flow into the filopodium.

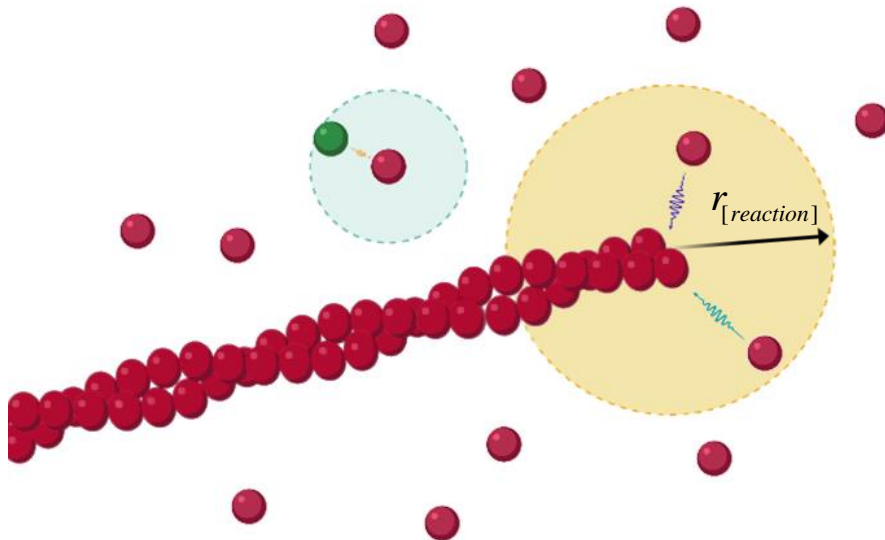


Figure 3.13: Interactions in filopodial dynamics are driven by distances. Every interacting particles in the system holds information about its chemical affinities and can react when close enough to others. It is defined specific “affinity radius” over which G-actins can be polymerized in filament plus-end or interact with ABPs following the rules described above. Image created by the author with BioRender.

As of note, the effects of temperature which are expected to alter the kinetics of particles and reactions will not be included in this model. The temperature will be assumed to be constant and stable throughout all processes. In the literature, an often used standard temperature is 25°C and the parameters used here were collected from studies that measured them under these conditions.

3.6 Filopodial elongation

Following further reports [28, 77], we use a compartmentalized domain that extends from the base of the filopodium up to its very tip. We define that a filopodium has a length $L(t) = L_c$. Although its time dependency, it is implicitly associated with the choices of N and k_{on} , and their impact on polymerization, and not only with the elapsed time. As the polymerization occurs, L_c increases and eventually displaces the membrane, a process emulated by the opening of new compartments.

The length of each compartment will be defined $h_c = 27$ nm, so that $L_c = n_c \cdot h_c$, with $n_c \in \mathbb{N}_+$ represents the number of compartments in which the domain is divided. Compartments will only be opened if all N filaments in the bundle reach the membrane, represented by the right boundary of the most advanced compartment. It simulates a limiting factor for growth, a fact predicted elsewhere [9, 28, 103]. Polymerization will occur evenly in the bundle allowing that filaments may extent up to same size, and then it can produce membrane deformation. Figure 3.14 illustrates the compartmentalized model proposed here.

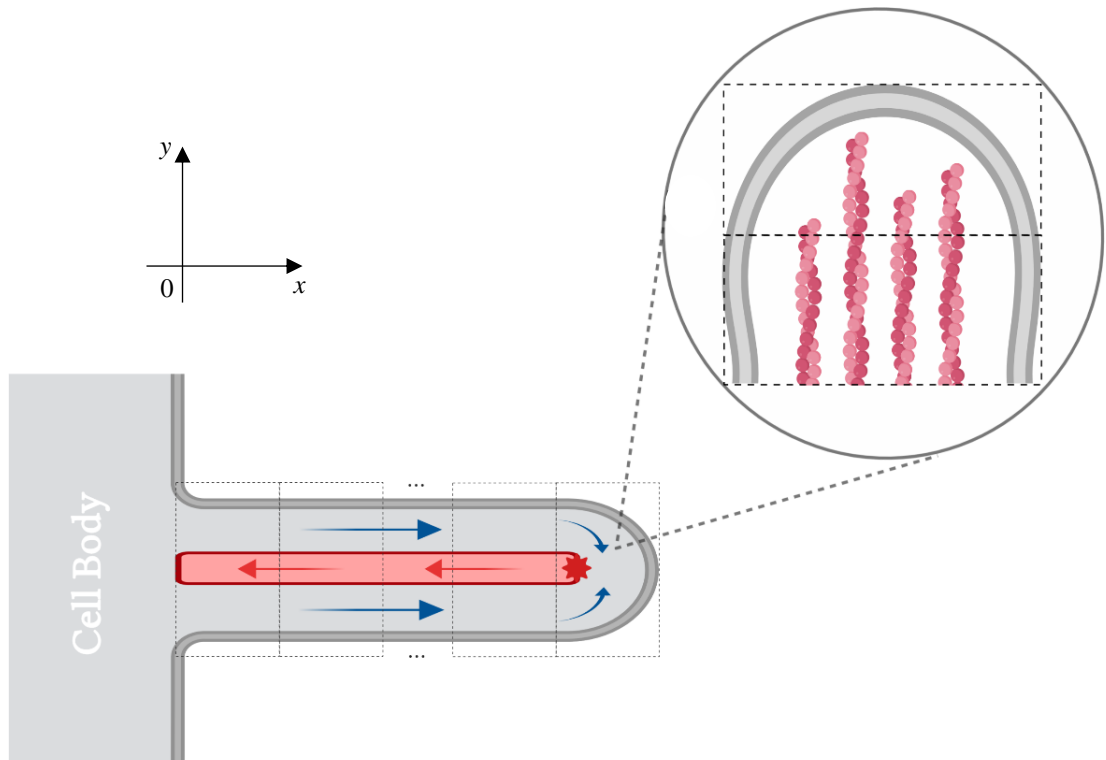


Figure 3.14: Filopodial compartmentalized model. Filopodium grows from $x = 0$ and has its length represented by a collection of compartments disposed over x -axis. Once every filament in the bundle reaches the right boundary of most advanced compartment, one more is opened so the filopodium may elongate. Image created by the author with BioRender.

We define $\delta = 2.7$ nm as the discrete fixed step on which the filament tip changes its position, that is, the contribution of a polymerized monomer in filament length. But, to the filopodial tip move forward, all filaments have to reach same size. Then, N G-actins must be equally polymerized in the N filaments for the tip to move forward. Therefore, in ten steps the tip walks a compartment length h_c , which means writing $h_c = 10\delta$. Then, defining n_p as a

dynamic count of polymerized monomers, it is possible to compute the distance l_p among F-actin bundle tip (red star in Fig. 3.14) and lower boundary of last compartment, which is:

$$l_p = \frac{n_p \cdot \delta}{2N}. \quad (3.18)$$

The bundle tip's position changes dynamically while the filopodium elongates and polymerization will always occur at some point x_p inside the last compartment. This means that x_p is separated from filopodial base a distance of $(n_c - 1)$ compartments plus l_p .

So, we can write:

$$x_p = (n_c - 1)h_c + l_p, \quad (3.19)$$

and then

$$x_p = 10 \cdot (n_c - 1)\delta + \frac{n_p \cdot \delta}{2N}. \quad (3.20)$$

3.7 Advection and its coupling with diffusion

Thus, we can start making assumptions about molecules' movement. Particles of a specie p diffuse within the growing filopodium on a continuous random walk with diffusion coefficient D_p . Despite the chaotic behavior of the motion process, there is a preference for a linear walking, but also a mechanism to make possible low and random “up and down” fluctuations in the particle's trajectory, since collisions are not explicitly simulated.

Here, as already said, particles will always move, but react just when they get close enough. It can be seen as an adaptation of the model described in [28], where each particle moves or reacts, not both, at each time step. The reactions will occur respecting parameters of chemical affinity held in every entity of the system, being particles or filaments.

So, consider a particle of type p diffusing in one dimension with diffusion coefficient D_p . According to [74], the mean time that p takes to diffuse from $x = 0$ to $x = h$ is

$$T_h|_p = \frac{h^2}{2D_p}. \quad (3.21)$$

If we compute simply $n \times T_h|_p$, with $n \in \mathbb{N}_+$, then we have the time that the same particle diffuses at a distance $l = n \cdot h$, which brings

$$T_l|_p = n \times \frac{h^2}{2D_p} = \frac{l \times h}{2D_p}. \quad (3.22)$$

From that, the average diffusion velocity $v_{dif}|_p$ of a particle p is

$$v_{dif}|_p = \frac{l}{T_l|_p} = \frac{nh}{\frac{nh^2}{2D_p}} = \frac{2D_p}{h}, \quad (3.23)$$

which will be treated as a diffusive contribution in the velocity of every particle p .

Coupled to $v_{dif}|_p$, we have the contribution of advection to the speed of particles. It is worth remembering that $v_{drift}|_p$ is closely related to the flow of volume out of the filopodium, quantified from inter-filament spacing estimate. According to [64], the drift part of G-actin flux is equal to the speed of filopodium extension, that is:

$$\frac{dL}{dt} = v_{drift}|_{actin}, \quad (3.24)$$

which in other terms can be written as:

$$v_{drift}|_{actin} = k_{on} \times d \times C(L) \times e^{\frac{\beta_{actin}}{N_0} \times \frac{L}{N_0}}. \quad (3.25)$$

This is due to the fact that membrane displacement during elongation implies an increase of internal volume that must be filled with input (and drag) of matter. Then, the right term of expression (3.25) quantifies how much filopodium dynamically increases in length, based on the number of polymerized subunits. Each molecule contributes with d in filament length. That depends on the assembly rate k_{on} , which in its turn is proportional to the local G-actin concentration.

The exponential factor is responsible for slowing protrusion rate with respect to the number N of filaments, which would require more or less polymerized monomers to grow. Important to notice that N_0 / N is also related to membrane resistance as a limiting factor of growth, since if $N_0 > N$, bundle is not enough stiff to perform mechanical effect on membrane. However, when filopodium is in a steady state (with no elongation or retraction), there is still the consumption of matter that induces an incoming flux of cytoplasm by hydrostatic pressure. For such situations, we use information about volume and speed of the outflowing matter and the inflowing flux of cytoplasm for mass conservation purposes.

Transcribing that in the notation used here, it follows:

$$v_{drift}|_p = \alpha k_{on} d C(L) e^{\frac{N_0}{N} \frac{\dot{V}}{\dot{V}_0}} + b \frac{S_{out} v_{out} \frac{\dot{V}}{\dot{V}_0}}{S_{in} \frac{\dot{V}}{\dot{V}_0}} M_p^{-1}. \quad (3.26)$$

In expression (3.26), drift by elongation and/or advection by flux are considered as possible contributions to particles' velocities. The parameters α and β are binary and used to control this process. Once there is elongation, $\alpha = 1$; otherwise, $\alpha = 0$. Also, basically $b = 1$, but we have the possibility to change it for purposes of virtual experimentation. Then, no physical effect on fluid motion will be lost. Moreover, representing molecular mass of particle p , a factor M_p was set to make speed rates proportional to particle mass. Since profilin, Ena/VASP, and actin do not have same size, it can induce different effects of the flux on each type of particle.

From that, we define

$$v_x|_p = v_{dif}|_p + v_{drift}|_p \quad (3.27)$$

in x -axis direction for every particle p .

Besides, particles may experience possible and random “up and down” fluctuations with a velocity $v_y|_p$, and then the velocity vector of particle p may be written as

$$\mathbf{v}|_p = v_x|_p \mathbf{i} + v_y|_p \mathbf{j}. \quad (3.28)$$

Every mentioned expression here was presented in their dimensionless form. Variables and parameters were properly rescaled due to compartment length and time scale involved during simulations.

So far, it has been established: means for the movement of particles, bases to justify the coupling of the described transport phenomena, foundation to calculate geometric parameters of F-actin bundle, and the systemic description of the reactions involved. Then, the construction of a mathematical formalization through a stochastic bias to describe the problem was presented and it will have its computational approach elaborated in the next chapter.

4 A NOVEL STOCHASTIC MODEL OF FILOPODIAL DYNAMICS: COMPUTATIONAL ASPECTS

In biological context, the structures involved hold fundamental properties that impact system dynamics. As examples, G-actins react with their regulating proteins following specific chemical affinities and each bond formed among them evolves according to parameters like reaction's strength and duration. Each molecule within filopodia moves driven by diffusion and drift (see Chapter 3).

Molecules' position change stochastically and influenced by eventual chemical interactions. The mechanical properties of F-actin bundle changes as its length or cross-linkage strength increases. Each filament is constituted by a number of actin monomers, whose variation change filopodial length dynamically.

To simulate all these processes, information about the entities considered should be computed, updated, and be made accessible at any time. Object Oriented Programming (OOP) is used as a computational foundation for the modeling strategy to allow the representation of any parameter. Biological structures can then be characterized as classes and their objects.

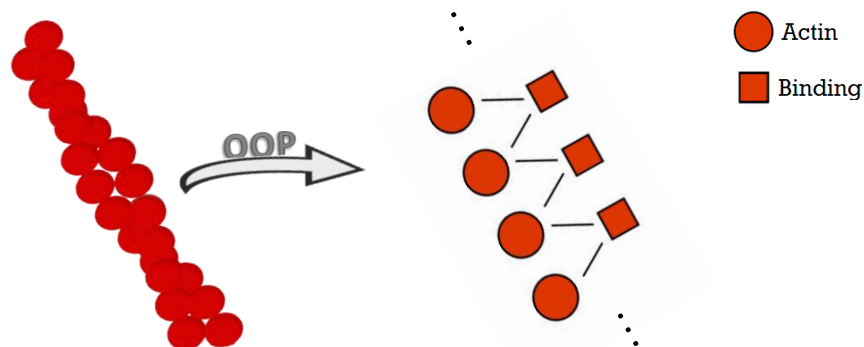


Figure 4.1: Molecules, bindings, and filaments as computational objects. The main players in filopodial dynamics should be computationally translated into data structures, with properties to store information and to update parameters after interacting with other players. Using OOP, actin filaments can be computationally represented as bipartite graphs, where each two actins are connected by a *binding object* containing physicochemical information referring to AA bonds. Image created by the author.

4.1 Computational Objects: defining the classes

The molecule class and the molecular-bond class are the two main classes here and their instances are the most fundamental players in the system. The bundle class is defined as a class

whose objects result from a reorganization of objects in the molecule class, which is caused by polymerization. F-actins also present a dynamical behavior and their computational counterparts store data about their mechanical parameters, that can be changed by physicochemical interactions. As an illustrative example, Figure 4.1 shows the representation of an actin filament by a bipartite graph composed of two types of computational objects: actin molecules and AA bonds.

In the molecules' class, we basically have three objects: Actin, Profilin and Ena/VASP. This can be changed if we want to include other proteins in the system. Each particle memorizes their own position, updated at each time step. There is also a counter to control how many molecules of each type are present in the simulation. Finally, the attribute *status* is used to inform if a particle is bound to another ('off') or free to react ('on'). Binding follows previously specified rules (related to their chemical affinities). Attributes such as shape, volume, speed, polarity, ATP/ADP regulation, among others may be included in the future to further refine the model. The class description in (pseudo) code (1) is:

Code (1):

```
class Molecules (name, pos_x, pos_y, number):
    mol.name = {Actin, Profilin, Ena/VASP}
    mol.position = [mol.pos_x; mol.pos_y]
    mol.name.num = number
    mol.status = 'on'
```

Objects of the *binding-class* are formed depending on which particles are involved. Free G-actins can be sequestered by profilin (AP); in that case, actin-profilin complexes that move near to the filament tip become highly attracted to any Ena/VASP present at the bundle tip. This configuration favors actin polymerization (AE then AA) through a catalytic reaction. When polymerized, we have *actin.status* = 'off '. In general, we can say that when *mol.status* is 'off ' for some particle its *bind.status* is 'active'.

We must remember that AA can only occur in the filament, since the free monomers have no affinity with each other. Also, there is a counter to control how many bonds of each type are present in the simulation. It is important to note that the binding-class objects have no position, no shape, and no volume. They are essentially a data structure to store information about the rules that govern how two interacting molecules ('mol_1' and 'mol_2' in code (2)) remain bonded. See the class description in the code (2) ahead.

Code (2):

```
class Bindings (mol_1, mol_2, name, number):
    bind.name = {AA, AE, AP, PE}
    bind.name.num = number
    bind.status = 'inactive'
```

When an actin monomer is polymerized, two objects are inserted in a filament: the monomer and an AA bond. So, F-actins are structured by bipartite graphs for containing these objects. A representative scheme can be seen in Figure 4.1. Those graphs are objects themselves in a class named *Bundle*, with a number N of filaments limited by the cited range in Table 1. The length L of the filopodium is computed considering elongation/retraction or being set as constant if we want to simulate steady state as a default configuration.

Filaments in the bundle are labeled from 1 to N . It is important to mention that L is increased just when all filaments have reached same length, what means that polymerization occurs equally over the N filament tips. Attributes such as polarity, bending, strength, stability, relation with links, etc. can be included to further refine the model. See the class description in code (3).

Code (3):

```
class Bundle (number):
    fil.length = 0
    fil.data = [ ]
    fil.num = number
```

The classes that refer to particles have methods to guide their objects within the dynamics or are used to obtain (or update) their parameters and properties. For example, the determination of a molecule position depends on a programming routine to simulate its movement. Also, the creation of *binding objects* is directly related to the proximity of two molecules with mutual affinity.

Polymerization and depolymerization are computationally simulated by inserting or removing data in filament-objects corresponding graphs as illustrated in the codes below. For instance, the code (4) shows that polymerization of one subunit increases F-actin length in 2.7

nm. In the other hand, depolymerization occurs as a function of the simulation time steps, whose rate is $k_{off} = 1$ subunit/step on a set of N_{step} filaments, what can be seen in code (5).

Code (4):

```
def insert (molecule, number):
    In fil.num == number:
        fil.append (molecule)
        fil.append (binding)
        fil.length = fil.length + 2.7          # in nanometers
        fil.num = fil.num + 1
```

Code (5):

```
def remove (number):
    In fil.num == number:
        fil.length = fil.length - 2.7          # in nanometers
        fil.num = fil.num - 1
        fil.data.pop (last_actin)
```

Notice that in each function above, the processes are performed on each filament of the bundle, since the command is made by identifying the filament number, described in the line “*In fil.num == number*”. Then, filament length and its number of subunits are updated, which is needed since we defined that the bundle only increases in size when each filament reaches the same length. For this, in the case of polymerization, the adding of particles is automatically directed to filaments that have not yet undergone polymerization in that time step, so that all filaments can grow equally and the bundle elongates. In case of depolymerization, N_{step} is accumulative and control an equally removal of particles in all filaments. Once we have $N_{step} = N$, the bundle retracts.

This representative scheme in Figure 4.2 illustrates in a simplified way the main interactions between the modeled phenomenological objects. The stochastic aspect of simulations is assured by particles motion towards filopodial tip and fluid reorganization as posed in Chapter 3. In Figure 4.2, circles were used to designate particles (color description follows in the figure caption) and squares represent the specific reactions formed between any two molecules.

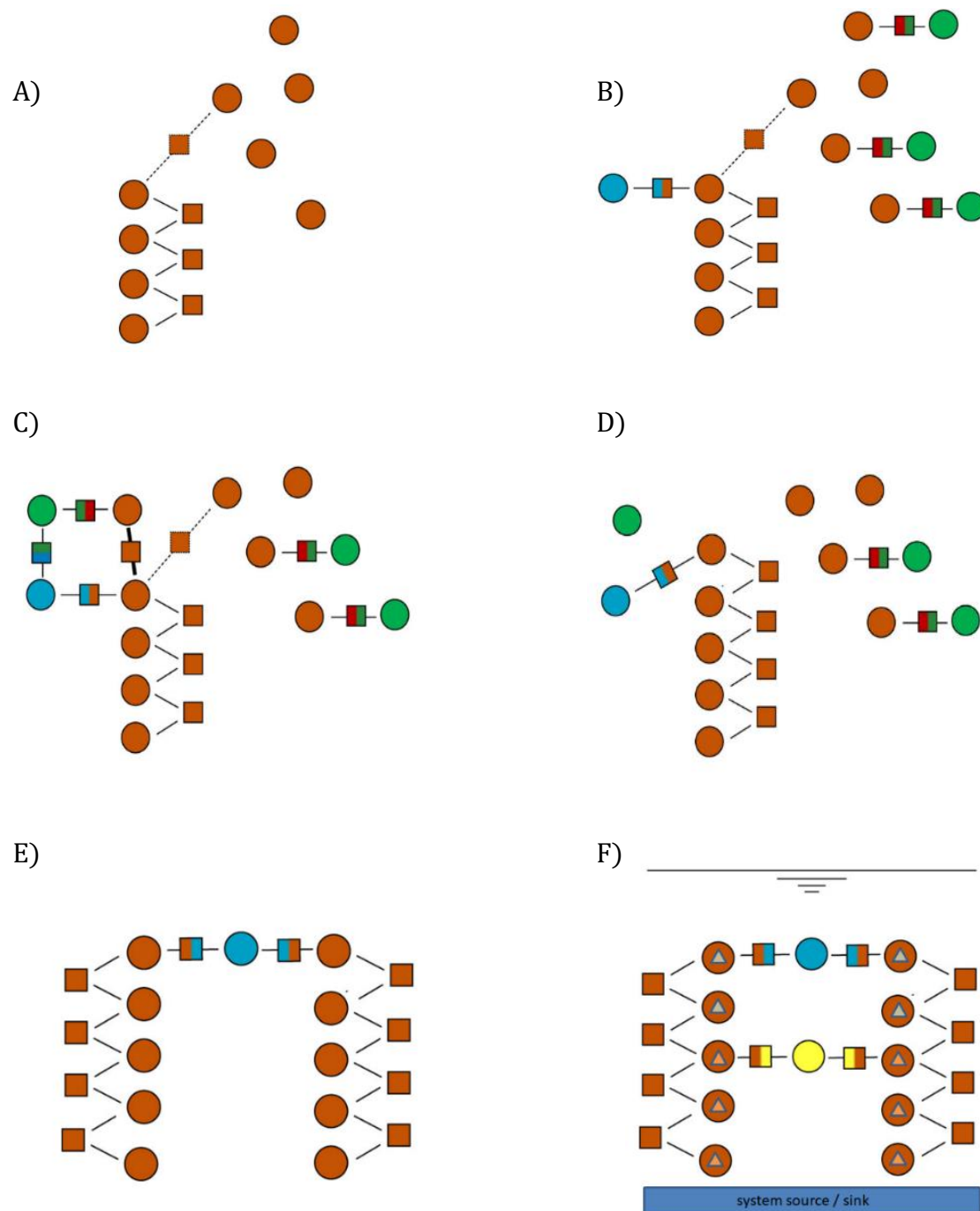


Figure 4.2: OOP scheme of actin dynamics in filopodia. (A) G-actins (orange) have attraction to F-actin tip; (B) Ena/VASP (blue) binds F-actin tip to prevent capping, while G-actins are sequestered by profilin (green); (C) as hetero-dimer, profilin has high affinity for Ena/VASP at the tip, promoting G-actin polymerization through a catalytic process; (D) Once G-actin is polymerized, Ena/VASP jumps to the new F-actin at the tip and profilin is released; (E) Ena/VASP also has a role in bundling filament tips; (F) Fascin (yellow) as cross-links actin filaments away from the tip, and ATP-Actin (circle with grey triangle) becomes ADP-Actin (circle with pink triangle); the bundle produces force against the membrane so that filament treadmilling occurs. Images kindly provided by A. Prokop.

4.2 Modeling filopodial geometry

The domain is two-dimensional and simulates the interior of a filopodium. We fix the origin of the coordinate system on the lower limit of the protrusion leading edge, which makes the whole domain to appear in the first quadrant. Here, the radius of a filopodium is $R = 100$ nm is displayed on the y -axis. The x -axis displays the length of filopodium, which varies with time due to elongation of the microfilament bundle. Once the filament bundle reaches a certain length, the membrane moves opening enough space for the polymerization to continue.

This strategy adapts the idea of a compartmentalized domain [77] and the filament-membrane interaction described elsewhere [28]. However, the procedures here differ considerably from the mentioned work to make the modeling as authentic as possible. We emphasize that the bundle pushes the membrane only when $N \geq N_0 = 13$ filaments, as cited in Table 1. Mechanically, $N > N_0$ implies that the bundle can elongate the filopodia even in curve when the filaments located in a sector of the bundle grow faster than the rest. This possibility will not be addressed in this work and the bundle growth performs just linear elongation.

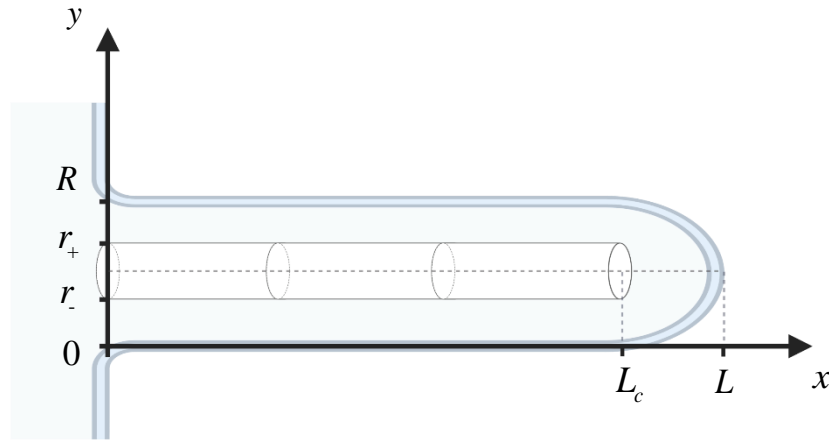


Figure 4.3: A geometric representation of the modeled domain. Image created by the author with BioRender.

Fluid enters the filopodium in the region $x = 0$ and $y \in [0, r_-) \cup (r_+, R]$, with a constant concentration C_0 . The region $[0, L_c] \times [r_-, r_+]$ represents the microfilament bundle, whereby the reorganized fluid outflows from the filopodium. In practice, while the first mentioned region acts as a source of inflowing cytoplasm, the filament bundle is treated as a sink with borders $y = r_-$ and $y = r_+$, which prevents the entry of volume between them. However, it follows the

attributes kept by each filament modeled using OOP, which allows to compute the individual filament lengths or any physical parameters of interest. Figure 4.3 brings an illustrative scheme of the modeled domain.

A comprehensive theory for shapes of membrane protrusions is still lacking [69]. So, we considered filopodial tips as a semi-sphere (or semi-circle, in our 2D model) with a reflective boundary condition, as Figure 4.4 shows. If a particle is not captured by a polymerization site and hits the curved membrane at the tip, it will be pushed back into the mainstream so it may be subjected to continue its dynamics. In the membrane-particle collision, we choose to set a loss of 20% of kinetic energy, which alters velocity and trajectory of that rebound particle. It is an estimate based on data about coefficients of restitution in collisions [92].

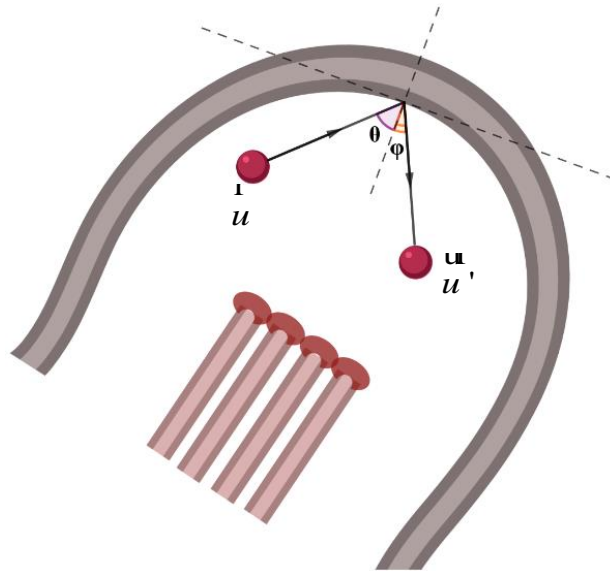


Figure 4.4: Boundary condition for membranes in filopodial tip. Image created by the author with BioRender.

This loss is computed as follows. Let's consider that a particle is travelling with velocity $\vec{u} = (u_x, u_y)$. Once kinetic energy decreases in 20%, its speed after hitting membrane would be

$$\vec{u}' = (u'_x, u'_y) \text{ with } |\vec{u}'| = \frac{2}{\sqrt{5}}|\vec{u}| \quad (4.1)$$

reflected over an angle φ of

$$\varphi = \arccos \frac{|\vec{u}'| \cos \theta}{|\vec{u}|} \quad (4.2)$$

The lateral surface of the cylinders which delimits the filopodium and filament bundle will be considered impermeable and frictionless with a *no-slip* boundary condition [84]. Although it is not known if in a real scenario there could be interaction between flows in opposite directions, causing turbulence or changes in both flow velocities. Then, this possibility will not be treated here, and the filament bundle will be imagined as a tube without interaction with the environment.

The filament bundle acts as a sink and mass conservation is fully satisfied. To clarify the balance, we need to understand how the phase fluid transition occurs at the polymerization site. Several physical factors (N , L , k_{on} , C , and ABPs) impact polymerization. Note that we have more information about the withdrawal of monomers by the retrograde flow of F-actins than the outflow of cytosol, which establishes a flow of unknown speed profile. This is a point that we should use the model to generate data.

To model polymerization, the reactions AA and EP will be promoted at a region of attraction Ω_p at the tip of the bundle, which directly add subunits of G-actin to some microfilament. We propose that the law of electrostatic attraction is obeyed inside Ω_p . These forces will act on the cross-section that contains the tip of the bundle tube and a semicircular area facing forward to it. Figure 4.5 gives an idea of how Ω_p (in light blue) will be located, highlighting that attraction force will not be equally exerted in all of its points.

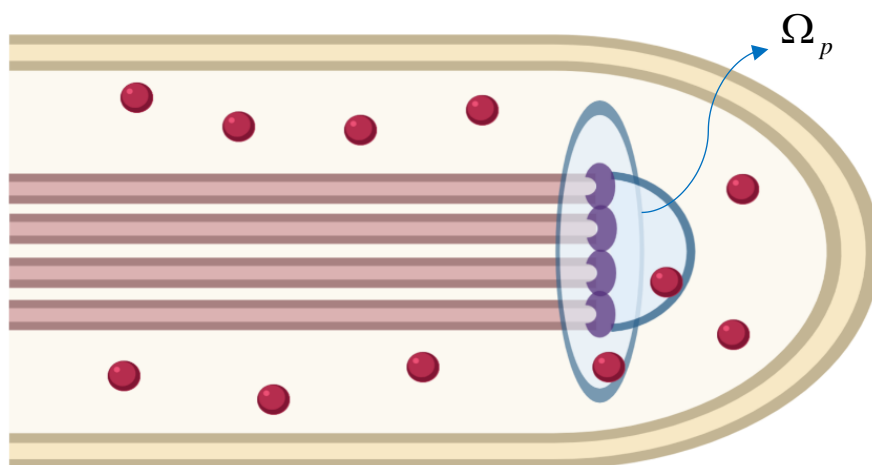


Figure 4.5: Region of attraction to polymerization. Image created by the author with BioRender.

4.3 Computational model for stochastic filopodial dynamics

The code (6) below indicates all procedures described in previous sections and shows the sequence of computational processes in simulations. Initially, classes and objects are instantiated with respective attributes and relevant methods. Once executing the program, the function “*Initialize classes*” indicates an initial construction of the most basic data structures that will serve to store objects. Two lists are created: one to record all the molecules in the system (inserted by “*Create molecules*” procedure); another to store information of each filament in the bundle.

Code (6):

Program “*Actin dynamics in filopodia*”

```

    Initialize classes;
    Set geometry;
    Set inputs;
    while (not final time):
        Create molecules;
        Brownian motion (particles);
        Search for reactions in domain;
            Polymerization (particles in the last compartment);
        Compute outflow cytosol volume;
        Update membrane;
        Check mass conservation;
    End of while;
    Obtaining data;
End of program.

```

Steps “*Set geometry*” and “*Set inputs*” build the computational domain and initial fluid configuration. Mixture composition, boundary conditions, and initial values for mechanical and physicochemical parameters are defined in these steps. Initial calculations about cross-section areas according to filopodial geometric configuration are also done here, as well as the input of simulation parameters. The user can choose to input data (as N , k_{on} , or inter-filament spacing) or any aspect of the system to perform tests on specific applications.

We consider $\Delta t = 10^{-4}$ sec in all simulations, a time step small enough to contemplate all possible chemical and diffusion phenomena, the simulation time run up to a previously defined final time $t_s = t_{final}$. In each step, a certain amount of molecules stochastically distributed flow towards the tip of filopodium from the source ($x = 0$), ruled by a random walk and interact if they are close enough (which was described in Chapter 3). In the last compartment, beyond usual interactions between particles, polymerization may occur.

Polymerization is modeled by the procedure in code 7 below:

Code (7):

```

Function "Polymerization";
    for 'G-actins' in last compartment:
        Check if any G-actin should be polymerized
        if 'yes':
            Change position of filament[N]'s tip
            Insert (molecule, number):
                actin.position = [actin.new_pos_x, actin.new_pos_y]
                actin.status = 'off'
        End of if;
    End of for;
End of function.

```

Notice that fluid is composed by “molecular part” and “colloidal water part”. These volumes are quantified separated and in total, controlling how much colloidal water outflows from filopodium with respect to F-actin treadmilling. “*Compute outflow cytosol volume*” generates a drop of hydrostatic pressure in the tip of the filopodium which drifts the fluid to compensate the cytosol volume removal. After that, if needed, another compartment can be opened in “*Update membrane*”, always obeying mass conservation.

The codes were implemented in Python language through Spyder developing environment. The computational resource used to run the simulations was a laptop with Intel Core i5, 8 Gb RAM, 1 Tb HD, and operational system Microsoft Windows 10. With this infrastructure, the developed model, and highlighted concepts, we proceed to the simulation of filopodial dynamics, approaching fundamental aspects of it, whose results can be seen in the chapter that follows.

5 RESULTS AND DISCUSSION

The sections in this chapter present virtual experimentations that reflect pertinent aspects of the filopodial dynamics. These experiments throw light on the physical phenomenology related to G-actin transport and provide important biological knowledge. Experiments and model validation are performed by varying a set of relevant parameters to observe variations in the resulting dynamics.

As our main result we recall that, in contrast with previous models in the literature, the model formulated here is able to represent filopodial elongation up to 40 μm of length, which is 20 times longer than certain results based only on diffusion (see Section 5.1.2). Nevertheless, this value is limited exclusively by computational cost and the model has potential to simulate even longer filopodia. Figure 5.1 illustrates briefly the relation of stationary lengths of the developed filopodia (lengths at the end of simulations) with a set of parameters whose values are strongly affected by computational cost. Relations between filopodial elongation and those parameters is schematically shown in Figure 5.2.

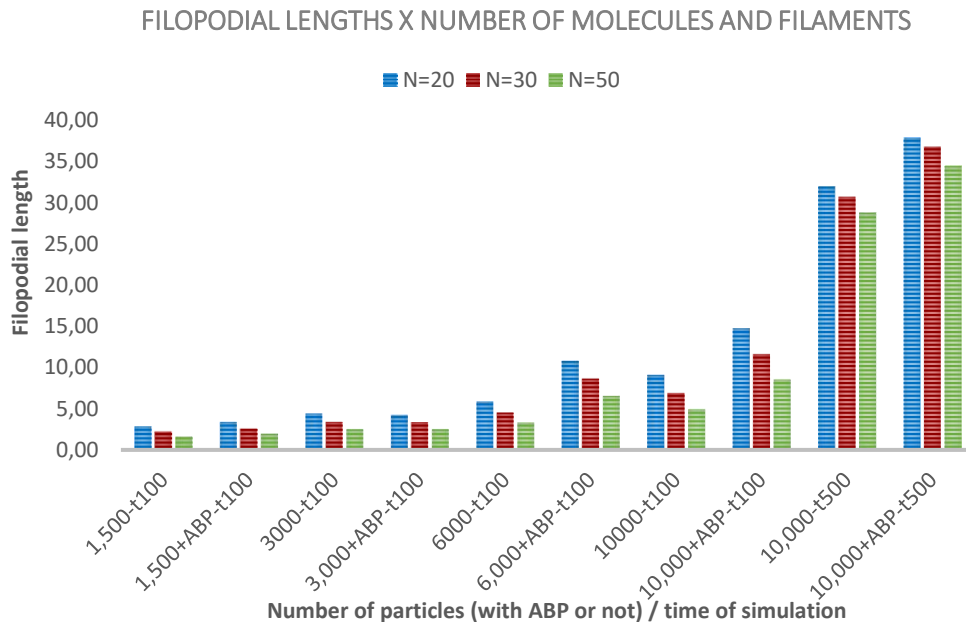


Figure 5.1: Reachable filopodial final lengths. As long as more molecules are interacting in the system $N_p = \{1500, 3000, 6000, 10000\}$, with (or not) presence of ABPs, and over certain ranges of simulation time $t_s = \{100, 500\}$, the developed filopodia may reach final lengths L of almost 40 μm . Besides, the model is capable to grow longer filopodia. The results of this chapter must be interpreted considering the computational processing cost as a limiting factor.

Moreover, results in Figure 5.1 present important analogy with cell biology. There is a biological foundation to explain why filopodia exhibit a lower efficiency of growth when the values of N grow in each set of parameters. Namely, the number of G-actins in the cell is limited or not replaced fast enough [64]. The limitation of molecules in the biological system (and in its model) is more than a technical issue. It is the right direction to represent what happens *in vivo*.

The model formulation integrates a coupling of physically-mediated and biologically-mediated processes related to G-actin transport which is fundamental to explore mechanical effects supporting filopodial dynamics. The model mimics processes that enhance filopodial growth rate. It allows us to inquire how specific parameters impact the filopodial dynamics. For instance, how does filopodium length L react when the number of filaments N in the bundle is increased? How does inter-filament spacing s impact filopodium growth? Does the amount of particles N_p alter significantly the filopodium length? How does each physical mechanism of transport contribute to particles movement? Is the total time of observation t_s relevant? A schematic illustration of filopodial elongation and all these parameters is presented in Figure 5.2.

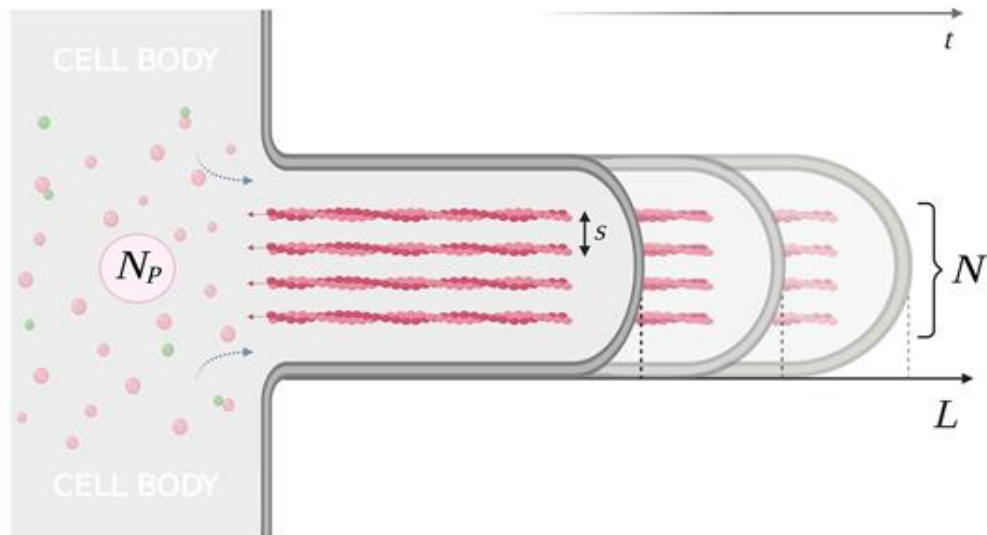


Figure 5.2: Standard simulation scheme. The proposed computational model simulates an inflow of cytoplasm (grey dashed arrows) with a total number of particles in the system N_p , which are reorganized into a bundle of N filaments through polymerization with a consequent treadmill-like outflow of actins and trapped cytosol within inter-filament spaces measuring s (red arrows). Analyzing different scenarios by varying these parameters, it is intended to establish relations between length L with N , s , and N_p , over a time t .

These coupled processes are analyzed in the following sub-sections to show what can be learned from virtual experiments. Each represented process provides a perspective of some aspects of the filopodial dynamics. We investigate how molecules' displacement, e.g. G-actin transport, is impacted by diffusion, cytoplasmic flow, and biological regulation. Figure 5.3 summarizes how this investigation will be performed and how the sub-sections are organized. It includes also information about the parameters variations considered. This plan results in biological knowledge, in the model validation, and leads to the formulation of additional hypotheses. Moreover, these virtual experiments provide evidence of the importance of cytosol flow in filopodial dynamics.

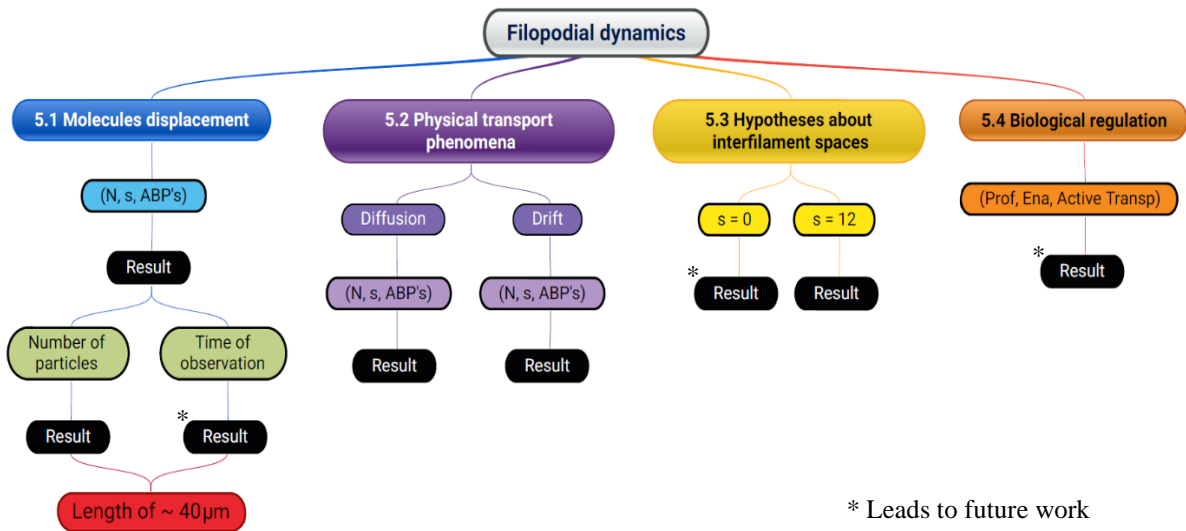


Figure 5.3: Roadmap of the particle-based computational model for filopodial dynamics and its main simulated aspects. Molecules' displacement, physical transport phenomena (diffusion and drift), extreme cases of hydration (the lowest and the highest considered values for inter-filament spacing), and biological regulations (by profilins, Ena/VASP, or motors) runs in parallel for a proper simulation of the filopodial dynamics.

At first, the displacement of particles within filopodial tube is set up as a fundamental platform to evaluate the G-actin monomers delivery to polymerization. We analyzed how the transport of monomers is impacted by varying the number of filaments in the bundle, the spacing between the filaments, the presence (or not) of ABPs, the number of particles, and the time of observation, affecting filopodial growth as a consequence. It is done gradually to have separated views of each parameter influence and, in a second moment, a perspective of the

dynamics in an integrated way, gaining knowledge from each virtual experiment. This is presented in Section 5.1 and identified in the blue branch in Figure 5.3.

To better understand how molecules are driven towards filopodial tip, we observe the contribution of diffusion and cytosol flow to molecules' velocities. This inquire also considers the variation of the quoted parameters to examine molecules displacement. In both investigations, ABP-mediation runs in parallel to complement the physically-mediated processes in a proper representation of the G-actin transport in filopodia. This is presented in Section 5.2 and identified in the purple branch in Figure 5.3.

The relations between flow rate and fluid volume are inspected in two hypothetical cases of inter-filament spacing: total hydration (i.e. $s = 0$) and no hydration layers whatsoever ($s = 12$). These experiments are detailed in Sections 5.3 and identified in the yellow branch in Figure 5.3. It shows a versatility of this computational model to explore the feasibility of specific propositions. At least, the model is used to answer how filopodial dynamics reacts to each regulatory protein and active transport by motors, which has been investigated elsewhere [5, 7, 41, 74, 81, 103] instead considering solely diffusion.

5.1 Filopodial growth and bundle configuration

In cytoskeletal dynamics, filopodium grows long enough so that diffusion becomes a limiting factor on which particles' velocities decreases [77]. As hypotheses, cytoplasm flow and/or active transport by motors may have relevant contribution in particles displacement to complement diffusion as coupled transport phenomena, supplying polymerization and sustaining filopodial growth.

Let us consider an incompressible mixture fluid occupying the domain. The described methods to quantify inflow and outflow volumes (in Chapter 3) ensure mass conservation in both phases. To make it clear, when it is mentioned *inflow volume*, it means cytosol and suspended particles; by *outflow volume*, we must understand filaments (with hydration layers or not) and the amount of trapped cytosol within the bundle spaces.

The fluid velocity within filopodium is defined by the movement of the particles. Since the inflow cytoplasm suffers effects of the physical transport phenomena and biological regulation, we consider that cytoplasm displacement does not differ much from the G-actin traffic. Computationally, these volumes are calculated at both phases, but the fluid is visualized just as an amount of moving particles since they have the same velocity as the fluid. Speed

variations are expected only for ABPs or hetero-dimers AP, once diffusion coefficients are weighted by their molecular masses. Once ABPs are within the domain, their steps of movement must be proportionally greater.

Moreover, *in vivo* microfilaments are kept together by cross-linking molecules, which we might wonder if they can act as barriers to the outflow fluid changing directions, pressure, or flow speed rates within the bundle spaces. But, as bindings between linkers and filaments are highly dynamic, they were not simulated. In this work, any flow within filopodia will be considered as laminar.

5.1.1 Inter-filament spacing slightly enhances filopodial growth

A sample of values for $N = \{20, 30, 50\}$ was chosen to estimate the variation of the filopodial length L (in micrometers) when inter-filament spacing is changed from $s = 0$ to $s = 12$ (in nanometers). Two fundamental scenarios have been considered: first, the fluid mixture contains only G-actins; second, actin monomers are regulated by ABPs. At this point, active transport is not involved. Its effect will be covered in Section 5.4.

Figures 5.4 to 5.6 show the distributions of 1500 G-actin particles at the end of a default time of observation $t_s = 100$. The distributed particles in red refer to moving G-actins. The domain represents a filopodial tube with length in micrometers and diameter in nanometers. F-actin bundle has N filaments computed individually, but it is embodied on a black rod reflecting the bundle actual length. The axes are not in their natural ratios.

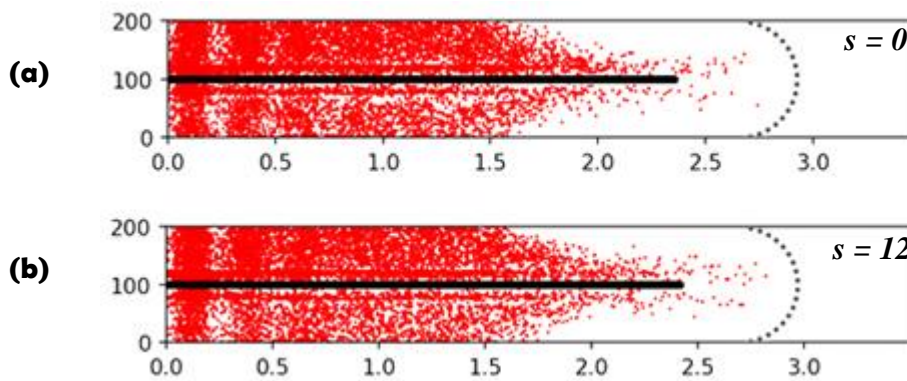


Figure 5.4: G-actins distribution with $N = 20$ and 1500 particles. In a) for $s = 0$, filopodial length reaches $L = 2.86 \text{ mm}$; in b) for $s = 12$, filopodial length reaches $L = 2.91 \text{ mm}$. The increase of s produced 1.75% of increase in L .

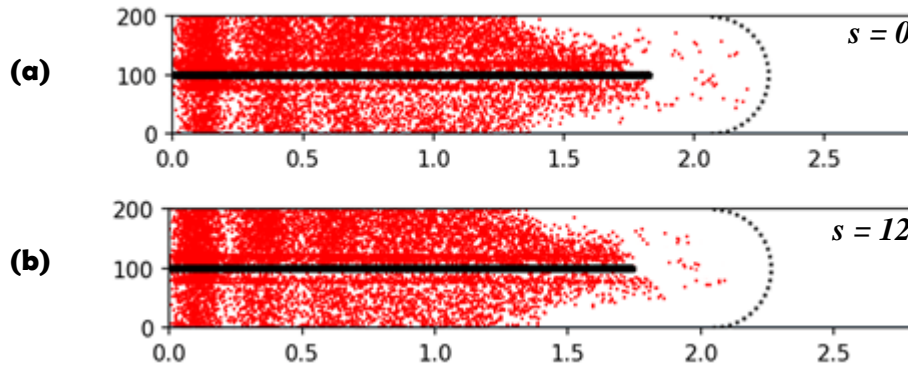


Figure 5.5: G-actins distribution with $N = 30$ and 1500 particles. In a) for $s = 0$, filopodial length reaches $L = 2.23 \text{ nm}$; in b) for $s = 12$, filopodial length reaches $L = 2.26 \text{ nm}$. The increase of s produced 1.34% of increase in L .

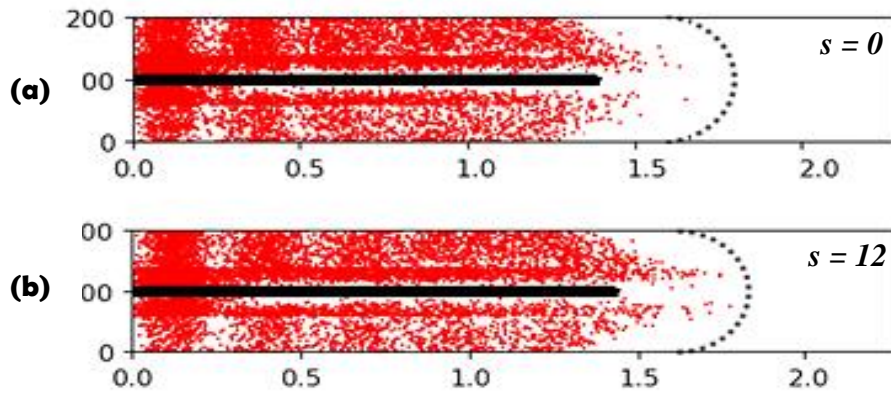


Figure 5.6: G-actins distribution with $N = 50$ and 1500 particles. In a) for $s = 0$, filopodial length reaches $L = 1.59 \text{ nm}$; in b) for $s = 12$, length reaches $L = 1.61 \text{ nm}$. The increase of s produced 1.26% of increase in L .

A first observation is that as higher N becomes, length L reaches shorter final values at both considered cases of inter-filament spacing s . This makes sense since more actin monomers have to be polymerized for the bundle to grow, shortening the final length L . This is in agreement with [64], which shows that higher values for N with lower s confers more mechanical efficiency and structural stability to filopodia, but filopodial length L has the tendency to be smaller as N increases.

In regard to inter-filament spacing s , all the scenarios present an increase in the length L when the inter-filament space value changes from $s = 0$ to $s = 12$. This indicates a mechanical relation between the bundle configuration and filopodial growth. To investigate this property, more parameters should be tested such as the number of moving particles. For 3000 particles in

the domain, the distribution of actin monomers at the end of simulations are shown in the Figures 5.7 to 5.9, for each chosen value of N :

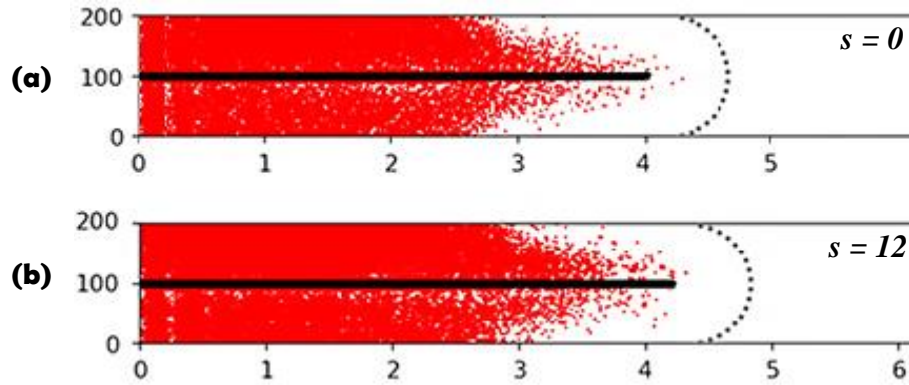


Figure 5.7: G-actins distribution with $N = 20$ and 3000 particles. In a) for $s = 0$, filopodial length reaches $L = 4.40 \text{ nm}$; in b) for $s = 12$, filopodial length reaches $L = 4.47 \text{ nm}$. The increase of s produced 1.59% of increase in L .

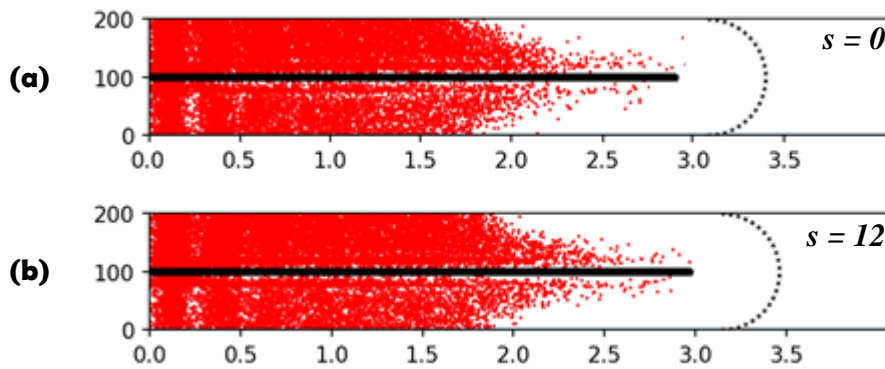


Figure 5.8: G-actins distribution with $N = 30$ and 3000 particles. In a) for $s = 0$, filopodial length reaches $L = 3.40 \text{ nm}$; in b) for $s = 12$, filopodial length reaches $L = 3.47 \text{ nm}$. The increase of s produced 2.06% of increase in L .

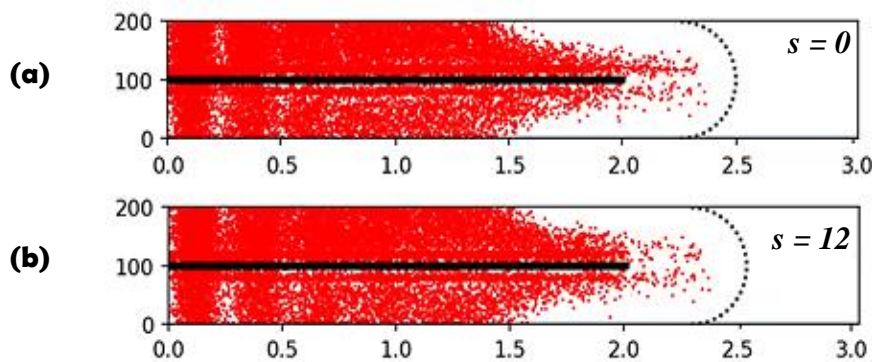


Figure 5.9: G-actins distribution with $N = 50$ and 3000 particles. In a) for $s = 0$, filopodial length reaches $L = 2.50 \text{ nm}$; in b) for $s = 12$, filopodial length reaches $L = 2.54 \text{ nm}$. The increase in s produces 1.60% of increase in L .

Table 2 summarizes lengths and their variation on each previously evaluated case. Figure 5.10 shows a comparison of all distributions in Table 2.

Table 2: Variation of L as function of s . Calculation done in each case were $\frac{L_{s=12} - L_{s=0}}{L_{s=0}} \times 100$.

Only G-actins				
$N_{\text{particles}}$	Length (in μm)	$N = 20$	$N = 30$	$N = 50$
1500	L for $s = 0$	2.86	2.23	1.59
	L for $s = 12$	2.91	2.26	1.61
	Variation	1.75 %	1.34 %	1.26 %
3000	L for $s = 0$	4.40	3.40	2.50
	L for $s = 12$	4.47	3.47	2.54
	Variation	1.59 %	2.06 %	1.60 %

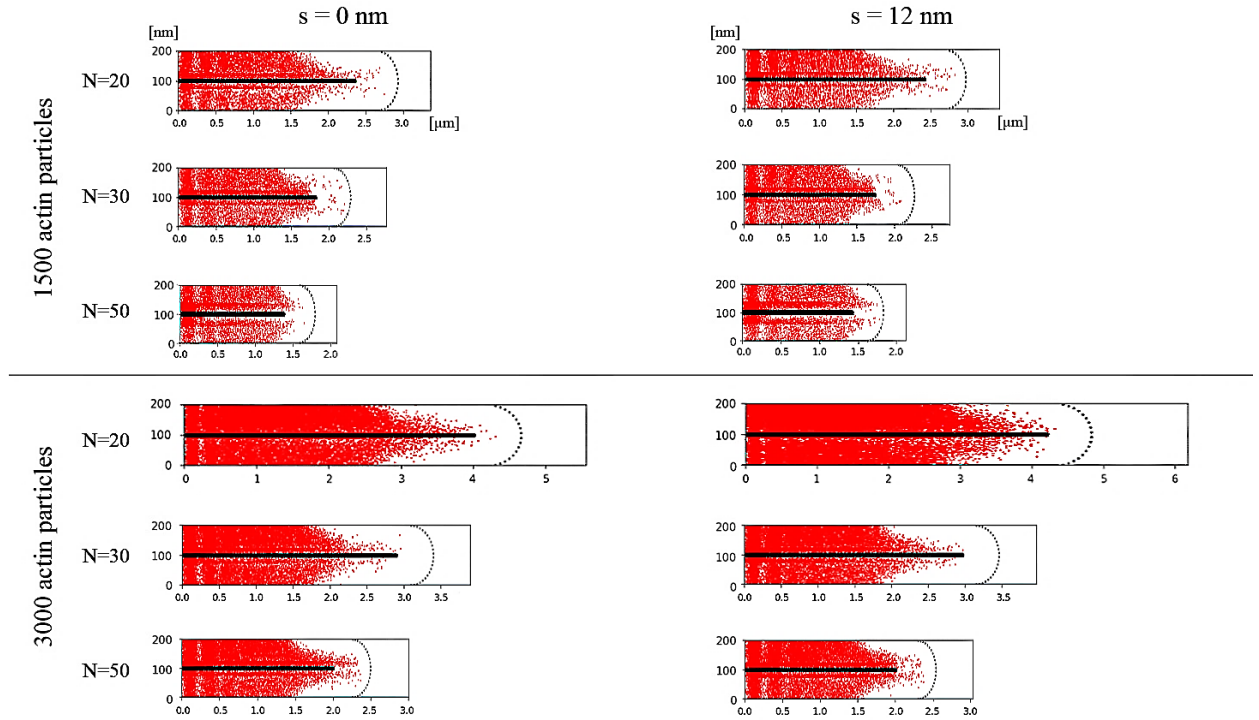


Figure 5.10: G-actins distribution combining values of $N = \{20, 30, 50\}$, $s = \{0, 12\}$, and $N_P = \{1500, 3000\}$. Lengths are those in Table 2 and the axes were re-scaled for comparison. Any image artefacts are due to a stretch to scale the graphs.

The inverse relation between N and L observed for 1500 particles persists for 3000 particles, which implicates in smaller final lengths of L even for a greater supply of G-actin monomers. In fact, this is verified mathematically when we write the expression (2.3) to obtain $L = L(N, C)$, when $C \gg C_{crit}$. This calculation will be presented in Appendix 2.

Two other points must be highlighted. First, the increase of N_p leads to higher values of L for all N . This can be physically explained by a greater supply of G-actins to polymerization. Second, for each fixed number of filaments, the filopodial length L increases whenever inter-filament spacing changes from $s = 0$ to $s = 12$. This bears a physical interpretation: an increase in outflowing volume induces an increase in the amount of drifting particles. This occurs since the cross-section outflowing area S_{out} increases along changes in s . In both points, higher removal of volume provokes a decrease in the outflow velocity, which produces as a consequence lower rate of filopodial elongation.

In order to confirm those highlighted facts, we must analyze filopodial dynamics behaves in response to the biological regulation of ABPs. In Figures 5.11 to 5.16, the yellow particles refer to moving hetero-dimers AP, in amounts of 1500 (Figures 5.11 to 5.13) and 3000 particles (Figures 5.14 to 5.16). The formation of hetero-dimers throughout filopodial interior is not taken into account; the inflowing particles are already dimerized.

Once hetero-dimers AP approach the Ena/VASP-mediated tips, they undergo the sequence of bindings (iii) described in Section 3.3. This means that EP reactions occur to polymerize actins, thus releasing profilins. The domain in following figures represents a filopodial tube with length in micrometers and diameter in nanometers, with the axes out of their natural ratios. Each filament in the bundle is computed individually, but they are embodied on a black rod which reproduces the actual bundle length.

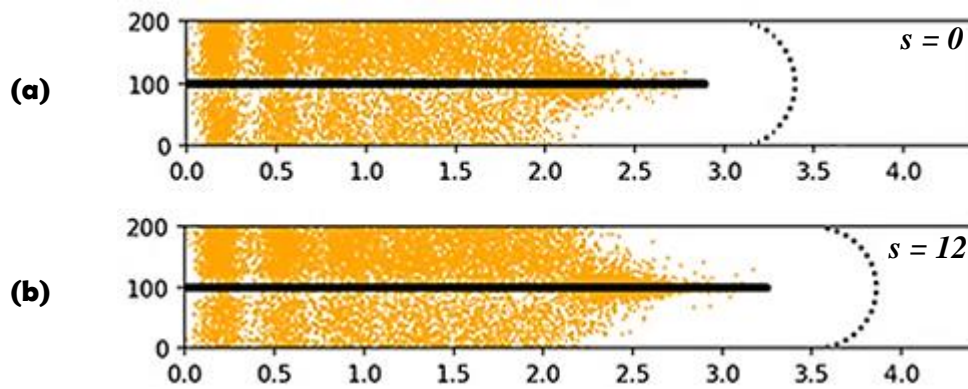


Figure 5.11: Hetero-dimers AP distribution with $N = 20$ and 1500 particles. In a) for $s = 0$, filopodial length reaches $L = 3.40 \text{ nm}$; in b) for $s = 12$, filopodial length reaches $L = 3.71 \text{ nm}$. The increase in s produces 9.18% of increase in L .

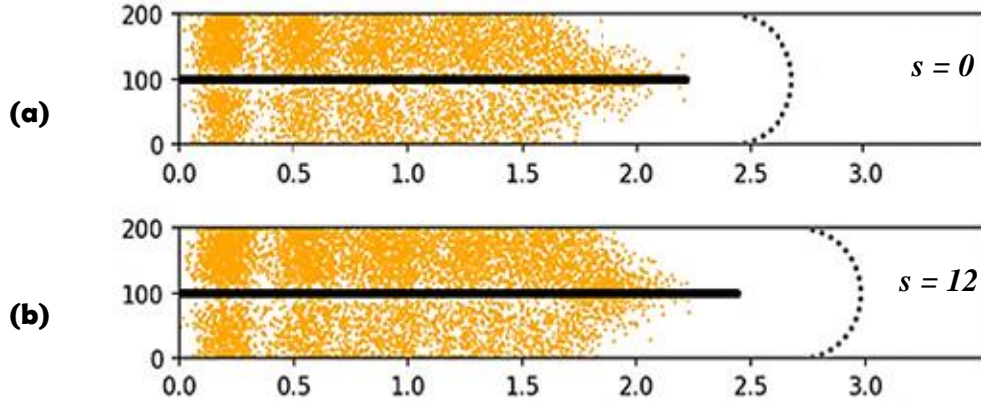


Figure 5.12: Hetero-dimers AP distribution with $N = 30$ and 1500 particles. In a) for $s = 0$, filopodial length reaches $L = 2.56 \text{ nm}$; in b) for $s = 12$, filopodial length reaches $L = 2.78 \text{ nm}$. The increase in s produces 8.59% of increase in L .

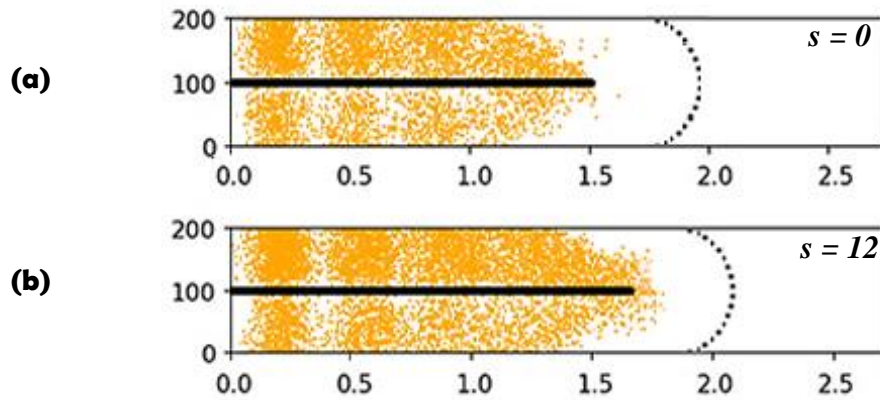


Figure 5.13: Hetero-dimers AP distribution with $N = 50$ and 1500 particles. In a) for $s = 0$, filopodial length reaches $L = 1.95 \text{ nm}$; in b) for $s = 12$, filopodial length reaches $L = 2.08 \text{ nm}$. The increase in s produces 6.70% of increase in L .

The above images showed 1500 moving hetero-dimers AP at the end of a simulation time ($t_s = 100$) in situations combining each chosen value of N with both considered cases of s . A deep investigation about ABPs influence and its impact on filopodial growth is addressed ahead in Section 5.4, but at this point we can already make a few comparisons with scenarios with no biological regulation. Filopodia have their growth enhanced up to approximately 27.5% in certain cases when ABPs are present when compared to correspondent cases without them. As an example, for the set of parameters $N = 20$, $s = 12$, and $N_p = 1500$ moving G-actins,

filopodial length reaches $L = 2.91 \text{ nm}$ ((b) in Figure 5.4), while for the same values of N and s , but particles being regulated by profilin and Ena/VASP, the filopodium grew up to $L = 3.71 \text{ nm}$ ((b) in Figure 5.11).

Regarding the investigated hypotheses, both were confirmed for similar parameters, which are: an inverse relation between the number of filaments N and filopodial length L , and an increase of inter-filament spaces s inducing more efficiency in filopodial growth. Due to the action of ABPs, the percentage of elongation from changes in s were much higher when compared to previous scenarios.

In order to complete this analysis, the distribution of 3000 hetero-dimers AP in the domain at the end of simulations should be investigated, for each chosen value of N . These distributions are exhibited in the figures below:

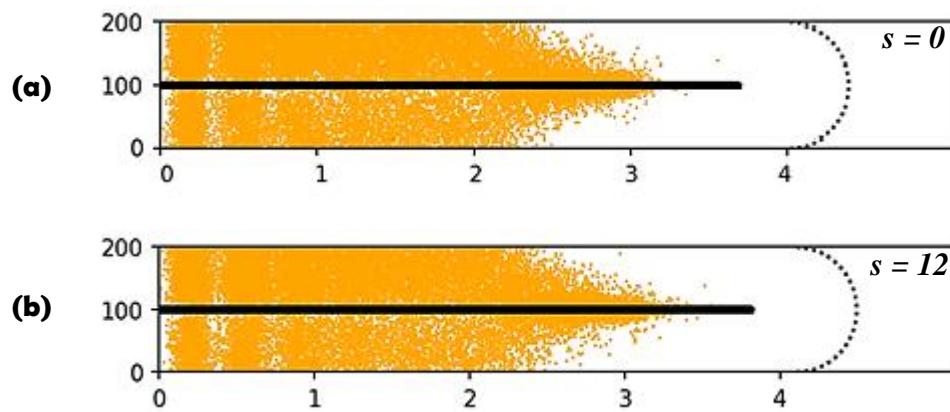


Figure 5.14: Hetero-dimers AP distribution with $N = 20$ and 3000 particles. In a) for $s = 0$, filopodial length reaches $L = 4.24 \text{ nm}$; in b) for $s = 12$, filopodial length reaches $L = 4.31 \text{ nm}$. The increase in s produces 1.65% of increase in L .

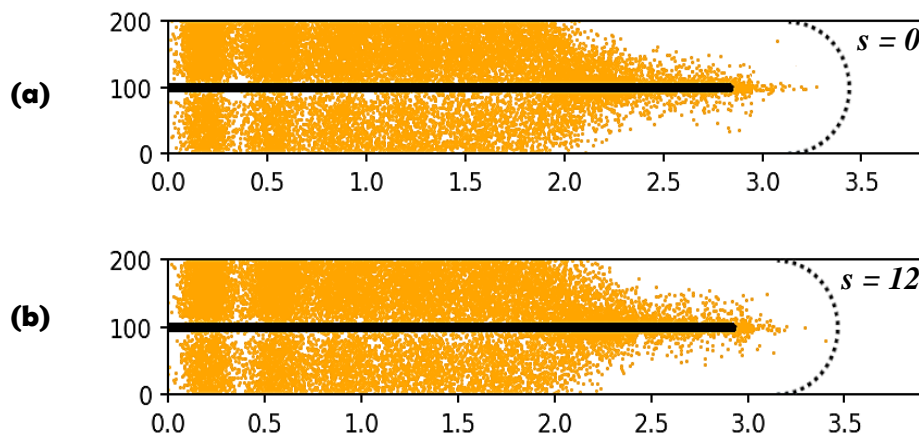


Figure 5.15: Hetero-dimers AP distribution with $N = 30$ and 3000 particles. In a) for $s = 0$, filopodial length reaches $L = 3.34 \text{ nm}$; in b) for $s = 12$, filopodial length reaches $L = 3.42 \text{ nm}$. The increase in s produces 2.39% of increase in L .

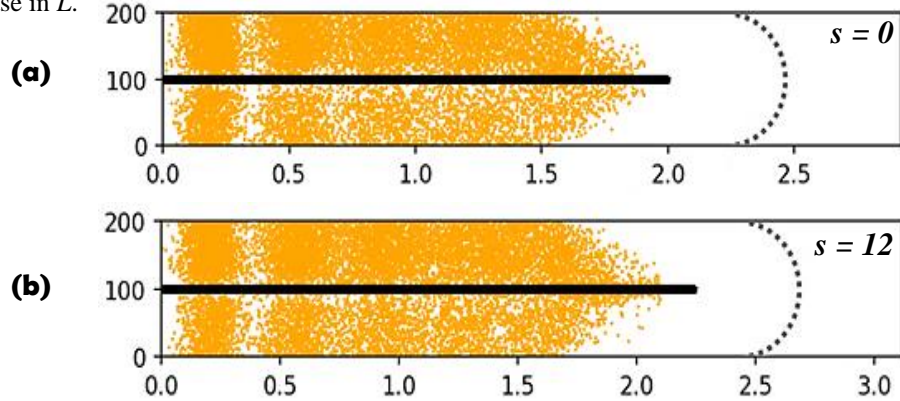


Figure 5.16: Hetero-dimers AP distribution with $N = 50$ and 3000 particles. In a) for $s = 0$, filopodial length reaches $L = 2.49 \text{ nm}$; in b) for $s = 12$, filopodial length reaches $L = 2.53 \text{ nm}$. The increase in s produces 1.61% of increase in L .

Several simulations were performed and the distributions slightly change from one run to another (due to the stochastic motion of particles) but results did not vary significantly. The chosen results were analyzed to capture an estimate (in %) of how length varies under each condition. This is useful to interpret how each set of parameters affects filopodial growth. Table 3 summarizes lengths and their variation on each previously evaluated case. Figure 5.17 shows a comparison of all distributions in Table 3.

Table 3: Variation of L as function of s in hetero-dimers AP distributions.
Calculations done in each case were $\frac{L_{s=12} - L_{s=0}}{L_{s=0}} \times 100$.

G-actins and ABPs				
$N_{\text{particles}}$	Length (in μm)	$N = 20$	$N = 30$	$N = 50$
1500	L for $s = 0$	3.40	2.56	1.95
	L for $s = 12$	3.71	2.78	2.08
	Variation	9.18 %	8.59 %	6.70 %
3000	L for $s = 0$	4.24	3.34	2.49
	L for $s = 12$	4.31	3.42	2.53
	Variation	1.65 %	2.39 %	1.61 %

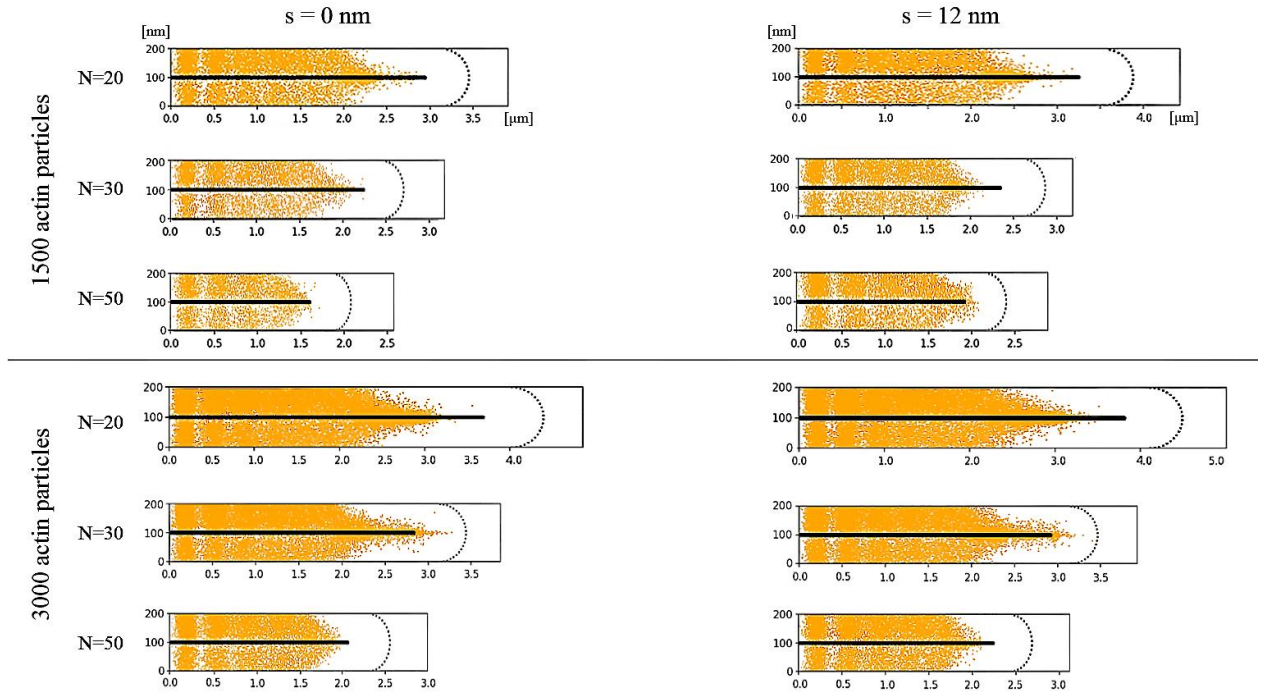


Figure 5.17: Hetero-dimers AP distribution combining values of $N = \{20, 30, 50\}$, $s = \{0, 12\}$, and $N_P = \{1500, 3000\}$. Lengths are those in Table 3 and the axes were re-scaled for comparison. Any image artefacts are due to a stretch to scale the graphs.

From Tables 2 and 3, interesting knowledge should be gained or highlighted. The main contributions of this section are:

- the verification of an inverse relation between the number of filaments N and filopodial length L , already approached by [64] although focusing on protrusions and diffusion as the transport mode;
- a novel relation between filopodial length L and inter-filament spacing s , where L increases whenever s changes from 0 to 12; although counterintuitive, as a greater space for the cytosol to outflow involves a smaller flux speed, but does not affect the proper supply of polymerization;

- the suggestion of a new hypothesis to be investigated in the Section 5.1.2, which is the direct relation between filopodial length L and the number of moving particles N_P ; the increase of N_P enhances filopodial growth in all tested scenario, despite a reduction in the percentage of length variation with respect to s .

5.1.1.1 Statistical evaluation of model stability

In the previous sub-section, the presented results were chosen from several performed virtual experiments to illustrate particles distributions. It should be clear that new runs generate different distributions mainly due to the randomness of the particles' movement. Besides, the pattern of results is not much beyond those shown, with average filopodial lengths not varying more than $\pm 0.2 \mu\text{m}$. To probe the stability of the model, Table 4 shows the variance σ between the final lengths of filopodia after 10 runs for each set of parameters tested in Section 5.1.1.

Table 4: Variance between the lengths after 10 runs for each considered case. The highest variance σ in the chosen sample is 0.00686 ($N_P = 10000$; $N = 20$; $s = 0$), which results in a difference of $0,248 \mu\text{m}$ between maximum and minimum values after 10 simulation runs for each set of parameters.

	N_P	N	s	σ
Only G-actins	1500	20	0	0.00059
			12	0.00024
		30	0	0.00013
			12	0.00020
		50	0	0.00010
			12	0.00009
	3000	20	0	0.00332
			12	0.00244
		30	0	0.00063
			12	0.00057
		50	0	0.00015
			12	0.00025
	6000	20	0	0.00251
			12	0.00355
		30	0	0.00119
			12	0.00039
		50	0	0.00025
			12	0.00051
	10.000	20	0	0.00686
			12	0.00280
		30	0	0.00184
			12	0.00205
		50	0	0.00101
			12	0.00105

These data in Table 4 indicates a notable stability of the model and the results obtained with it. The ranges in which filopodial lengths vary represents amounts of 15 to 50 monomers polymerized per filament. This represents 0.018% in length or 0.01% in the number of monomers in place. As the methodology of variance calculation is maintained for all cases, the evaluation of scenarios with G-actins and ABPs will be omitted.

5.1.2 Amount of particles enormously enhances filopodial growth

In the results exhibited in the previous section, we could note an increase in the filopodial lengths when analogous cases are compared. That is, for each set of parameters N and s , the final value of L becomes greater as long as the number N_p of moving particles increases. This leads to conclude that N_p greatly influences filopodial elongation. Conveniently rewriting the data in Tables 2 and 3, we can observe how L is influenced by N_p . Tables 5 and 6 present these comparisons for cases with only G-actins and those that include ABPs.

Table 5: Comparison of cases with different N_p and only G-actins in the system. Filopodial length increases considerably when N_p changes from 1500 to 3000 particles. Lengths are in micrometers.

Length variations for only G-actins				
s	$N_{\text{particles}}$	$N = 20$	$N = 30$	$N = 50$
$s = 0$	1500	2.86	2.23	1.59
	3000	4.40	3.40	2.50
Variation		53.85 %	52.47 %	57.23 %
$s = 12$	1500	2.91	2.26	1.61
	3000	4.47	3.47	2.54
Variation		53.61 %	53.54 %	57.76 %

Table 6: Comparison of cases with different N_p and ABPs in the system. Filopodial length increases considerably when N_p changes from 1500 to 3000 particles. The percentage rates are smaller in this case, but final lengths are still greater for each tested set of parameters. Lengths are in micrometers.

Length variations for G-actins and ABPs				
s	$N_{\text{particles}}$	$N = 20$	$N = 30$	$N = 50$
$s = 0$	1500	3.40	2.56	1.95
	3000	4.24	3.34	2.49

<i>Variation</i>		24.71 %	30.47 %	27.69 %
$s = 12$	1500	3.71	2.78	2.08
	3000	4.31	3.42	2.53
<i>Variation</i>		16.17 %	23.02 %	21.64 %

These data point to the direction of a clear and important relation between the number of moving particles and the stationary length of the filopodium, when considering a certain observation time. When there are just G-actins in the domain, L increases approximately from 52.4% to 57.8%. When filopodial dynamics involves ABPs, these growth rates remain between 16.2% and 30.5%.

Despite a still stable and relevant length increasing, the variation is lower in the second case. This can be explained by a more efficient G-actin supply to barbed ends primarily due to the action of the regulating proteins, with a consequent filopodium elongation faster than the first case. In fact, the lengths are higher for both values of N_p , which shortens their difference thus producing lower percentages of variation. Also, it is reasonable to think that particles must flow further and further to be polymerized in longer filopodial tubes and at the same time of observation which may produce a limiting effect.

Both hypotheses require more investigation to confirm if these tendencies stand for other values of N_p , that is, if the number of particles greatly enhances filopodial lengths and a possible effect of time on this computation. Then, following the same criteria and ranges of parameters, we can inquire about the model to perform experiments for $N_p = 6000$ and $N_p = 10000$. Tables 7 and 8 present those results, followed by discussion. Particles distributions were not generated. The focus is on the final length of filopodia in each case and its consequent variation (in %) due to the increase of N_p .

Table 7: Comparing filopodial length for $N_p = 6000$ and $N_p = 10000$ G-actins in the system. A higher number of particles reflects a substantial increase in the final length of the filopodium in every tested set of parameters. Lengths are in micrometers.

Length variations for only G-actins				
s	$N_{\text{particles}}$	$N = 20$	$N = 30$	$N = 50$
$s = 0$	6000	5.89	4.53	3.30
	10000	9.11	6.90	4.91
Variation		54.67 %	52.32 %	48.79 %
$s = 12$	6000	5.94	4.63	3.39
	10000	9.20	7.01	5.02
Variation		54.88 %	51.40 %	48.08 %

Table 8: Comparing filopodial length for $N_p = 6000$ and $N_p = 10000$ particles, with ABPs regulating G-actins in the system. A higher number of particles reflects a relevant increase in the final length of the filopodium in every tested set of parameters. Lengths are in micrometers.

Length variations for G-actins and ABPs				
s	$N_{\text{particles}}$	$N = 20$	$N = 30$	$N = 50$
$s = 0$	6000	10.81	8.64	6.52
	10000	14.75	11.60	8.52
Variation		36.45 %	34.26 %	30.67 %
$s = 12$	6000	10.95	8.72	6.69
	10000	14.78	11.69	8.79
Variation		34.98 %	34.06 %	31.39 %

We can observe that the impact of the number of particles on filopodial length is extremely relevant. The analyzes done for $N_p = \{1500, 3000\}$ can be extrapolated, for example, to $N_p = \{6000, 10000\}$, producing filopodia of almost 15 μm length with an unchanged simulation time $t_s = 100$. This exhibits a high efficiency of particles' transport when we integrate into our investigations the various aspects of the filopodial dynamics and structure, such as

diffusion, drift, and reactions, in addition to the number of filaments in the bundle and its inter-filament spaces, and the number of particles.

If we cross all information we have at this point, considering corresponding cases, that is, using the same set of filopodial physical/structural parameters, the effect of N_p on L becomes even more evident. For example, a filopodium that has $N = 20$, $s = 12$, and $N_p = 1500$ particles, including ABPs (see Table 6) reaches maximum length 3.71 μm , while a scenario with the same parameters, but with $N_p = 10000$ (see Table 8), the filopodium grows up to 14.78 μm , almost four times greater.

5.1.3 More time of experimentation greatly improves filopodial growth

The time of observation is a limiting factor to simulations. This is observed by recalculating the data for $N_p = 10.000$ with ABPs in Table 8 but running for $t_s = 500$. This experiment provides the data in Table 9, where L reaches $\sim 38.4 \mu\text{m}$. However, the absolute length values have not been the research focus so far, but the contribution of each parameter to the extension of filopodia. For future work, a relation between the simulation time and the real-time of interactions and reactions between molecules in a filopodial environment can provide even more tangible data about time influence over this dynamics.

Table 9: Simulation of filopodia with 10.000 particles and 500 time steps.

Final lengths for only G-actins				
s	t_s	$N = 20$	$N = 30$	$N = 50$
$s = 0$	$t_s = 100$	9.11	6.90	4.91
	$t_s = 500$	31.97	30.67	28.77
$s = 12$	$t_s = 100$	9.20	7.01	5.02
	$t_s = 500$	32.20	30.92	29.01
Final lengths for G-actins and ABPs				

s	t_s	$N = 20$	$N = 30$	$N = 50$
$s = 0$	$t_s = 100$	14.75	11.60	8.52
	$t_s = 500$	37.89	36.71	34.43
$s = 12$	$t_s = 100$	14.78	11.69	8.79
	$t_s = 500$	38.36	37.24	34.94

Besides, it is important to note that the influence of changes in the inter-filament spacing observed in the previous section can still be perceived, that is, higher values of s reflects in filopodial extension, although in a more subtle way than other observed parameters. The number of interacting particles in the system has a greatest impact, on which filopodia presents remarkable growth.

Even in longer simulations, the extension remains stable, generating filopodia with length of almost $40\text{ }\mu\text{m}$. Modeling providing this amplitude of filopodial elongation is not found in the literature. We emphasize that this brings a relevant contribution from the proposed mathematical-computational model.

5.2 Predominance of each transport phenomenon

The spatial distribution of particles within filopodia provides a picture of how important are inter-filament spacing, the number of particles, and time in filopodial growth when diffusion, drift, and those reactions relevant to actin dynamics are considered. Nevertheless, the mechanisms that drive particle flow along the filopodium need to be investigated. An immediate question in this direction is the effect of each phenomenon separately.

In the following, a broader understanding of the transport mechanisms is provided by inspecting *velocity profiles* of the inflow mixture for given conditions. This allows us to understand which of the three processes is more effective and where. We analyze also their individual contributions and how these transport phenomena relate to fundamental parameters such as the inter-filament spacing s , the number of filaments in the bundle N , the length of the filopodium L , or chemical aspects like biological regulation.

Curves in Figures 5.18 to 5.20 represent velocity profiles of inflowing cytoplasm with G-actins dispersed. In green profiles, movement is driven by diffusion, while in red profiles, by drift. The blue profiles represent the composition of both phenomena. The curves were obtained varying the values of $N = \{20, 30, 50\}$ and $s = \{0, 12\}$. The x -axis registers the filopodial length, in micrometers. Flow velocities given by each phenomenon along filopodial length are set on y -axis, in micrometers per second. The total simulation time for all profiles is $t_s = 100$.

In each figure, a sketch of the modeling domain is shown at the top to locate the velocities. Besides, the last graph deploys the three previous profiles highlighting which speed is more important. The axes are not in their natural ratios.

Then, for $s = 0$, the velocity profiles for N are as follows:

- $N = 20$

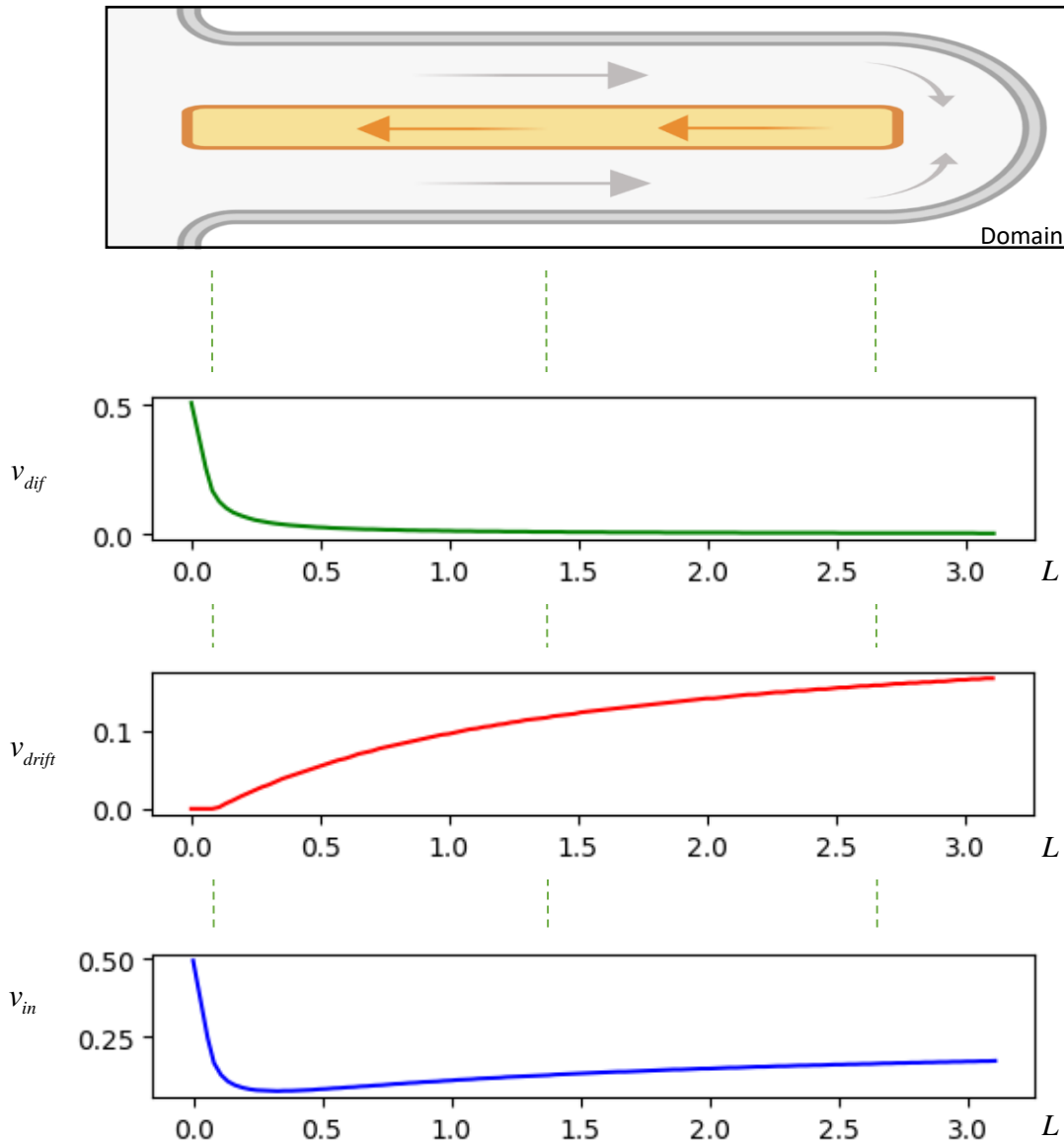


Figure 5.18: Velocity profile driven by each transport phenomena, with $N = 20$ and $s = 0$. In green, diffusion; in red, drift; in blue, inflow velocity by the coupled processes. The last image joins the three previous curves. Length is marked on x -axis and velocity is on y -axis. Diffusion contribution is much higher in protrusions and drift takes place in motion as long as particles approach the polymerization point.

○ $N = 30$

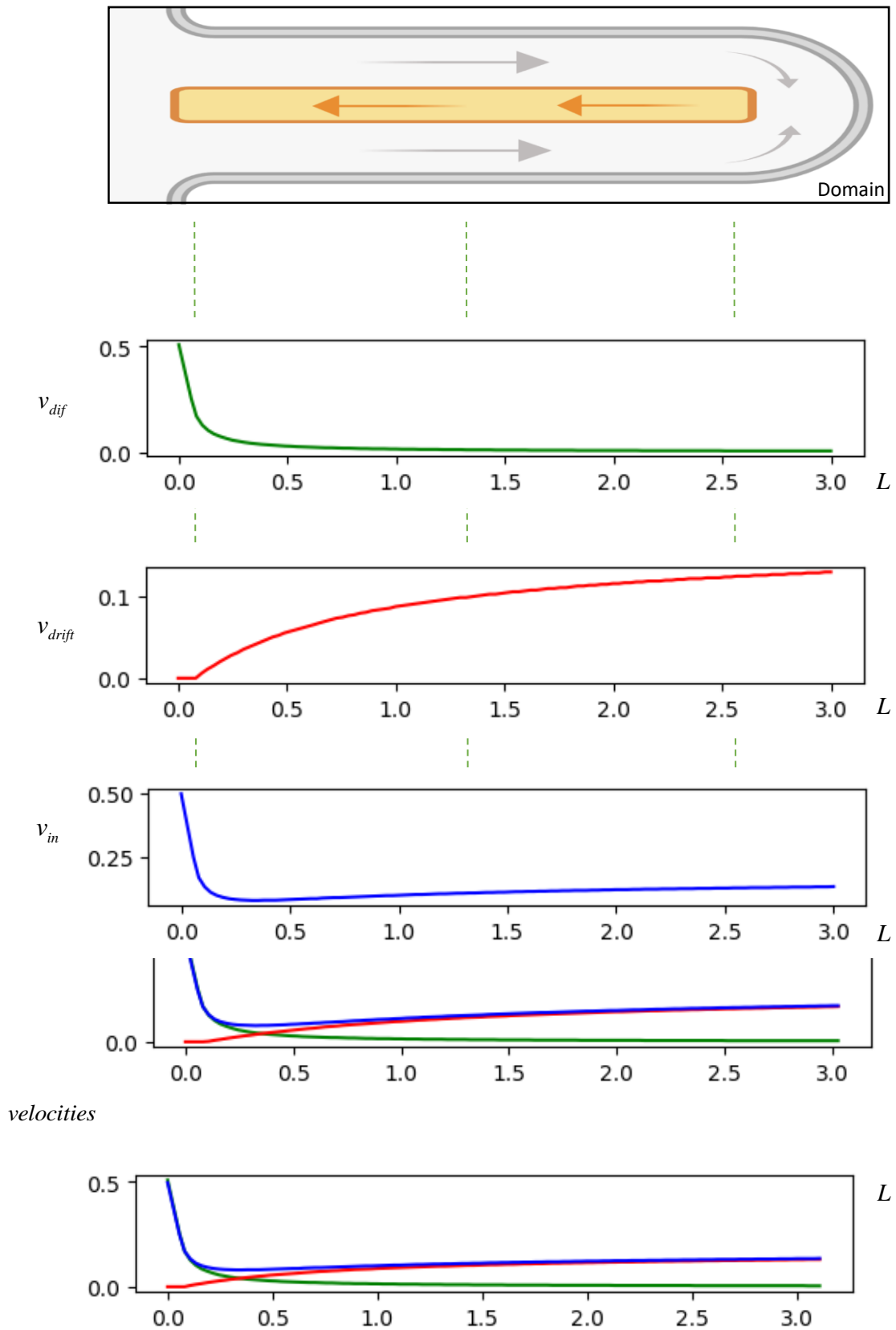


Figure 5.19: Velocity profile driven by each transport phenomena, with $N = 30$ and $s = 0$. In green, diffusion; in red, drift; in blue, inflow velocity by the coupled processes. The last image joins the three previous curves. Length is marked on x -axis and velocity is on y -axis. Diffusion contribution is much higher in protrusions and drift takes place in motion as long as particles approach the polymerization point, but with a slightly lower intensity than in the previous case.

○ $N = 50$

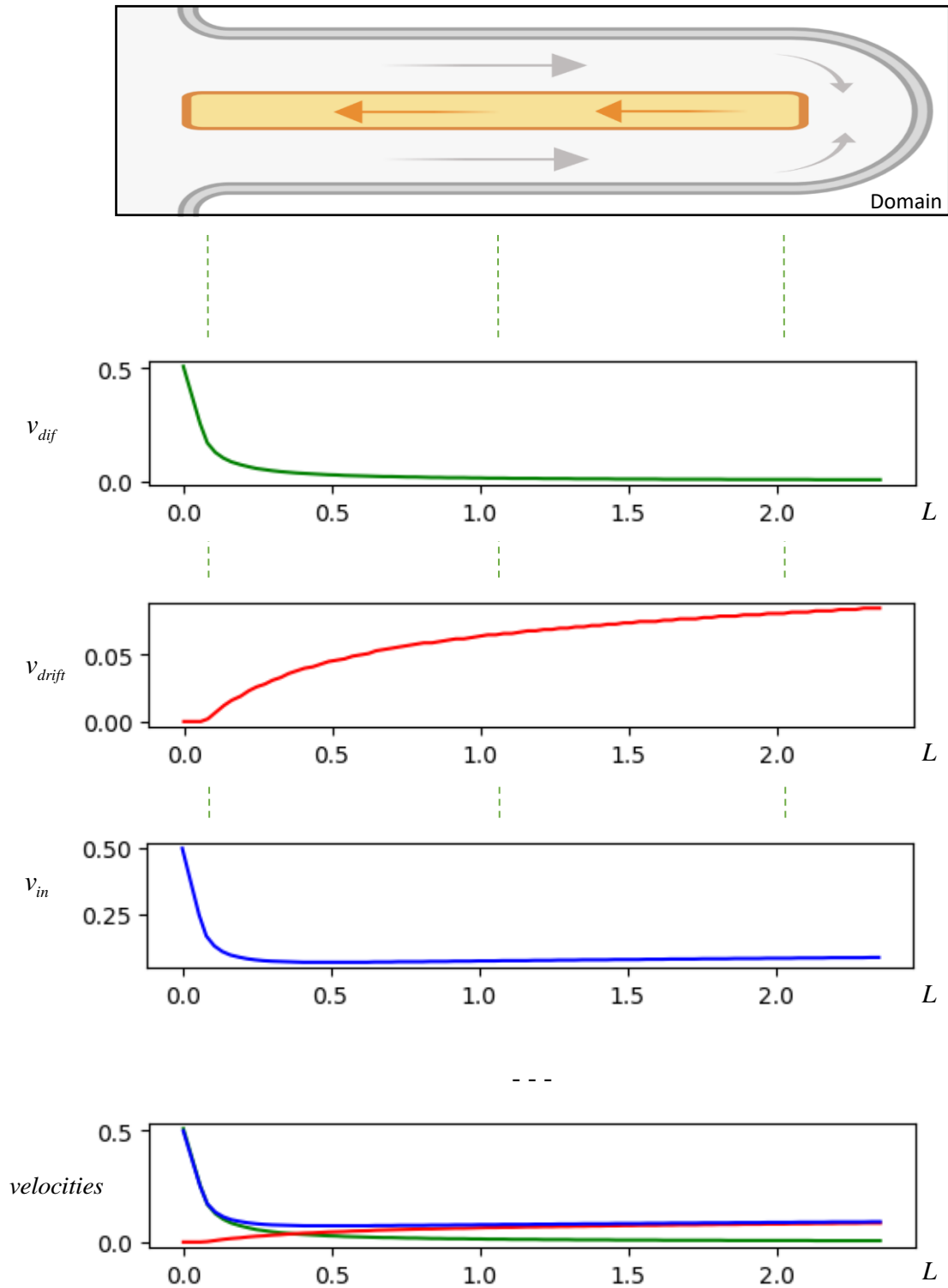


Figure 5.20: Velocity profile driven by each transport phenomena, with $N = 50$ and $s = 0$. In green, diffusion; in red, drift; in blue, inflow velocity by the coupled processes. The last image joins the three previous curves. Length is marked on x -axis and velocity is on y -axis. Diffusion contribution is much higher in protrusions and drift takes place in motion as long as particles approach the polymerization point. Since outflow velocity is lower due to the greater consumption of volume at barbed ends, filopodial growth tends to be less efficient at the end of the simulation.

With the purpose of comparing the contributions of the three flow modes, Figures 5.21, 5.22, and 5.23 display together the curves for different N values for each mode: diffusion, drift, and inflow velocity, with inter-filament spacing $s = 0$. This provides a more friendly visualization of the curves. These new figures point to important features of the physical phenomena involving particle movements in filopodia.

First (Figure 5.21), diffusion alone quickly becomes fairly ineffective to deliver actin to polymerization. The speed absolute value tends to zero once filopodial length becomes higher than $1 \mu\text{m}$ for all three values of N . Further, the relation between N and L discussed in Section 5.1 is perceived: length becomes longer for lower number of filaments in the bundle, and vice versa.

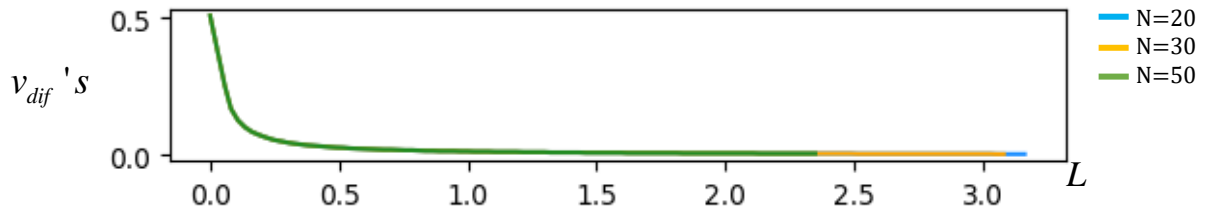


Figure 5.21: Diffusion contribution to flow velocity in a filopodium with only G-actins. As long as filopodium elongates, diffusion rapidly becomes inefficient to sustain G-actin transport. Also, greater number of filaments diminishes filopodial final length.

The fast decay of diffusion velocity is a known result (Section 2.2), but it is interesting to see that diffusion is related to filopodial configuration. An important question is how diffusion relates to drift, which has its contribution for chosen N deployed in Figure 5.22. In the virtual experiments, drift increases for almost the entire process, except for a short time in the initial stage of growth when its value is not significant in comparison to diffusion.

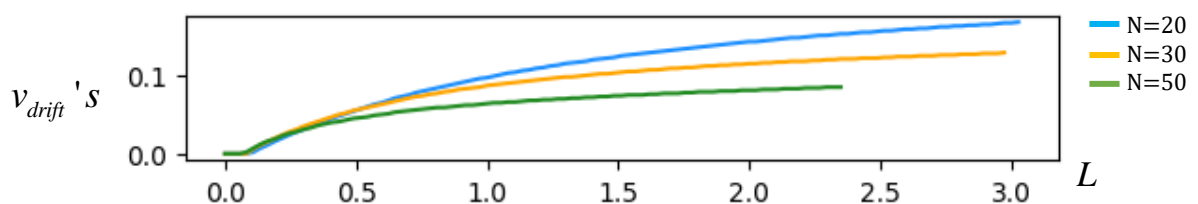


Figure 5.22: Drift contribution to flow velocity in a filopodium with only G-actins. As long as filopodium elongates, with consequent diffusion decay, drift becomes the main physical transport phenomenon, with higher velocity for lower number of filaments.

In figures 5.18 to 5.20, we saw the composition of both phenomena, i.e. diffusion and drift, in blue. This composition means the total inflow cytoplasm velocity v_{in} , defined in Section 3.2 as $v_{in} = v_{dif} + v_{drift}$. Besides, the total speed v_{in} can be interpreted by two central features of the filopodial domain: the *source* of matter at the filopodial base and the *sink* in the polymerization point, which induces an increasing advective effect due to the volume removal and consequent drop of hydrodynamic pressure at filopodial tip.

Hence, the curve v_{in} is approximated by diffusion curve in the beginning of the filopodial tube, while v_{in} approaches drift magnitude in the end of it. For each value of N , drift become more prominent as diffusion value tends to zero. These curves are plotted in Figure 5.23 for comparison.

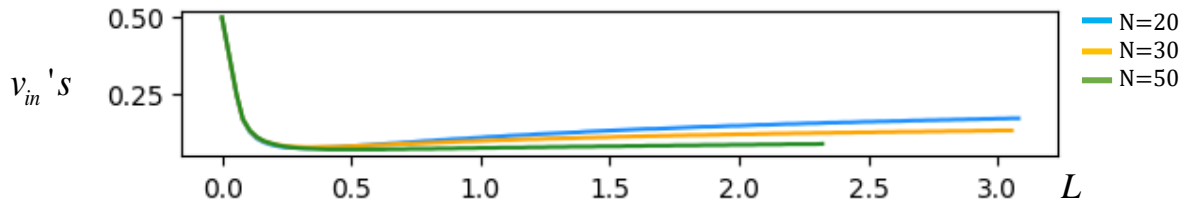


Figure 5.23: Total velocity of inflow cytoplasm in a filopodium with only G-actins. As long as filopodium elongates, with consequent diffusion decay, drift becomes the prominent physical transport phenomenon, with higher velocity for lower number of filaments.

These patterns emerge for all parameter sets, with greater or smaller contribution of different mechanisms at specific locations. For example, for $N = 30$, the drop of diffusion curve and the rise of drift curve are slightly more pronounced, which is caused by factor as: a higher demand of G-actins by polymerization, a greater volume of hydrated cytosol, and/or a larger inter-filament spacing for the cytosol to outflow. In comparison, due to the inverse relation between N and L , the total speed leads to similar dynamics for $N = 20$, but with its curve exhibiting lower growth close to the sink.

For $N = 50$, with an even faster exchange of predominant phenomena, a lower efficiency in filopodial extension is perceived. However, this result is expected: since the demand for monomers increases, and as the bundle spaces enlarge, slower will be the outflow through it.

As consequence, the pressure exerted on filopodial tip also decreases, which causes the smoothing of the advective induction of compensatory matter.

In the following, the dynamics is simulated under a different value for parameter s to observe if similar features emerge. So, when $s = 12$, profiles in Figures 5.24 to 5.26 are obtained:

- $N = 20$

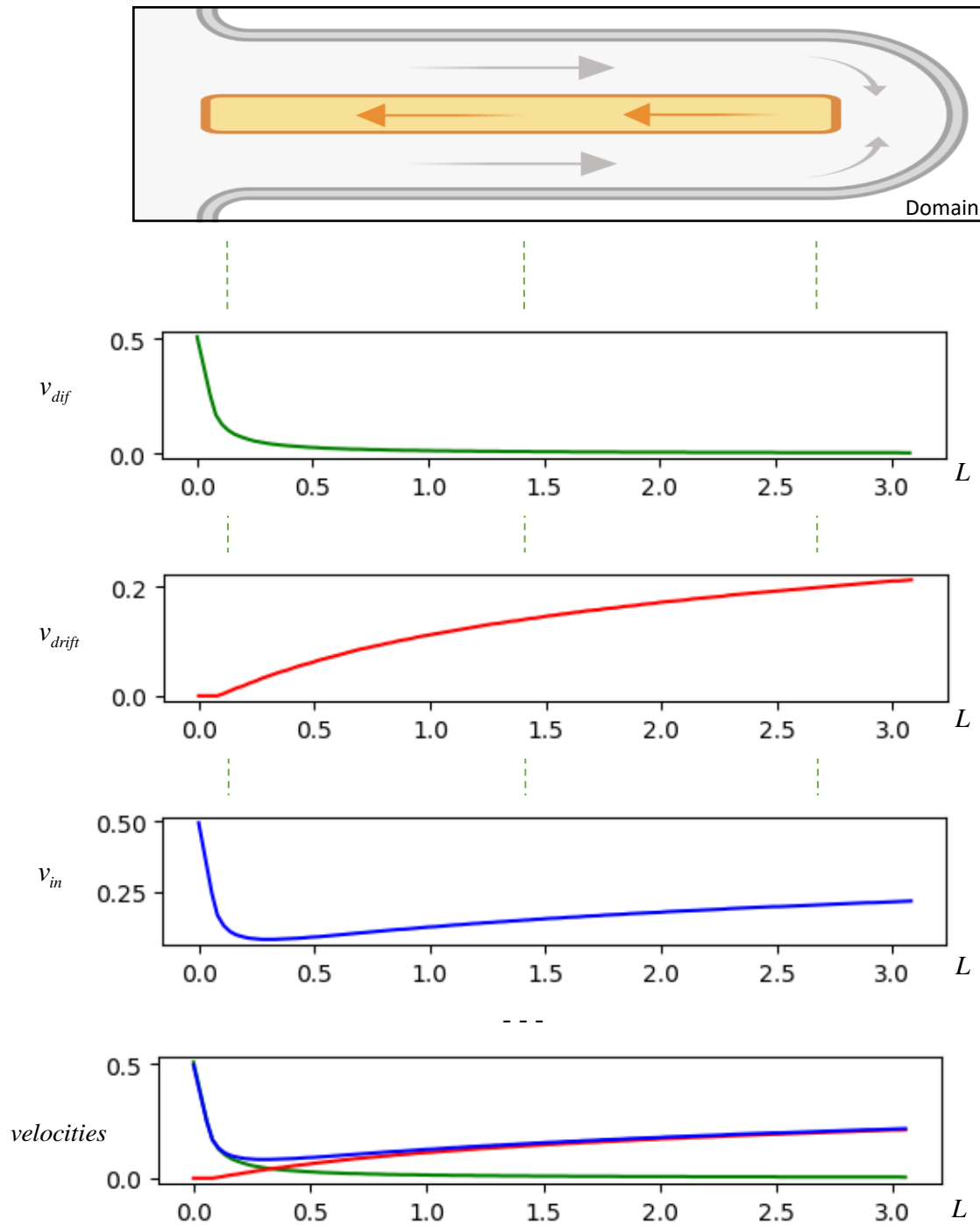


Figure 5.24: Velocity profile driven by each transport phenomena, with $N = 20$ and $s = 12$. In green, diffusion; in red, drift; in blue, the sum of both processes. The last image joins the three previous curves. Length is marked on x -axis and velocity is on y -axis. Diffusion contribution is much higher in protrusions and drift takes place in motion as long as particles approach the polymerization point. Drift exhibits more intensity for this value of s .

○ $N = 30$

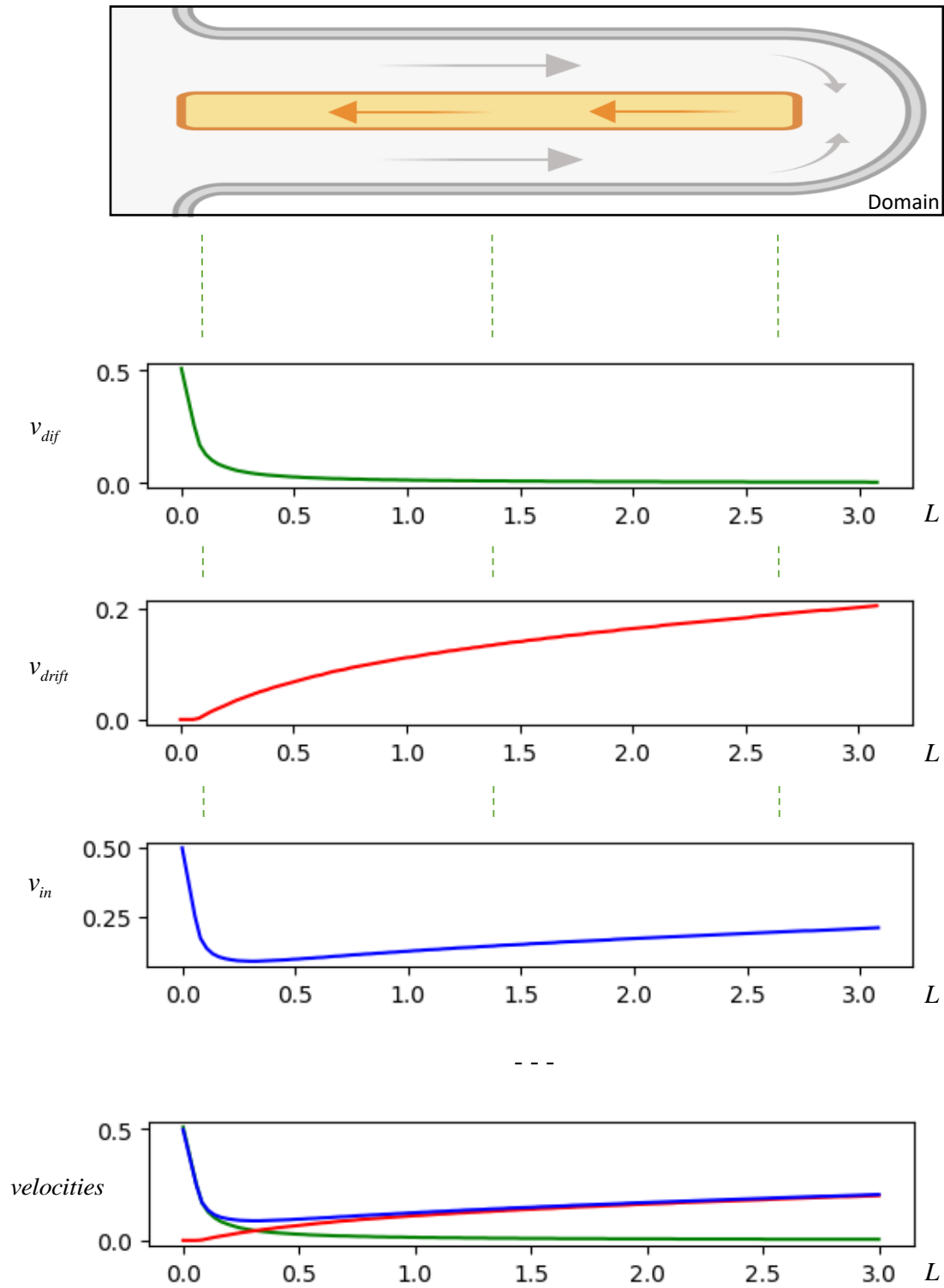


Figure 5.25: Velocity profile driven by each transport phenomena, with $N = 30$ and $s = 12$. In green, diffusion; in red, drift; in blue, the sum of both processes. The last image joins the three previous curves. Length is marked on x -axis and velocity is on y -axis. Diffusion contribution is much higher in protrusions and drift takes place in motion as long as particles approach the polymerization point. Drift exhibits more intensity for this value of s .

○ $N = 50$

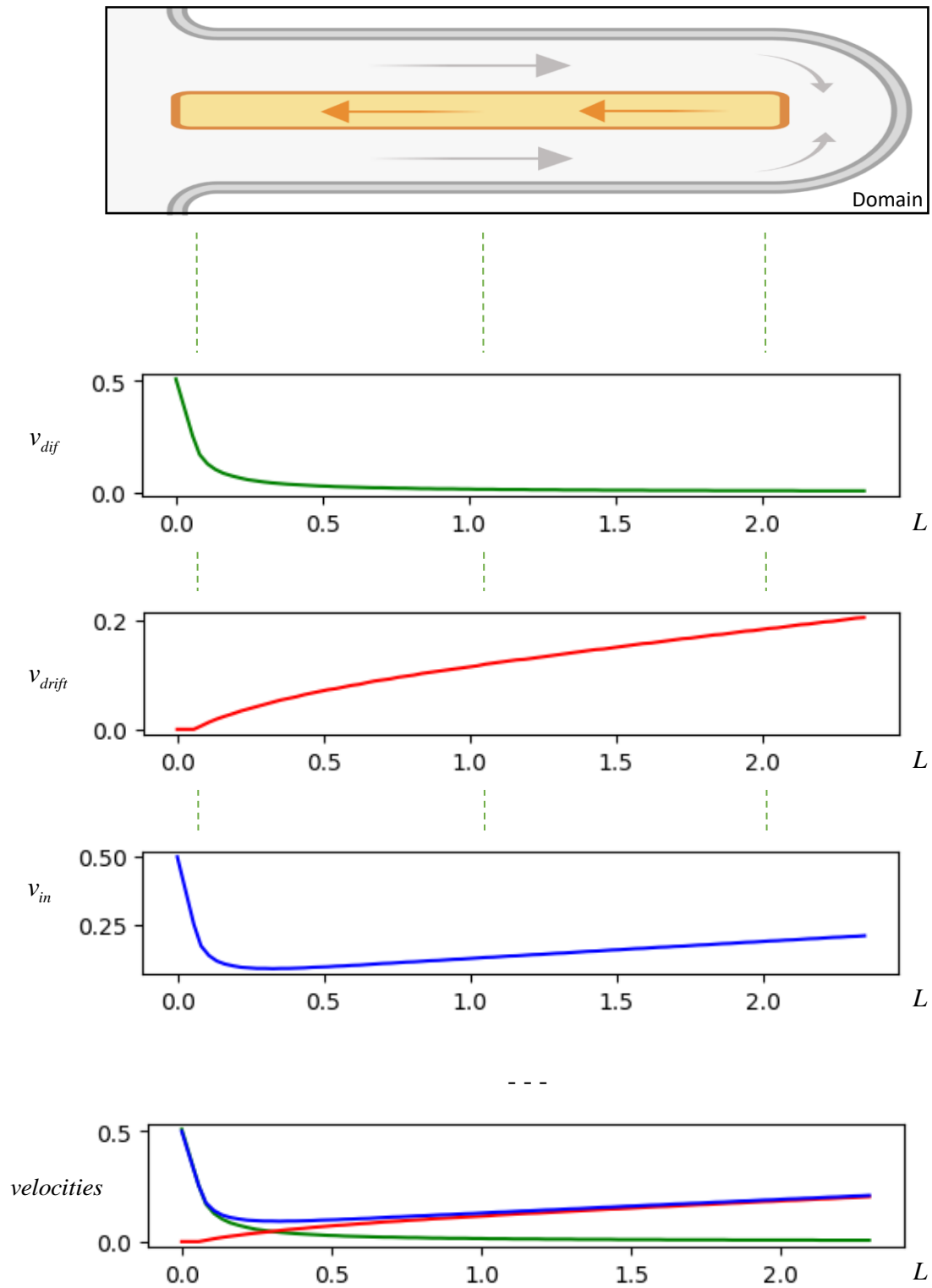


Figure 5.26: Velocity profile driven by each transport phenomena, with $N = 50$ and $s = 12$. In green, diffusion; in red, drift; in blue, the sum of both processes. The last image joins the three previous curves. Length is marked on x -axis and velocity is on y -axis. Diffusion contribution is much higher in protrusions and drift takes place in motion as long as particles approach the polymerization point. Drift exhibits more intensity for this value of s .

The profiles obtained for $s = 12$ are similar to those with $s = 0$, but a perceptible difference is the slightly higher intensity of drift for all N values, especially $N = 50$. This is related to the discussion in the previous section about greater supply for polymerization providing greater consumption of matter, which induces more drag of cytoplasm. In Figure 5.27, we find the three curves of each phenomenon presented for cases where the inter-filament space is $s = 12$. This eases to observe the higher intensity of drift in comparison to those in Figure 5.22, for $s = 0$.

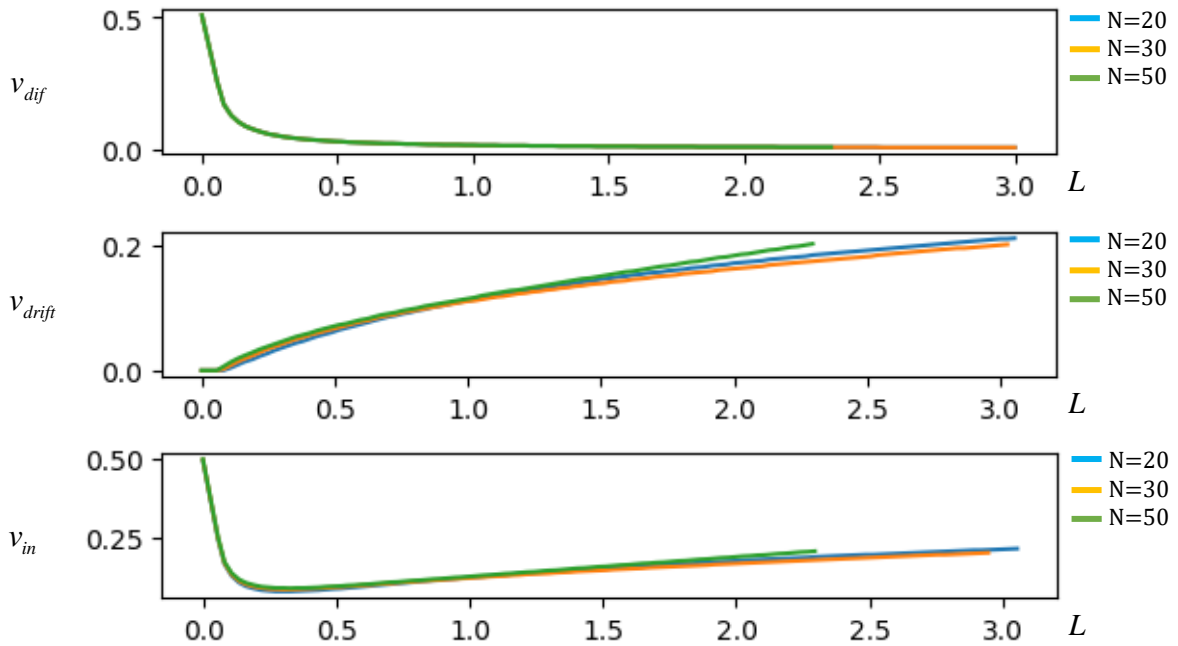
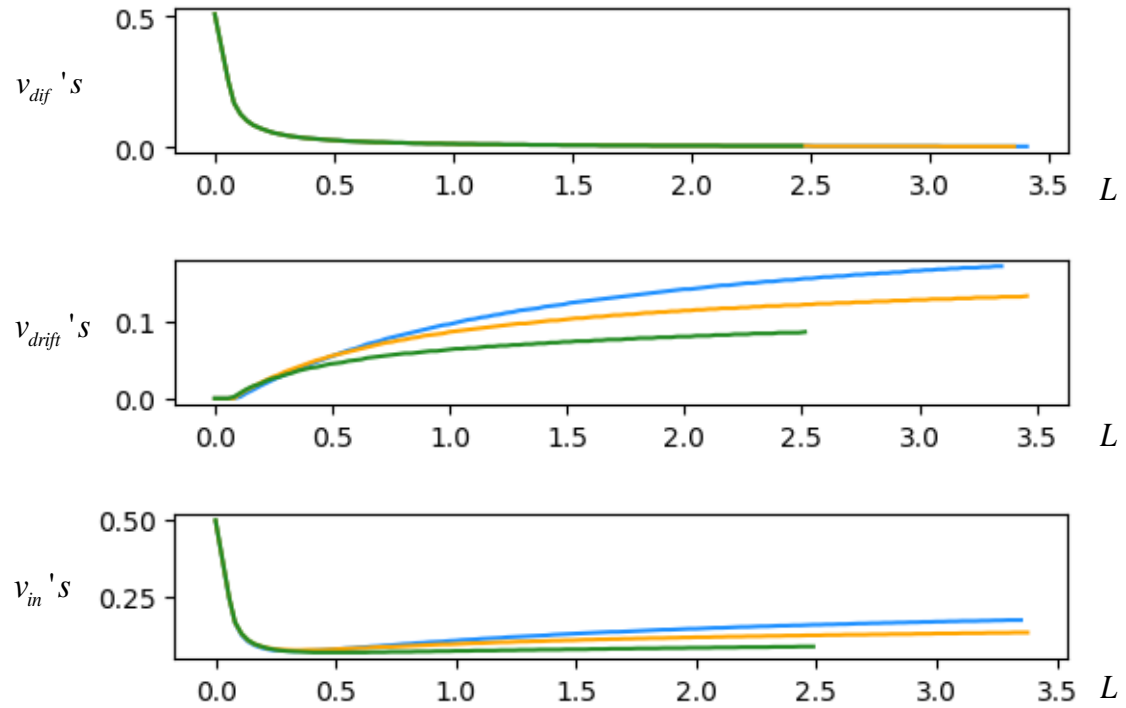


Figure 5.27: Physical transport phenomena contributions to flow velocity in a filopodium with only G-actins and $s = 12$. As long as filopodium elongates, with consequent diffusion decay, drift becomes the main physical transport phenomenon, with higher velocity for lower number of filaments. As a novelty, in this case, the higher intensity of drift when compared to drift for $s = 0$, where the flow top speed reaches two times those in the first case. It is due to more consumption of volume in filaments' tips.

At last, analogous observations can be done when ABPs are present in the domain and curves display patterns deeply similar to those in the scenarios analyzed individually, with solely G-actins. The most relevant contribution of ABPs lays in terms of larger maximum filopodial lengths when considering the default time of observation $t_s = 100$. Figure 5.28 shows different instances combining N and s , but with constant regulation of ABPs. Although the pattern is similar in each case, which is expected, the main contribution of these following

velocity profiles is to observe the maintenance of flow behavior under each considered physical transport phenomena and their bearing on the efficiency of filopodial growth.

$$s = 0$$



$$s = 12$$

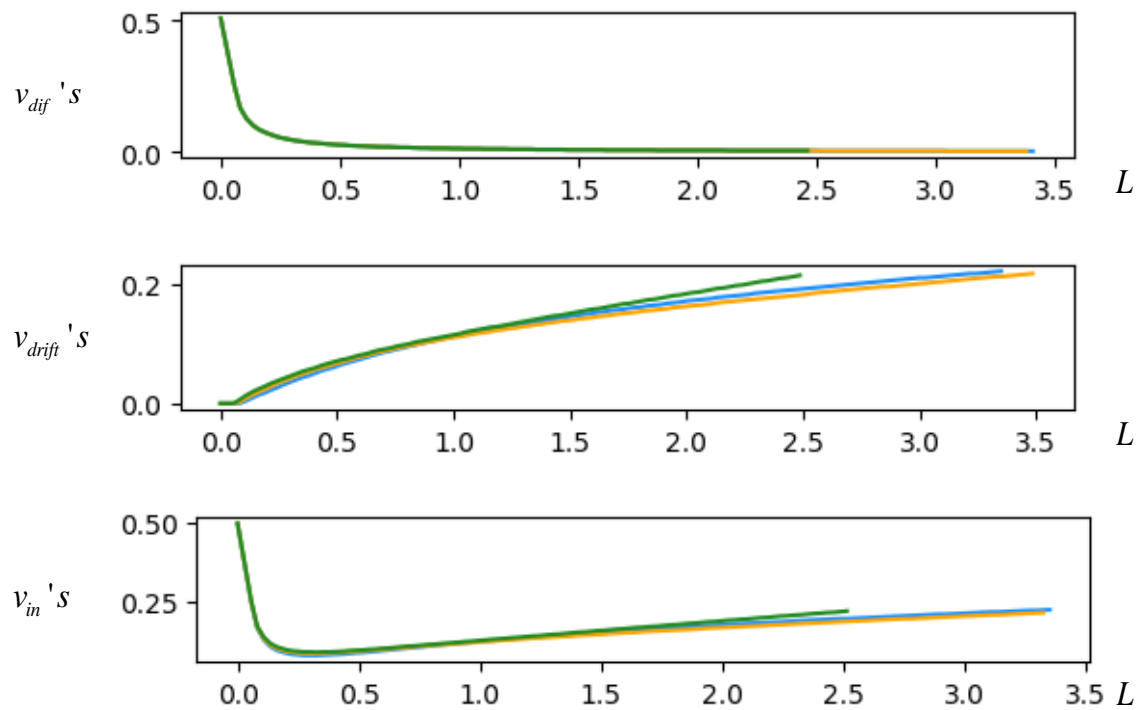


Figure 5.28: Velocity profiles of the cytoplasm flux in a filopodial dynamics mediated by ABPs. In (a), the diffusion contribution, in (b) the drift's, and (c) the total inflow velocity of flow. Curves in blue represent filopodia with $N = 20$; in yellow, curves for $N = 30$; and in green, curves for $N = 50$. Length is marked on x -axis and velocity is on y -axis. ABPs regulation essentially provides a larger final filopodial length.

So far, we have investigated the effects of transport mechanisms, coupled and isolated, as well as their relationship with physical parameters and the own structure of the filopodium. Other issues can be inquired when observing F-actin bundle geometry, for example, if more or less spaces within the bundle can alter cytosol flux in filopodia.

In the two following tests, we will analyze the feasibility of two particular hypotheses. In the first, we seek to know if in cases where the diameter of the bundle is sufficiently wide, i.e., for higher values of N and s , the incoming flow may enter within filopodium also through the inter-filament spaces. The second test briefly explores the hypothesis that the whole outflowing cytosol is encapsulated to F-actin filaments into hydration coats and, thus, this package of polymers and cytosol may outflow of the filopodium with the retrograde flow velocity.

5.3 Testing original hypotheses about inter-filament spaces

As discussed in Section 3.4, hydrated F-actin bundle has a straight relation with inter-filament spaces. As long as hydration occurs, the apparent filament radius r is enlarged by the shells of water molecules. This shortens the inter-filament spacing s linearly according to expression $s = -2r + 20$, defined in Section 3.4. The opposite situation is analogous; no hydration implies in lower value for r and higher for s .

In the following sections, a hypothesis about each extreme value of s is tested: $s = 12$ in Section 5.3.1 and $s = 0$ in Section 5.3.2. Thus, some assumptions about the relation between hydration and the bundle spaces must be done.

- When $s = 0$, we consider the maximum hydration, in which the enlargement of r makes filaments in the bundle tangent to each other. As a consequence, the cross-sectional area S_{out} is minimum. To illustrate this, Figure 3.10 can be re-called.
- Otherwise, when $s = 12$, F-actins are not hydrated at all. This scenario provides the maximum inter-filament spacing, which brings a maximum value for S_{out} . For this situation, Figure 3.11 can be referred.

5.3.1 Inflow cytoplasm within bundle spaces stops compensatory mechanisms

Consider the following hypothesis: in the case of total absence of hydration, which is, when $s = 12$, the cross-linkers maintain the maximum inter-filament spacing where cytosol can flow. This flow is not likely to be influenced by the bundle retrograde flow. We inspect now if the incoming flux would flow through these bundle spaces.

For this value of s , it is reasonable to assume that there is no outflowing of cytosol through the bundle interior. The entire outflow volume in the filopodium would come from fluid reorganization, with actin monomers removal from the cytoplasm realized by polymerization process. The question we approach here is: how would mass balance within the filopodium impact in- and outflowing matter and the supply of G-actins to filaments' tips?

To investigate this, the number of filaments is fixed as $N=50$. Molecules like profilin, Ena/VASP, and specially G-actins do not flow through inter-filament spaces due to their polarities and that of F-actin. Molecular polarity was not considered in the model. From these assumptions, we can perform simulations making:

$$S_{in} = S_{filop} - (N \times S_C) \quad (5.1)$$

or

$$S_{in} = pR^2L - NS_C L_o, \quad (5.2)$$

so that the cytoplasm inflows through the filopodial inner spaces except those occupied by F-actins.

Initial conditions are set for three situations:

- Only G-actins in the system
- G-actins and ABPs
- G-actins, ABPs, and motors

For each situation, we aimed to answer three questions.

1) Is the incoming volume of cytosol (mixture) equal to the volume of polymerized actins?

Answering this question shows if inflow and outflow volumes are in balance, satisfying mass conservation. The answer is “yes” just if the volumes are balanced during all the simulation time. A tolerance of 0.1 was set for the difference between those values to prevent approximation errors.

2) Is polymerization properly supplied by actin monomers?

This simulation calculates the percentage of cases where $N_p > N_{ret}$ (as in Section 2.2).

The answer is “yes” if polymerization is supplied during all the simulation time.

3) What is inflowing flux velocity?

Parameter to be compared with the results of other cases.

Then, the results of the computation were the following:

✓ Test “Only G-actins in the system”

1) *Is incoming volume of cytosol (mixture) equal to volume of polymerized actins?*

Yes, within the tolerance (difference in values: 0.01450312).

2) *Is polymerization properly supplied by actin monomers?*

No.

% of “yes”: 0.629 % of “no”: 99.371

3) *What is inflowing flux velocity?*

$$v_{in} = 0.508 \text{ nm} / \text{s}$$

✓ Test “G-actins and ABPs”

1) *Is incoming volume of cytosol (mixture) equal to volume of polymerized actins?*

Yes, within the tolerance (difference in values: 0.0195187).

2) *Is polymerization properly supplied by actin monomers?*

No.

% of “yes”: 0.853 % of “no”: 99.1467

3) *What is inflowing flux velocity?*

$$v_{in} = 0.676 \text{ nm} / \text{s}$$

✓ Test “G-actins, ABPs, and motors”

1) *Is incoming volume of cytosol (mixture) equal to volume of polymerized actins?*

Yes, within the tolerance (difference in values: 0.02379677).

2) *Is polymerization properly supplied by actin monomers?*

No.

% of “yes”: 1.056 % of “no”: 98.944

3) *What is inflowing flux velocity?*

$$v_{in} = 0.828 \text{ mm/s}$$

Analyzing these results, we conclude that polymerization is rarely supplied if there is no hydration. Even with the aid of regulators and motor proteins, the appropriate supply occurs only in the case of very mild filopodial protrusions ($L < 0.5 \text{ mm}$). There is a slight increase in the incoming fluid speed as polymerization is boosted by biological processes (compare question 3 of each test), due to the consequently higher volume removal. However, it has no influence and polymerization is still not properly supplied. Thus, the hypothesis of not having outflow of cytosol through bundle spaces in filopodia must be discarded.

5.3.2 Encapsulated outflow cytosol is a viable possibility

In the previous investigation, we tested a scenario that involves the absence of F-actin hydration. Likewise, we can establish a hypothesis for cases of total hydration, that is, $s = 0$. Imagine that the entire bundle is filled with water (colloid) associated with the filaments by hydration. In this situation, every volume that flows out of the filopodium is given by the filaments, and cytosol as a hydration shell that occupies the entire interior of the bundle and F-actin surroundings with same velocity as the retrograde flow.

For this, we consider that the encapsulated outflowing volume would be given by

$$V_{outflow} = V_{bundle} = 0.75 \times S_H \times N \times L_o \quad (5.3)$$

and outflows at the speed of the retrograde flow v_{ret} . The calculations aim to answer whether this dynamic is feasible in these terms.

The same initial conditions of the previous test are used in this one:

- Only G-actins in the system
- G-actins and ABPs
- G-actins, ABPs, and motors

For each situation, the computations seek to answer three questions.

1) Is incoming volume of cytosol (mixture) equal to volume of outflowing encapsulated bundle with hydration shells?

Answering this question shows if inflow and outflow volumes are in balance, satisfying mass conservation. The answer is “yes” just if the volumes are balanced during all the simulation time. A tolerance of 0.1 was set for the difference between those values to prevent approximation errors.

2) Is polymerization properly supplied by actin monomers?

This simulation calculates the percentage of cases where $N_p > N_{ret}$ (as in Section 2.2).

The answer is “yes” if polymerization is supplied during all the simulation time.

3) What is inflowing flux velocity?

Parameter to be compared with the results of other cases.

For simplicity, in this first approximation, we do not consider water molecules “bind-unbind” reactions with F-actins at any point of its length. As polymerization, hydration occurs at filaments’ tips. But since the initial filopodial length is zero, the bundle will be hydrated during the whole process. It was chosen $N = 30$ to perform this simulation.

Then, the results of the computation were the following:

✓ Test “Only G-actins in the system”

1) Is incoming volume of cytosol (mixture) equal to volume of outflowing encapsulated bundle with hydration shells?

Yes, within the tolerance (difference in values: 0.005455).

2) *Is polymerization properly supplied by actin monomers?*

No.

% of “yes”: 60.8 % of “no”: 39.2 (first “no” occurring at $C = 1.36 \mu\text{M}$)

3) *What is inflowing flux velocity?*

$$v_{in} = 0.509 \text{ nm} / s$$

✓ Test “Presence of actin binding proteins”

1) *Is incoming volume of cytosol (mixture) equal to volume of outflowing encapsulated bundle with hydration shells?*

Yes, within the tolerance (difference in values: 0.00423675).

2) *Is polymerization properly supplied by actin monomers?*

No.

% of “yes”: 81.5 % of “no”: 17.5 (first “no” occurring at $C = 1.78 \mu\text{M}$)

3) *What is inflowing flux velocity?*

$$v_{in} = 0.677 \text{ nm} / s$$

✓ Test “Presence of ABPs and active transport by motors”

1) *Is incoming volume of cytosol (mixture) equal to volume of outflowing encapsulated bundle with hydration shells?*

Yes, within the tolerance (difference in values: 0.00281771).

2) *Is polymerization properly supplied by actin monomers?*

Yes.

% of “yes”: 100.0 % of “no”: 0.0

3) *What is inflowing flux velocity?*

$$v_{in} = 0.83 \text{ nm} / s$$

The question 2 of the last test brings biologically relevant information that leads to further investigation. For the case where all biological interesting dynamic aspects are considered, we verify that the hydration of filaments may not be simply an osmotic cell control mechanism, but also sustains the flow of matter in filopodia. Hydration shells around filaments displacing together with the F-actins treadmilling process contribute to keep the balance of mass within the filopodium.

This assumption does not contradict the previous hypotheses and results, as well as the vast field of knowledge available in the literature. It gives us a perspective of extreme cytosol flow patterns – with or without total hydration. When the spaces in the bundle are larger, the total volume of outflow cytosol can be decomposed into a colloidal flux (whose speed tends to be much greater than v_{ret}) and hydration shells around filaments (flowing with speed v_{ret}). This further increases the inflow of molecules to support polymerization.

This is a novel and relevant finding, which paves the way for further mind-boggling investigations. This picture can be widely improved by simulating a completely particulate fluid representing colloidal water molecules flowing with charged actins and their regulators. In this case, the formation of the hydration shells can be simulated and to enhance the understanding of the previous analyzes proposed.

5.4 Influence of ABPs and active transport in filopodial growth

The purpose of this section is to evaluate specific scenarios of filopodial dynamics, where particular reacting particles are “*turned on*” or “*turned off*” to observe differences in system behavior. This leads to a deeper understanding the influence of the presence or absence of several combinations of actin-regulator molecules and by observing how the filopodium evolves in each case.

We investigate the influence of profilin, Ena/VASP, and/or motors in filopodial dynamics. Active transport by motors is analyzed only briefly by increasing the polymerization rate in 30%, as mentioned in Section 2.3 [103]. It is important to notice that some of these results have been discussed in the literature [5, 7, 41], although these previous efforts use exclusively diffusion as physical molecules transport mode. These simulations also demonstrate that our model is a viable tool to investigate these and similar biological interdependencies.

For reference, G-actin critical concentration C_{crit} is represented by a red line in the graphs. This parameter denotes the concentration of G-actin monomers at the tip which

polymerization rate is not supplied efficiently. This implies that the filopodial length fluctuates around L_{crit} , which is the length where the monomer concentration becomes C_{crit} . Filopodial length diminishes when $C > C_{crit}$ and elongates when $C < C_{crit}$ until more monomer to travel towards the tip. The G-actin critical concentration is defined and computed in Appendix 1.

The following results have comparable simulation times, which are shorter than the previous ones. This happens due to a slight difference in the way of computing time iterations. Also, the computational resource¹² presents difficulties to run long-time simulations or simulations with a larger number of particles. Thus, the number of particles is fixed $N_p = 1500$ particles. This is why the t_s in this section are shorter as well as the final filopodial length. The purpose here is to investigate the biological impact of molecular regulation in dynamics.

5.4.1 Basic filopodial model (Ena/VASP = ‘off’ and Profilin = ‘off’)

In this test, the main ABPs are not present. G-actins are responsible for the dynamics influenced solely by transport physical processes. The movement of particles occurs freely, that is, with no sequestration-type reactions. Polymerization occurs as long as the monomer concentration is enough to feed the filaments’ plus-ends. In Figures 5.29 and 5.30, the filopodial length varies for $t_{final} = 200$ and $t_{final} = 2000$. In both tests, $N = 30$ and $s = 12$.

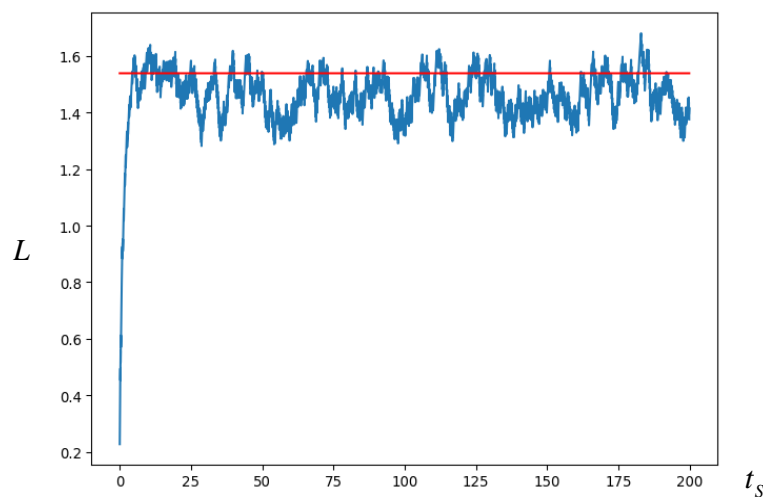


Figure 5.29: Filopodial length for $t_s = [0, 200]$. Red line represents the critical concentration, which is the fundamental parameter to limit the length of a filopodium when no biological regulation is present.

¹² Intel Core i5, 1 Tb HD, 8 Gb RAM, operational system Windows 10, coded in Python.

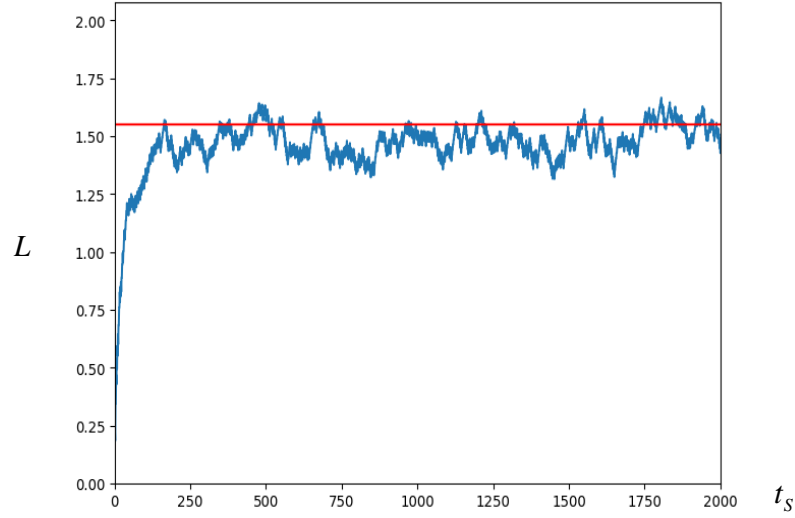


Figure 5.30: Filopodial length for $t_s = [0, 2000]$. Red line represents the critical concentration, which is the fundamental parameter to limit the length of a filopodium when no biological regulation is present. Longer simulations do not change the pattern of results.

Although these simulations comprise two different time ranges, the global pattern of length variation does not change considerably. In both situations, the relation between flow velocity and concentration acts as the limiting factor to elongation. Along the time range, the filopodial length fluctuates around L_{crit} where the critical concentration is reached. In both cases above, C_{crit} occurs when the filopodial length is approximately $L_{crit} = 1.57 \text{ nm}$.

5.4.2 Filopodial growth is improved (Ena/VASP = ‘on’ and Profilin = ‘on’)

In this test, we activate the dimerization actin-profilin (AP) and the association of Ena/VASP with filament tips to observe how the coupling of diffusion, drift, and ABP-regulation impact filopodial growth. Comparing Figure 5.31 with 5.29, we observe that these regulators enhance elongation of the filopodium, which reaches higher length values for the same simulation time. As in the previous test, we have $N = 30$ and $s = 12$.

For these parameters, the critical concentration threshold becomes higher than when computed without them (Section 5.4.1). The critical concentration occurs when filopodial length is $L_{crit} = 2.16 \text{ nm}$, which represents an increase of approximately 37.6%. From the results of Section 5.1, this is an expected outcome, with the presence of ABPs bringing more efficiency of elongation.

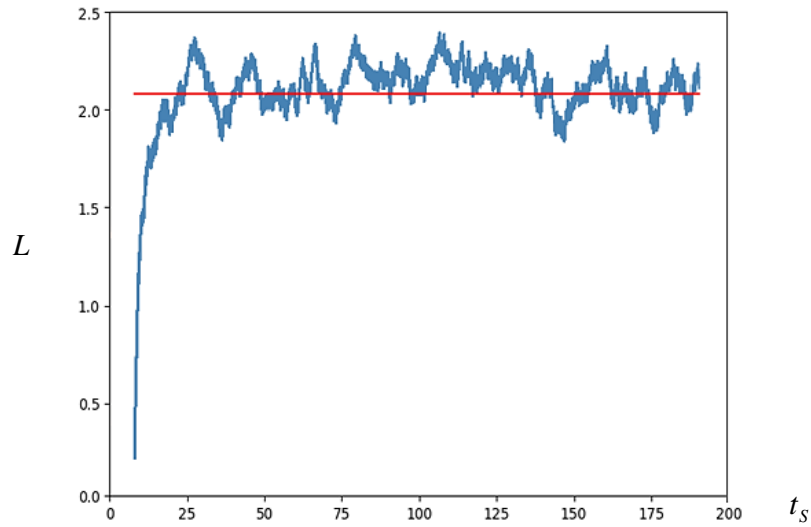


Figure 5.31: Filopodial length with mediation of profilin and Ena/VASP. Simulation with $t_s = [0, 200]$. Filopodial lengths are highly impacted by the regulating proteins of G-actins.

5.4.3 G-actin is sequestered (Ena/VASP = ‘off’ and Profilin = ‘on’)

The influence of profilin is better perceived in this test, where there is no Ena/VASP regulating the filament tips. Only free G-actin monomers can be polymerized, and not those in hetero-dimer AP. In this case, profilin produces a G-actin sequestration effect. This occurs because AP reactions prevent the polymerization of the profilin-dimerized G-actins when there is the impossibility of an EP reaction at the tips to perform actin polymerization. In Figure 5.32, different percentages of moving hetero-dimers AP are tested. The black line marks $x = 0$.

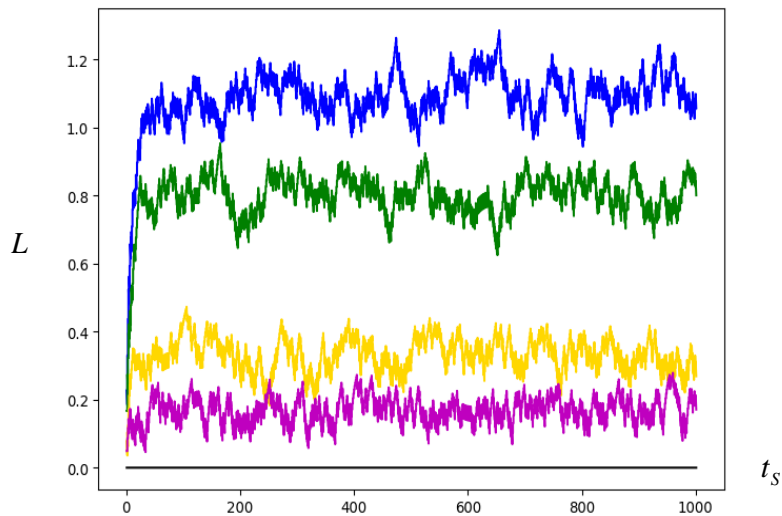


Figure 5.32: Influence of profilin. Four values for percent of actin sequestration due to the AP reactions were tested: in blue, 0% (all the G-actins are free); in green, 20%; in yellow, 50%; and in magenta, 60%. As more G-actins are in association with profilin, less actins are polymerized, which shortens filopodial length. Simulation with $t_s = [0, 1000]$.

Close to 70% of sequestration, filopodial length approaches to zero, almost stops polymerization, and prevents elongation. In Figure 5.33, a new simulation with same parameters as those in Figure 5.29, but with 70% of sequestration (in magenta). Notice that at some points, $L < 0$. Obviously, in biological context, it does not make sense, since $L = 0$ may already result in a complete filopodial extinction. But we intended to show that this behavior is present during the whole simulation. The black line marks $x = 0$.

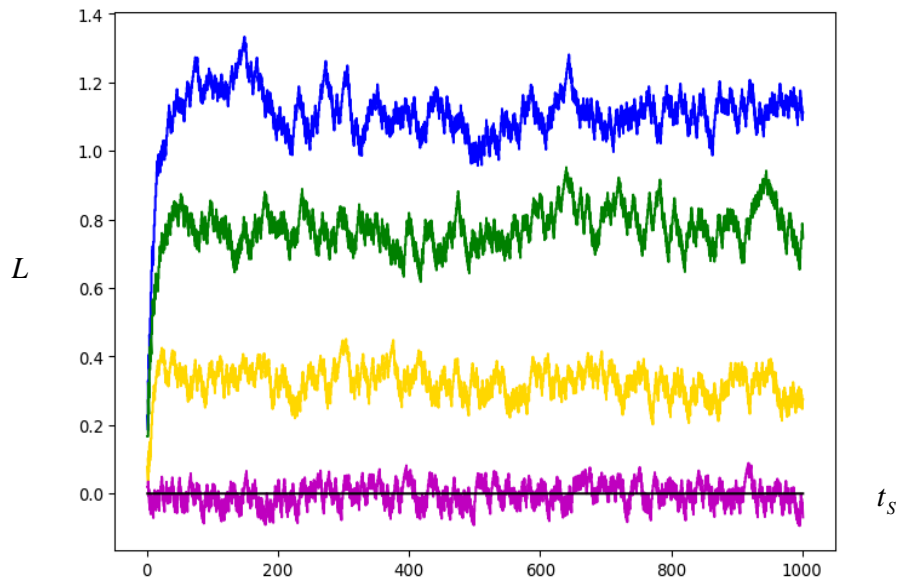


Figure 5.33: Influence of profilin and filopodial extinction. Values for percent of actin sequestration: in blue, 0%; in green, 20%; in yellow, 50%; and in magenta, 70%. Simulation with $t_s = [0, 1000]$.

5.4.4 Decrease in polymerization rate (Ena/VASP = ‘on’ and Profilin = ‘off’)

When Ena/VASP regulates filament tips, G-actin are only polymerized when it is bonded with profilin. In this test, AP reactions do not occur throughout the domain as well as no hetero-dimer AP are dispersed in the cytosol. Ena/VASP is suspended in fluid and reacts with the F-actin tips at a fixed time $t_s = 100$ chosen previously. From that moment on, the filopodium length rapidly contract. Figure 5.34 shows a simulation of this described situation.

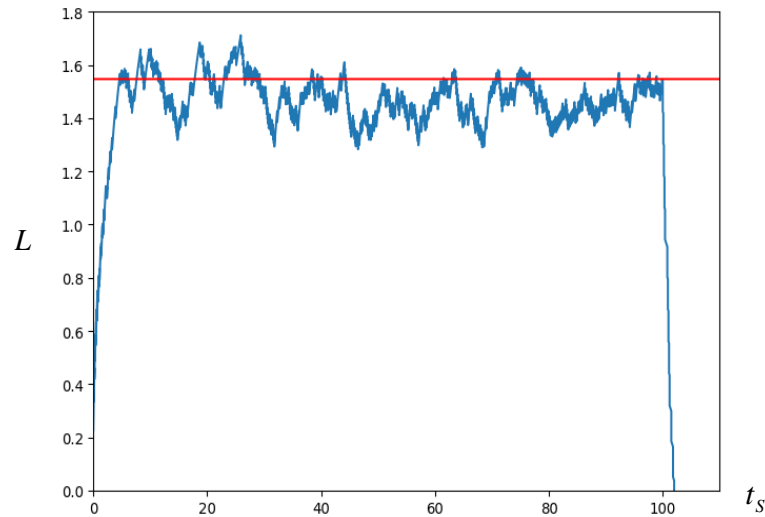


Figure 5.34: Ena/VASP regulating bundle tip with no profilin in the system. In this test, just G-actins are dispersed in the fluid and it is simulated a binding of Ena/VASP in bundle tip at $t_s = 100$. It causes a rapid reduction of polymerization if we consider that G-actin must be in a hetero-dimer with profilin to react with Ena/VASP and, as consequence, polymerize actin monomers.

In Figure 5.35, it is supposed a hybrid hypothesis between this test and that in Section 5.4.3. Consider that an amount of profilin dispersed in the fluid performs $P\%$ of G-actin sequestration and Ena/VASP molecules start to regulate F-actin tips from a certain moment. With this new input, $(1 - P)\%$ of G-actin monomers are polymerized, while $P\%$ remains bonded into hetero-dimers AP. From the moment that Ena/VASP binds to the tips, $P\%$ of profilin-bonded actins are polymerized, while $(1 - P)\%$ of them remains sequestered. The following figure shows this situation for different values of P .

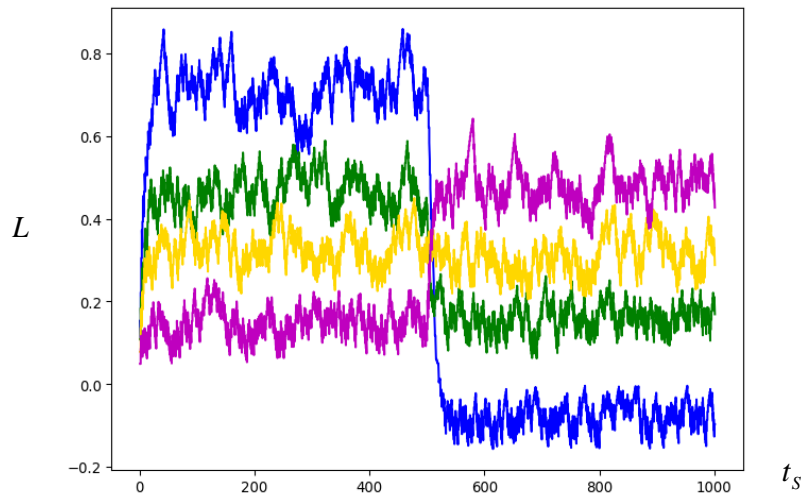


Figure 5.35: Ena/VASP molecules regulating bundle tip with profilin in the system. Values for percent of actin sequestration: in blue, 25%; in green, 40%; in yellow, 50%; and in magenta, 60%. Simulation with $t_s = [0, 1000]$ and Ena/VASP binding tip at $t_s = 500$.

5.4.5 Motors have a quite relevant contribution

(Active transport = ‘on’, Ena/VASP = ‘off’, Profilin = ‘off’)

Motors have their contribution visualized in this test. Even without other regulation modes, G-actin delivery is enhanced by active transport. The following results show filopodial length evolution with the same parameters as those in Section 5.4.1, but including motors in the system. We observe that L reaches a maximum value of around 27 - 30% higher compared with the simulation without them, which is in agreement with [103] about motors that do not contribute much more than 30% in actin delivery.

The contribution of 30% in polymerization rate was set as an input to the model. Figure 5.36 exhibits the evolution of the filopodial length values; in (a) for $t_s = [0, 200]$ and in (b) for $t_s = [0, 2000]$. This makes them comparable to those results in Section 5.4.1, which is presented in Table 9.

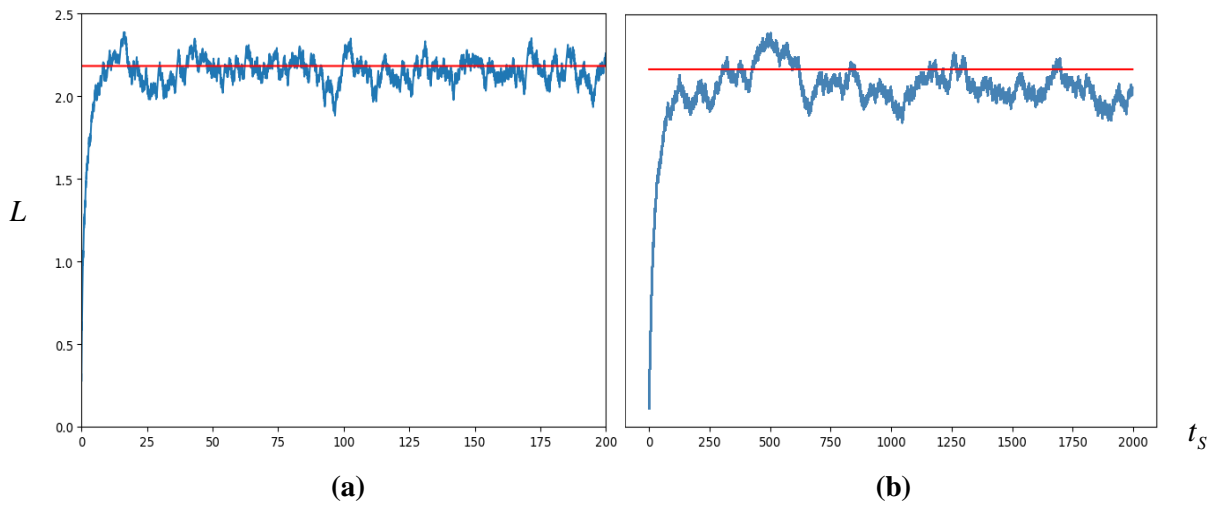


Figure 5.36: Influence of active transport in filopodial length, for $t_s = [0, 200]$ in (a) and for $t_s = [0, 2000]$ in (b). Comparing with test 5.4.1, for the same t_s , filopodial length has an increase of almost 30%, according to data in the literature.

Table 9 below shows that motors contribute around 30% in G-actin delivery to polymerization. The following data compares minimum (L_{min}), maximum (L_{max}), and critical lengths (L for C_{crit}) of the corresponding simulations in this test and those in Section 5.4.1, with an estimate of elongation (in %) in the presence of motors.

Table 10: Contribution of active transport in filopodial elongation. Lengths are in micrometers.

Time	Length	In (5.4.1)	In (5.4.5)	% of increase
200 (Figs. 5.26 and 5.33)	L_{min}	1.22	1.85	29.48
	L_{max}	1.73	2.39	27.62
	L_{crit}	1.55	2.17	28.57
2000 (Figs. 5.27 and 5.34)	L_{min}	1.32	1.88	29.79
	L_{max}	1.67	2.37	29.34
	L_{crit}	1.55	2.19	29.22

5.4.6 Coupling all modeled filopodia aspects leads to consistent elongation (Active transport = ‘on’, Ena/VASP = ‘on’, and Profilin = ‘on’)

In this test, the physical transport phenomena and the biological regulation processes considered in the model are simulated: molecules driven by diffusion and drift towards the tip, regulated by Ena/VASP and profilin, and counting with the contribution of active transport by motors.

As the critical concentration is computed by considering solely diffusion and drift, C_{crit} value is overtaken by the G-actin supply when biological regulators (including motors) are coupled. In fact, C_{crit} is updated and becomes higher, thus enhancing filopodial growth. Besides that, motors motion does not depend on fluid flow exclusively, but on “bind-unbind” reactions between their tails and F-actins. This justifies an increase in the G-actin supply beyond the updated critical concentration affords.

Figure 5.37 show filopodial length evolution for $t_s = [0, 2000]$. The red line indicates L_{crit} computed without biological regulation.

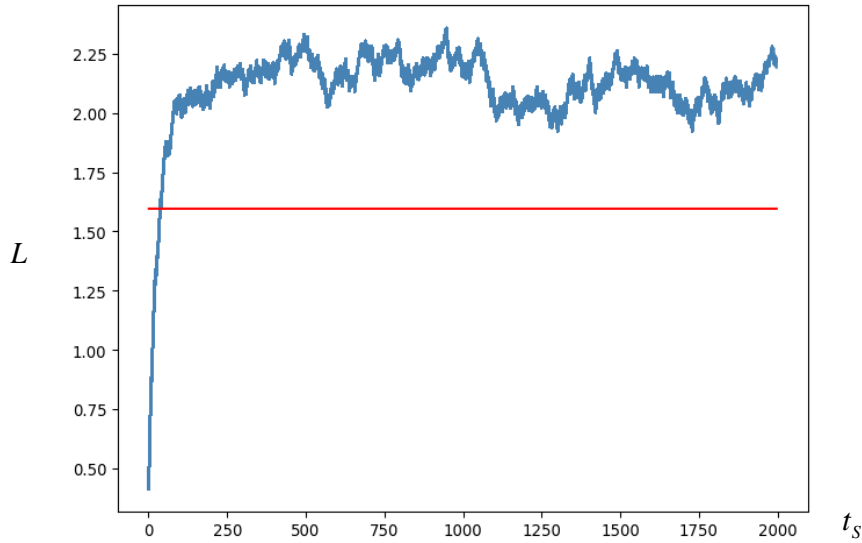


Figure 5.37: Actin regulators and active transport influence in filopodial length. Time is in the range $t_s = [0, 2000]$, represented in the x -axis, and y -axis representing L , in micrometers. The red line shows L_{crit} computed without biological regulation. Filopodial growth is improved 31.84% in comparison with the results in Section 5.4.1, for the same time of simulation.

In this case, the filopodial maximum length increases in 31.84% compared to the results in Section 5.4.1 and 3.26% to those in Section 5.4.5, for $t_s = [0, 2000]$. This expresses a quite decisive influence of active transport, mainly because it does not depend on the filopodial configuration parameters (as N , s , or L itself). Instead limited, active transport by motors provides an approximately constant rate of G-actin delivery to polymerization.

CONCLUSIONS AND FUTURE WORK

Biology has on laboratory experiments its main way to gain knowledge through research results. But, in specific cases, methods are limited in their accuracy or there is low feasibility in performing some essays. To unravel the complexity of biological issues, mathematical modeling and computational simulations rise as efficient tools in this process and may significantly complement experimental investigation. Hence, works have been published on several biological fields coupling those approaches to enhance biological comprehension, and sometimes with relevant medical applications.

For example, actin cytoskeleton is a critical regulator of cytoplasmic architecture and mechanics. It has extreme importance in mediating axon growth and its maintenance, which brings implications for neural development, aging, regeneration, and degeneration. However, cytoskeletal machinery is highly intricate and dynamic. So, in this context, a good starting point is to observe the regulation of actin dynamics within very simple, finger-like structures called filopodia, which protrude at the plasma membrane leading edge of growing neurons or migrating cells. Due to this, the present work focused on formulating a novel approach to computationally simulate aspects of filopodial dynamics.

In the description of the matter flow inside filopodia, it was proposed the addition of cytoplasm flow advective effects (drift) to diffusion as a combined physical transport phenomenon of molecules suspended on cytosol. That is justified by the biological knowledge that volume is withdrawn from the filopodia, providing a pump mechanism for compensatory inflow. From that, this research intended to approach some open questions, such as: (1) relations between the number of filaments in the bundle and several physical parameters, like flow velocity, G-actin concentration, elongation–retraction of the filopodia, inter-filament spacing, and others; (2) the influence of Actin Binding Proteins on filopodial dynamics; and (3) how the outward movement of the filament bundle affects the laminar inward flow.

During simulations, we took into account that filopodial behavior resembles flow in highly flexible pipes as well that they always show a swift adaptation to regulatory stimuli. Thus, to better describe molecular motion and flow properties were required a multi-scale particle-based scheme. Particles movement could be properly simulated with Brownian motion, with its reactions occurring dynamically through the domain. In this way, the modeling multi-scaling feature allows us to treat cytosol fluid as a mixture of molecules like it really is.

Mathematically, the proposed model has a stochastic bias, because we agree that for the determined purposes it would be a better mean to obtain results in both molecular and flow

visualization scales. The questions addressed required individual relations and displacements to be considered, without neglecting the overall behavior. In this way, the movements of the particles are calculated individually, with reactions occurring dynamically according to experimental parameters, for later acquisition of physical and mechanical effects that emerge from the molecular interactions. It is also important to highlight the tendency perceived in the literature to work with deterministic models and this research collaborates in the other direction.

Then, the model proposed here provides us the possibility to experiment a wide range of hypotheses. This is the main contribution of this work: the production of a tool containing a variety of joint concepts and capable to grow filopodia up to almost 40 μm in length. All these features are unusual to find in the literature. In the future, other parameters can be introduced into the model and more ABPs may have their effects studied based on a proper description of them as new computational objects. Also, the model can be improved in order to deeply investigate problems that we had briefly approached in this work.

For example, at the tip of the filament bundle, the mixture-flow bends in the direction of the polymerization site, guided by the molecular organization around it, where the incoming G-actins are incorporated through polymerization into the backflowing F-actin bundle. The bending flow might even produce outward forces in the membrane that could further help sustain its shape. The data obtained in the first application of this work may be a starting point to unravel this question. As mentioned in the text, improvements, in order to simulate water molecules displacement, would provide an opportunity to better understand the hydration process and its influence on the dynamics of filopodia.

The model presented brought adaptations of some cited works, but also insertions of an authorial nature, aiming to answer the proposed questions and open space to approach other related problems. However, models can be improved, refined, and have their efficiency significantly increased or with a focus on solving other problems. Therefore, several simplifications or choices that were made in this model development can be explored in next works. Each new addition can be studied individually, for the purpose of comparison with the previous modeling step, constituting a source of great exploration of the effects that new parameters would cause in the entire system.

More possibilities that can be explored in this model through minor changes or additions which we can mention are: simulation of physical collisions during the displacement of the molecules; dynamic alteration of the links positions in the bundle formation; description of water molecules causing the volume to be entirely particulate; exchange the moving method of particles for stochastic differential equations; among others. A new model with three-

dimensional domain can give a good new perspective of the analyzes carried out in this work and the use of cylindrical coordinates might be useful. Furthermore, according to this research, investigations of flow interacting with the plasma membrane at the tip of the filament is an issue that has not received enough attention in the literature. Depending on the complexity that the model description reaches, parallel-wise computation should be required.

A key prerequisite for successful modeling is the existence of biological data and concepts/cartoon models. Since there is no single cellular system used in biological research which would alone provide sufficient insights and experimental data, the only feasible strategy to develop conceptual models for filopodial dynamics is to integrate mechanistic conclusions obtained from a wide range of very different cellular systems [30, 35, 57, 62, 65].

However, this approach can be misleading since the properties of filopodia may vary between animal species and cell types. Ideally, it would be desirable to have a single and standardized experimental system so that data and mechanistic concepts can be reliably integrated. This would enormously facilitate the experimental validation of predictions made from mathematical modeling, especially if these predictions concern the interface between different parameters or elements.

As biological systems suitable for studying filopodia, growth cones are particularly well suited since they are rich in actin networks and reliably display filopodia as a prominent and functionally important structural feature [21, 36]. Growth cones are the motile tips of growing axons, the long and slender processes of nerve cells which form the cables that wire the nervous system. To lay these cables during development or regeneration, the growth cones at their tips navigate along specified paths, and their prominent filopodia act as sensors facilitating proper navigation [89]. Apart from the fact that growth cones display prominent filopodia with a clearly defined function, there is a good conceptual understanding of the fundamental roles that actin plays in growth cones, and their actin machinery is well investigated in this context [70, 73].

A promising biological model might be provided by growth cones of the fruit fly *Drosophila melanogaster* which are accessible to detailed studies of the cytoskeleton and systematic genetic dissections of its various regulators [87, 89, 90]. For example, a systematic study used filopodial number and length as a simple readout to understand the systemic contributions and functional interfaces of seven different ABPs, which included formins, Ena/VASP, profilin, and capping proteins.

Besides, flies and humans have common evolutionary roots and 75% of human disease genes have a match close enough to be studied in flies (Figure 6.1). It often inspires and

enormously accelerates research on these genes in mice or even humans. This clearly demonstrated how *Drosophila* growth cones can be used to deduce cartoon models of filopodial dynamics [78, 90]. Given the relative speed and ease with which experiments can be carried out in *Drosophila* neurons, this system is ideal for partnering up with the mathematical/computational modeling of filopodial dynamics [87].

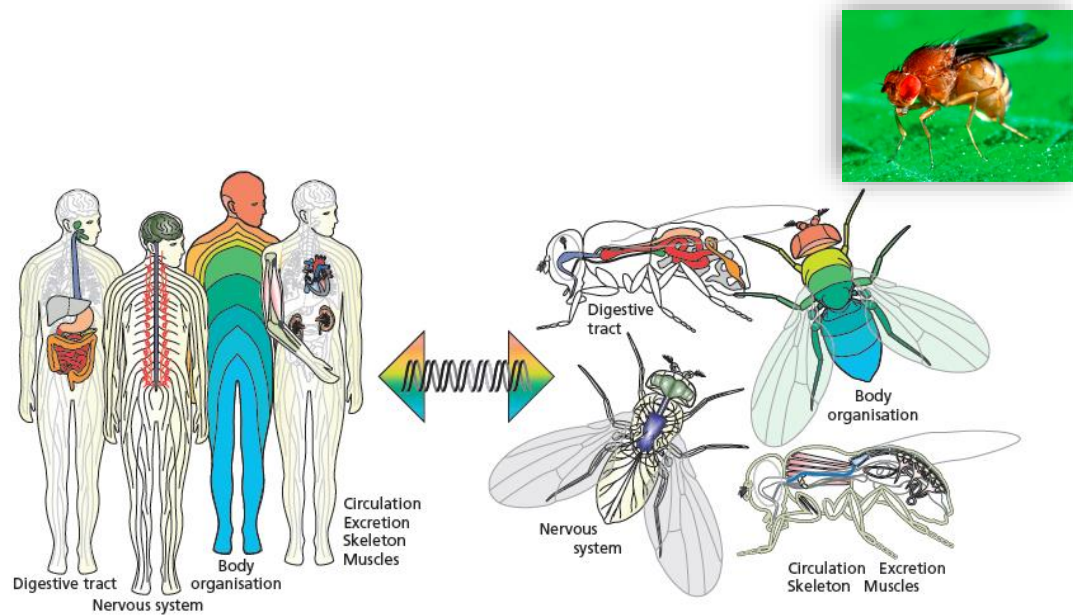


Figure 6.1: *Drosophila* as a versatile biological model to study filopodial dynamics. Research in *Drosophila* (in detail) is fast and has practical advantages at many levels of the investigative process. For most human organs there is a match in flies, and common genes tend to regulate their development, organization, and function. Image¹³ kindly provided by A. Prokop.

Understanding cytoskeletal dynamics, in particular in filopodia, has extreme clinical relevance. The elongated shape of filopodia suggests sensory and exploratory functions. In neuronal growth, this role guides axons contact of nearby cells in order to establish early synapses. Complete comprehension of this process may help to develop mechanisms to minimize the damage of diseases such as epilepsy or Alzheimer's. In non-nerve cells, but with a migratory characteristic, growth and mobility of these protrusions can impact on pathologies related since embryonic development to cancer metastasis.

More recently, research findings showed that actively polymerized filopodia are exploited during virus entry, trafficking, spread, and development of viral pathologies. These observations have caused a surge in investigating this fact and now it is clear that filopodia can provide unique opportunities for many viruses to invade host cells and that may subsidize

¹³ Available at [https://www.research.manchester.ac.uk/portal/en/publications/fruit-flies-in-biological-research\(9addecf9-d08c-4950-9c5b-ded33f67f397\).html](https://www.research.manchester.ac.uk/portal/en/publications/fruit-flies-in-biological-research(9addecf9-d08c-4950-9c5b-ded33f67f397).html)

discussions of future therapeutic possibilities [12]. Additionally, the way filopodia in migrating cells explore their surrounding during motion is one target of research in tissue engineering, which deals with replacement or regeneration of cells and tissues, or restoration of organs normal function.

Thereby, we realize the high complexity of this natural system, which has its own mechanisms of self-regulation, response to chemical stimuli, and mechanical effects that play vital roles for cellular functions. Researching the physicochemical processes involved by combining computational methods with laboratory experiments allows us to advance in its understanding and seeking applications. Even with a vast literature available, there is still a long way to go through, either in the formulation of new approaches or in the acquisition of new data. And when it means to make progress towards curing so challenging diseases for the human condition, efforts should not be spared. This is the beauty of the human gift that drives us to scientifically unravel the mysterious phenomena of Nature.

REFERENCES

- [1] Alberts, B., Johnson, A., Lewis, J., Raff, M., Roberts, K., and Walter, P. Molecular Biology of the Cell. New York: Garland Science (2002).
- [2] Atilgan, E., *et al.* Mechanics and dynamics of actin-driven thin membrane protrusions. Biophysical Journal vol. 90,1, 65-76 (2006).
- [3] Baines, A.J. The spectrin-ankyrin-4.1-adducin membrane skeleton: adapting eukaryotic cells to the demands of animal life. Protoplasma 244 (2010).
- [4] Bathe, M., Heussinger, C., Claessens, M.M., Bausch, A.R., Frey, E. Cytoskeletal bundle mechanics. J. Biophys. 94, 2955-2964 (2008).
- [5] Bear, J.E., Gertler, F.B. Ena/VASP: towards resolving a pointed controversy at the barbed end. J. Cell Sci. 122 (2009).
- [6] Bindschadler, M., Osborn, E.A., McGrath, J.L. A mechanistic model of the actin cycle. Biophys J. 86(5), 2720-2739 (2004).
- [7] Birbach, A. Profilin, a multi-modal regulator of neuronal plasticity. Bioessays 30 (2008).
- [8] Blagoev, K.B., Shukla, K., Levine, H. We need theoretical physics approaches to study living systems. Phys. Biol. 10, 040,201 (2pp) (2013).
- [9] Blanchoin, L., Boujemaa-Paterski, R., Plastino, C.S.J. Actin dynamics, architecture, and mechanics in cell motility. Physiol. Rev. 94 (2014).
- [10] Breitsprecher, D., Goode, B.L. Formins at a glance. J. Cell Sci. 126, 1-7 (2013).
- [11] Carlsson, A.E. Actin dynamics: from nanoscale to microscale. Ann. Rev. Biophys. 39, 91-110 (2010).
- [12] Chang, K., Baginski, J., Hassan, S.F., Volin, M., Shukla, D., and Tiwari, V. Filopodia and Viruses: An Analysis of Membrane Processes in Entry Mechanisms. Front. Microbiol. 7:300 (2016).
- [13] Chesarone, M.A., Goode, B.L. Actin nucleation and elongation factors: mechanisms and interplay. Curr. Opin. Cell Biol. 21, 28-37 (2009).
- [14] Cohen, J.E. Mathematics is biology's next microscope, only better; biology is mathematics' next physics, only better. PLoS. Biol. 2, e439 (2004).
- [15] Collart-Dutilleul, P., *et al.* Initial stem cell adhesion on porous silicon surface: molecular architecture of actin cytoskeleton and filopodial growth. Nanoscale Res. Lett. 9, 564 (2014).
- [16] Cooper, G.M. The Cell: A Molecular Approach. 2nd edition. Sunderland (MA): Sinauer Associates. Structure and Organization of Actin Filaments (2000).

- [17] Copley, A.L. Hemorheology and Ischemia. In: Zülch K.J., Kaufmann W., Hossmann KA., Hossmann V. (eds) Brain and Heart Infarct II. Springer, Berlin, Heidelberg (1979).
- [18] Dawes, A.T., Ermentrout, G.B., Cytrynbaum, E.N., Edelstein-Keshet, L. Actin filament branching and protrusion velocity in a simple 1d model of a motile cell. *J. Theor. Biol.* 242, 265-279 (2006).
- [19] Demirdzic, I., Peric, M. Finite volume method for prediction of fluid flow in arbitrarily shaped domains with moving boundaries. *Int. J. Numer. Methods Fluids* 10, 771-790 (1990).
- [20] Dent, E.W., Gertler, F.B. Cytoskeletal Dynamics and Transport in Growth Cone Motility and Axon Guidance. *Neuron*. Volume 40, Issue 2, Pages 209-227 (2003).
- [21] Dent, E.W., Gupton, S.L., Gertler, F.B. The growth cone cytoskeleton in axon outgrowth and guidance. *Cold Spring Harb. Perspect. Biol.* 3, a001, 800 (2011).
- [22] De Vos, K.J., Grierson, A.J., Ackerley, S., Miller, C.C.J. Role of Axonal Transport in Neurodegenerative Diseases. *Annual Review of Neuroscience* 31:1, 151-173 (2008).
- [23] Ditlev, J.A., Mayer, B.J., Loew, L.M. There is more than one way to model an elephant. Experiment-driven modeling of the actin cytoskeleton. *Biophys. J.* 104, 520-532 (2013).
- [24] Dumas, D., *et al.* Membrane Fluidity and Oxygen Diffusion in Cholesterol-enriched Endothelial Cells. 1 Jan.: 255-261 (1999).
- [25] Edidin, M. Lipids on the frontier: a century of cell membrane bilayers. *Nature Rev. Mol. Cell Biol.* 4, 414-418 (2003).
- [26] Edwards, M., Zwolak, A., Schafer, D.A., Sept, D., Dominguez, R., Cooper, J.A. Capping protein regulators fine-tune actin assembly dynamics. *Nat. Rev. Mol. Cell Biol.* 15, 677-689 (2014).
- [27] Eltsov, M., Dubé, N., Yu, Z. *et al.* Quantitative analysis of cytoskeletal reorganization during epithelial tissue sealing by large-volume electron tomography. *Nat. Cell Biol.* 17, 605-614 (2015).
- [28] Erban, R., Flegg, M.B., Papoian, G.A. Multiscale stochastic reaction-diffusion modeling: application to actin dynamics in filopodia. *Bull. Math. Biol.* 76, 799-818 (2014).
- [29] Evans, M., Harlow, F.H. The particle-in-cell method for hydrodynamic calculations. Technical Report, LA-2139, 73p. Los Alamos Scientific Laboratory, New Mexico (1957).
- [30] Faix, J., Breitsprecher, D., Stradal, T.E.B., Rottner, K. Filopodia: complex models for simple rods. *Int. J. Biochem. Cell Biol.* 41(8-9), 1656-1664 (2009).
- [31] Fife, C.M., McCarroll, J.A., and Kavallaris, M. Cytoskeleton and cancer metastasis. *Br. J. Pharmacol.*, 171: 5507-5523 (2014).
- [32] Fletcher, D.A., Mullins, R.D. Cell mechanics and the cytoskeleton. *Nature* 463, 485-492 (2010).

- [33] Fujiwara, I., Vavylonis, D., Pollard, T.D. Polymerization kinetics of adp-and adp-pi-actin determined by fluorescence microscopy. *Proc. Natl. Acad. Sci. USA* 104, 8827-8832 (2007).
- [34] Fuller, N., Rand, R.P. Water in Actin Polymerization. *Biophysical Journal*, Volume 76, Issue 6, Pages 3261-3266 (1999).
- [35] Gallo, G. Mechanisms underlying the initiation and dynamics of neuronal filopodia: from neurite formation to synaptogenesis. *Int. Rev. Cell. Mol. Biol.* 301, 95-156 (2013).
- [36] Gomez, T.M., Letourneau, P.C. Actin dynamics in growth cone motility and navigation. *J. Neurochem.* 129(2), 221-234 (2013).
- [37] Grazi, E. What is the diameter of the actin filament?, *FEBS Letters*. Volume 405, Issue 3, Pages 249-252 (1997).
- [38] Gunawardena, J. Beware the tail that wags the dog: informal and formal models in biology. *Mol. Biol. Cell.* 25, 3441-4 (2014).
- [39] Gunawardena, J. Models in biology: accurate descriptions of our pathetic thinking. *BMC Biol.* 12, 29 (2014).
- [40] Hahn, I., Voelzmann, A., Liew, Y.-T., Costa-Gomes, B., Prokop, A. The model of local axon homeostasis - explaining the role and regulation of microtubule bundles in axon maintenance and pathology. *Neural Dev.* 14 (2019).
- [41] Harker, A.J., *et al.* Ena/VASP processive elongation is modulated by avidity on actin filaments bundled by the filopodia cross-linker fascin. *Molecular Biology of the Cell* 30:7, 851-862 (2019).
- [42] Herrmann, H., Aebi, U. Intermediate Filaments: Structure and Assembly. *Cold Spring Harbor Perspectives in Biology*. 8 (2016).
- [43] Islam, M.A. Einstein-Smoluchowski diffusion equation: a discussion. *Phys. Scripta* 70, 120-125 (2004).
- [44] Janmey, P.A., McCulloch, C.A. Cell mechanics: integrating cell responses to mechanical stimuli. *Annu. Rev. Biomed. Eng.*, 9: 1-34 (2007).
- [45] Jansen, S., *et al.* Mechanism of actin filament bundling by fascin. *The Journal of Biological Chemistry* vol. 286, 34:30087-96 (2011).
- [46] Jasnin, M., *et al.* Actin filament architecture in comet tails. *Proceedings of the National Academy of Sciences*, 110 (51) 20521-20526 (2013).
- [47] Kabir, S.R., *et al.* Hyper-mobile water is induced around actin filaments. *Biophysical Journal*. Vol. 85, 5: 3154-61 (2003).
- [48] Katz, M.M., Hargens, A.R., Garfin, S.R. Diffusion versus convection. Intervertebral disc nutrition. *Clin. Orthop. Relat. Res.* Sep 243-245 (1986).

- [49] Kucik, D.F., Elson, E.L., Sheetz, M.P. Forward transport of glycoproteins on leading lamellipodia in locomoting cells. *Nature* 340, 315-317 (1989).
- [50] Kumar, S., Mansson, A. Covalent and non-covalent chemical engineering of actin for biotechnological applications. *Biotechnology Advances*. Volume 35, Issue 7, Pages 867-888 (2017).
- [51] Lan, Y., Papoian, G. The stochastic dynamics of filopodial growth. *Biophys. J.* 94, 3839-3852 (2008).
- [52] Liu, C., Zhigang, L. On the validity of the Navier-Stokes equations for nanoscale liquid flows: the role of channel size. *AIP Adv.* 1, 032, 108 (2011).
- [53] Mallavarapu, A., Mitchison, T. Regulated actin cytoskeleton assembly at filopodium tips controls their extension and retraction. *J. Cell. Biol.*, 146, pp. 1097-110 (1999).
- [54] Matsudara, P.T., Burgess, D.R. Identification and organization of the components in the isolated microvillus cytoskeleton. *The Journal of Cell Biology* vol. 83, n. 3, p. 667-673 (1979).
- [55] Matsuo, T., *et al.* Difference in the hydration water mobility around F-actin and myosin subfragment-1 studied by quasielastic neutron scattering. *Biochemistry and Biophysics Reports* vol. 6, 220-225 (2016).
- [56] Mattila, P.K., Lappalainen, P. Filopodia: molecular architecture and cellular functions. *Nat. Rev. Mol. Cell. Biol.* 9, 446-54 (2008).
- [57] McGrath, J.L., Tardy, Y., Dewey, C.F., Meister, J.J., Hartwig, J.H. Simultaneous measurements of actin filament turnover, filament fraction, and monomer diffusion in endothelial cells. *Biophys. J.* 75, 2070-2078 (1998).
- [58] McMurray, C. Neurodegeneration: diseases of the cytoskeleton?. *Cell Death Differ.* 7, 861-865 (2000).
- [59] Mellor, H. The role of formins in filopodia formation. *Biochim. Biophys. Acta* 1803(2), 191-200 (2009).
- [60] Mescher, A. Junqueira's Basic Histology Text & Atlas, 14 ed.: Lange (2016).
- [61] Mitchison, T.J., *et al.* Actin-Based Cell Motility and Cell Locomotion. *Cell*, Volume 84, Issue 3, 371-379 (1996).
- [62] Mogilner, A., Edelstein-Keshet, L. Regulation of actin dynamics in rapidly moving cells: a quantitative analysis. *Biophys. J.* 83, 1237-1258 (2002).
- [63] Mogilner, A., Oster, G. Cell motility driven by actin polymerization. *Biophys. J.* 71, 3030-3045 (1996).
- [64] Mogilner, A., Rubinstein, B. The physics of filopodial protrusion. *Biophys. J.* 89, 782-795 (2005).

- [65] Mogilner, A., Allard, J., Wollman, R. Cell polarity: quantitative modeling as a tool in cell biology. *Science* 336, 175-179 (2012).
- [66] Mörters, P., Peres, Y. Brownian motion. Cambridge University Press vol. 30, pg. 2 (2010).
- [67] Moura, C.A. de, Kritz, M.V., Leal, T.F., Prokop, A. Mathematical-Computational Simulation of Cytoskeletal Dynamics In: *Mathematical Modeling and Computational Intelligence in Engineering Applications*. 1 ed.: Springer-Verlag, p. 15-36 (2016).
- [68] Mullins, R.D., Hansen, S.D. *In vitro* studies of actin filament and network dynamics. *Curr. Opin. Cell Biol.* 25, 6-13 (2013).
- [69] Novak, I.L., Slepchenko, B.M., Mogilner, A. Quantitative analysis of G-actin transport in motile cells. *Biophysical Journal*, 95(4), 1627-1638 (2008).
- [70] Oosawa, F., Asakura, S., Ooi, T. G-F transformation of actin as a fibrous condensation. *J. Polym. Sci.* 37, 323-336 (1959).
- [71] Oshima, H., Hayashi, T., Kinoshita, M. Essential Roles of Water in Actin-Myosin Binding. *Biophysical Journal*. Volume 110, Issue 3, 300a (2016).
- [72] Oshima, H., Hayashi, T., Kinoshita, M. Statistical Thermodynamics for Actin-Myosin Binding: The Crucial Importance of Hydration Effects. *Biophysical Journal*, 110(11), 2496–2506 (2016).
- [73] Othmer, H. Actin cytoskeleton, multi-scale modeling. In: Engquist, B. (ed.) *Encyclopedia of Applied and Computational Mathematics*, pp. 17-23. Springer, Berlin/Heidelberg (2015).
- [74] Pak, C.W., Flynn, K.C., Bamberg, J.R. Actin-binding proteins take the reins in growth cones. *Nat. Rev. Neurosci.* 9, 136-47 (2008).
- [75] Perelson, A.S., Coutias, E.A. A moving boundary model of acrosomal elongation. *J. Math. Biol.* 23, 361-379 (1986).
- [76] Perrin, J.B. Facts. NobelPrize.org. Nobel Media AB. Accessed: Mar 14th (2020). Available at: <https://www.nobelprize.org/prizes/physics/1926/perrin/facts/>
- [77] Peskin, C.S., Odell, G.M., Oster, G.F. Cellular motions and thermal fluctuations: the Brownian ratchet. *Biophys. J.* 65, 316-324 (1993).
- [78] Pimentel, C.G., Gombos, R., Mihály, J., Sánchez-Soriano, N., Prokop, A. Dissecting regulatory networks of filopodia formation in a *Drosophila* growth cone model. *PLoS. One* 6, e18, 340 (2011).
- [79] Pollard, T.D. Regulation of actin filament assembly by arp2/3 complex and formins. *Ann. Rev. Biophys. Biomol. Struct.* 36, 451-477 (2007).
- [80] Pollard T.D, Borisy G.G. Cellular motility driven by assembly and disassembly of actin filaments. *Cell*. Feb 21 112(4):453-65 (2003).

- [81] Pollard, T.D., Cooper, J.A. Actin and actin-binding proteins. a critical evaluation of mechanisms and functions. *Ann. Rev. Biochem.* 55, 987-1035 (1986).
- [82] Pollard, T.D., Goldman, R.D. Overview of the cytoskeleton from an evolutionary perspective. *Cold Spring Harbor perspectives in biology* 10.7 (2018).
- [83] Portera-Cailliau, C., Yuste, R. Sobre la función de los filopodios dendríticos. *Rev. Neurol.* 33 (12), 1158-1166 (2001).
- [84] Potter, D. *Computational Physics*. Wiley, New York (1973).
- [85] Prokop, A., Beaven, R., Qu, Y., Sánchez-Soriano, N. Using fly genetics to dissect the cytoskeletal machinery of neurons during axonal growth and maintenance. *J. Cell Sci.* 126, 2331-41 (2013).
- [86] Prokop, A., Sánchez-Soriano, N., Calves Pimentel, C.G., Molnár, I., Kalmar, T., Mihály, J. DAAM family members leading a novel path into formin research. *Commun. Integr. Biol.* 4, 538-542 (2011).
- [87] Prokop, A., Küppers-Munther, B., Sánchez-Soriano, N. Using primary neuron cultures of *Drosophila* to analyse neuronal circuit formation and function. In: Hassan, B.A. (ed.) *The making and un-making of neuronal circuits in Drosophila*, vol. 69, pp. 225-247. Humana Press, New York (2012).
- [88] Pronk, S., Geissler, P.L., Fletcher, D.A. Limits of filopodium stability. *Phys. Rev. Lett.* 100, 258, 102 (2008).
- [89] Sánchez-Soriano, N., Tear, G., Whittington, P., Prokop, A. *Drosophila* as a genetic and cellular model for studies on axonal growth. *Neural Dev.* 2, 9 (2007).
- [90] Sánchez-Soriano, N., Pimentel, C.G., Beaven, R., Haessler, U., Ofner, L., Ballestrem, C., Prokop, A. *Drosophila* growth cones: a genetically tractable platform for the analysis of axonal growth dynamics. *Dev. Neurobiol.* 70, 58-71 (2010).
- [91] Schäfer, C., *et al.* The filopodium: a stable structure with highly regulated repetitive cycles of elongation and persistence depending on the actin cross-linker fascin. *Cell Adhesion & Migration* vol. 5, 5 (2011).
- [92] Schau, H., Johannes, M., Bochart, Jana. Impact behavior of rocking rigid bodies subjected to seismic loads, 23rd Conf. on Structural Mechanics in Reactor Technology, Manchester, UK (2015).
- [93] Schwienbacher, C., Magri, E., Trombetta, G., Grazi, E. Osmotic properties of the calcium-regulated actin filament. *Biochemistry* 34 (3), 1090-1095 (1995).
- [94] Singer, S.J., Nicolson, G.L. The fluid mosaic model of cell membranes. *Science* 175, 720-731 (1972).
- [95] Svitkina, T.M., Bulanova, E.A., Chaga, O.Y., *et al.* Mechanism of filopodia initiation by reorganization of a dendritic network. *J Cell Biol.* 160(3):409-421 (2003).

- [96] Tobin, A.J., Dusheck, J. Asking about life. Cengage Learning (2005).
- [97] Vavylonis, D., Yang, Q., O'Shaughnessy, B. Actin polymerization kinetics, cap structure, and fluctuations. *Proc. Natl. Acad. Sci. USA*, 102, 8543-8548 (2005).
- [98] Waterman-Storer, C.M., Desai, A., Bulinski, J.C., and Salmon, E.D. Fluorescent speckle microscopy, a method to visualize the dynamics of protein assemblies in living cells. *Curr. Biol.* 8:1227-1230 (1998).
- [99] Wegner, A. Head to tail polymerization of actin. *J. Mol. Biol.* 108, 139-150 (1976).
- [100] Wilson, K.G. Grand challenges to computational science. *Futur. Gener. Comput. Syst.* 5, 171-189 (1989).
- [101] Wriggers, W., Schulten, K. Stability and dynamics of G-actin: back-door water diffusion and behavior of a subdomain 3/4 loop. *Biophysical Journal*, Volume 73, Issue 2, Pages 624-639 (1997).
- [102] Yamazaki, D., Kurisu, S., Takenawa, T. Regulation of cancer cell motility through actin reorganization. *Cancer science*, 96, 379-86 (2005).
- [103] Zhuravlev, P.I., Der, B.S., Papoian, G.A. Design of active transport must be highly intricate: a possible role of myosin and Ena/VASP for G-actin transport in filopodia. *Biophys. J.* 98, 1439-1448 (2010).
- [104] Zhuravlev, P.I., Papoian, G.A. Protein fluxes along the filopodium as a framework for understanding the growth-retraction dynamics: the interplay between diffusion and active transport. *Cell Adhes. Migr.* 5, 448-456 (2011).
- [105] Zicha, D., Dobbie, I.M., Holt, M.R., Monypenny, J., Soong, D.Y., Gray, C., Dunn, G.A. Rapid actin transport during cell protrusion. *Science* 300, 142-145 (2003).

APPENDIX 1

In Section 2.2, by calculating $C = C(L, N, k_{on})$ we argue to show that polymerization only can be properly supplied in filopodial protrusions. More data was computed in that analysis to reinforce those conclusions. First, a critical G-actin concentration was found making:

$$N_p < N_{ret} \Rightarrow 11NC < 26N \Rightarrow C < \frac{26}{11} \approx 2.36$$

giving $C_{crit} = 2.36 \mu\text{M}$, which is the highest concentration value for $N_p < N_{ret}$. This value is represented by a red line in Figures A1.1 and A1.2, where concentration is defined as a function of L and N , respectively.

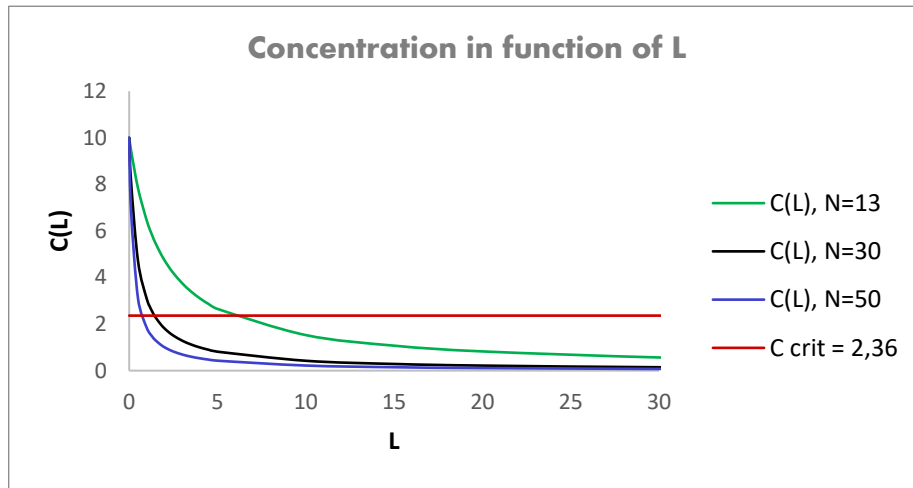


Figure A1.1: Concentration as function of length. Used data: $k_{on} = 11.6$. Simulated by the author.

Figure A1.1 shows the evolution of concentration with respect to filopodial length, for different values of N . When we set higher values for N , polymerization is inefficiently supplied by diffusion, and concentration is under its critical value before L reaches $5 \mu\text{m}$. Even when $N = N_0$, the length is not expressive, confirming that diffusion is a limiting factor to filopodial growth. In Figure A1.2, the behavior of concentration as a function of N is exhibited for a sample of lengths L , which for certain N , diffusion is no longer sufficient to sustain the process since the beginning of filopodial elongation.

But observing both graphics, we might notice that the effect of L on the concentration is greatly overcome by the number of filaments in the bundle, where we can see a relevant and implicit dependency. Since N increases, L hardly can reach expressive values when diffusion is the main transport phenomenon involved.

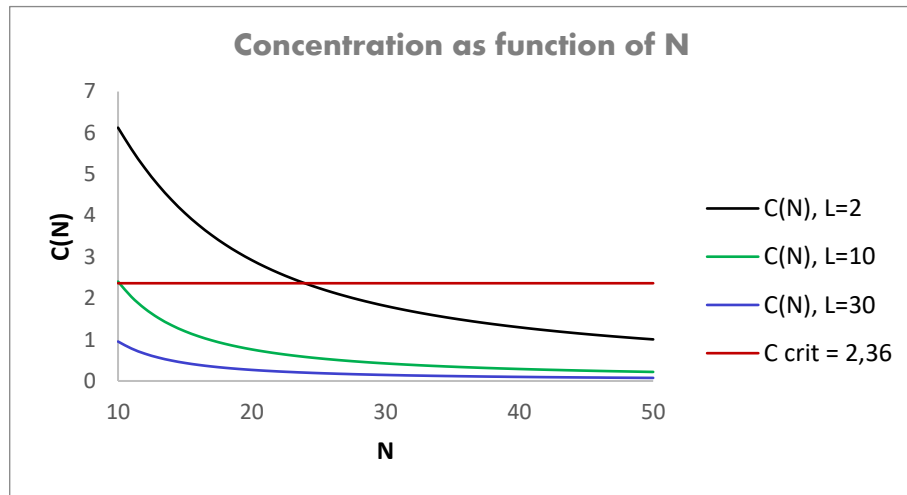


Figure A1.2: Concentration as function of number of filaments. Used data: $k_{on} = 11.6$. Simulated by the author.

From this, we can enquire about the influence of polymerization rate k_{on} on the concentration of actins along filopodial tube. A small sample of values of L and N was chosen to calculate $C = C(L, N, k_{on})$ and these data are presented in Table 10. For this, we consider minimum, maximum, and average values used for k_{on} in literature, also mentioned in Table 1. Then, we determined the standard deviation σ between the values obtained for C in each case.

Table 11: Concentration estimative as function of polymerization rate

	C, L = 2, N = 13	C, L = 20, N = 20	C, L = 50, N = 30
K_{ON} MIN = 10	5,111203047	0,457000146	0,10177946
K_{ON} AVE = 10.8	4,918825917	0,424585585	0,094311344
K_{ON} MAX = 11.6	4,740405006	0,396464739	0,087864262
σ	0,185442789	0,030293072	0,006963839

As we can see, k_{on} seems not to have a great impact in concentration like that produced by N . A more concrete observation can be done through Figures A1.3 and A1.4.

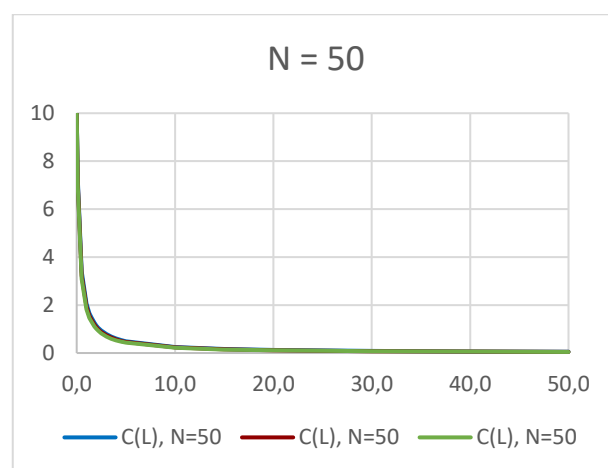
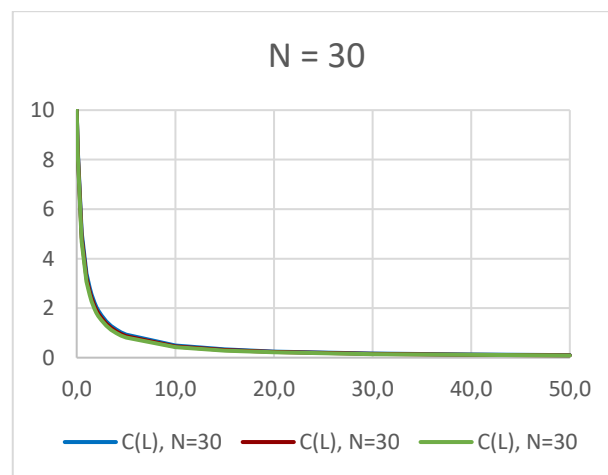
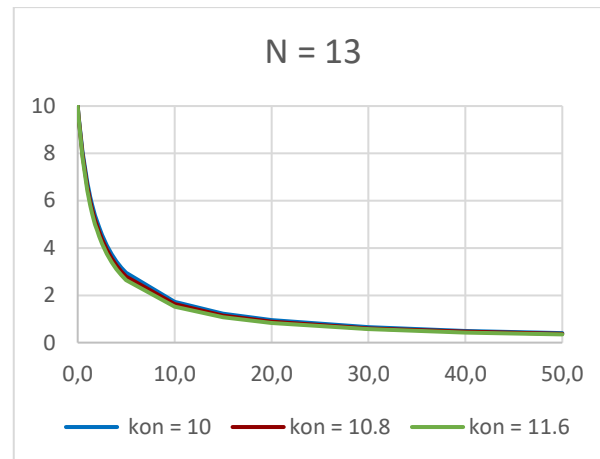


Figure A1.3: Influence of k_{on} in $C(L)$, for different N . Simulated by the author.

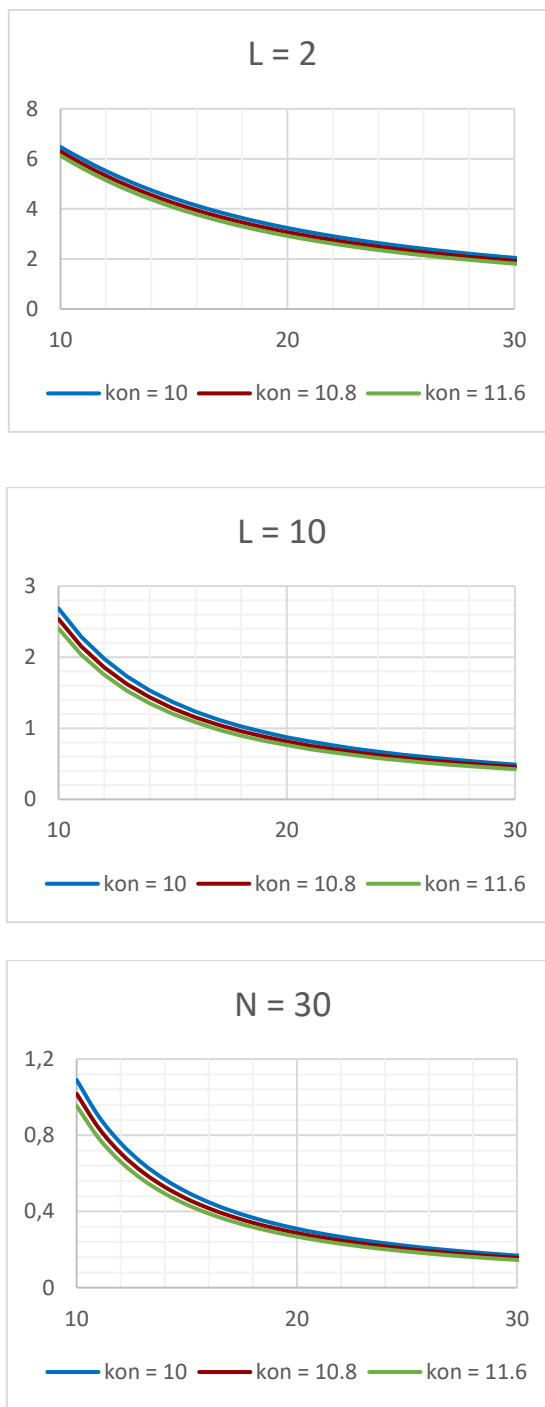


Figure A1.4: Influence of k_{on} in $C(N)$, for different L . Simulated by the author.

Therefore, the use of different values for the polymerization rate does not produce a prominent modification in numerical terms. This is evident in the graphs above where the curves with different k_{on} values are almost indistinguishable in some cases. Hence, starting from Section 2.2, we chose to use the average value among those most cited in the literature, namely,

$$k_{on}|_{average} = 10.8 \mu M^{-1} s^{-1}.$$

APPENDIX 2

In Section 5.1, simulations of particles distribution suggested that as the number of filaments in the bundle N increases, filopodial length L tends to reach shorter stationary values at both measures of inter-filament spacing s . As said, [64] investigates the relation between N and L , which validates the observations here.

From statements and concepts developed in this proposal, it can be mathematically verified the inverse relation between N and L . To do this, the expression (2.3) should be written to obtain L as a function of N and concentration C , and then evaluate the obtained expression $L = L(N, C)$ when C is fixed.

Since expression (2.3) is

$$C = C(L, N, k_{on}) = C_o - \frac{C_o L}{L + (D\eta e^{N_o/N}) / (k_{on} N)},$$

we can assume $k_{on} = k_{on}|_{average}$ and parameters cited in Table 1, it follows that

$$L = L(N, C) = \left(\frac{C_o - C}{C} \right) \left(\frac{D\eta e^{N_o/N}}{k_{on} N} \right).$$

Figure A2.1 shows the surface that represents a plot for L as a function of C from 0 to 10 and N from 20 to 50. Despite the discrete nature of N , which should be an integer, it was plotted as a real interval to a better visualization.

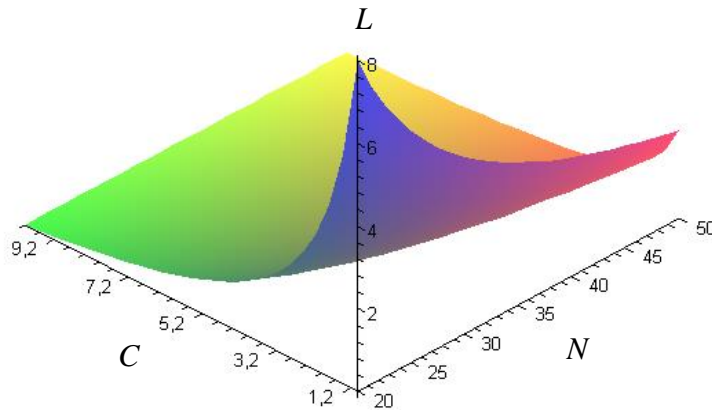


Figure A2.1: Surface representing function $L = L(N, C)$, for $N = [20, 50]$ and $C = [0, 10]$. Plot created by the author.

It is possible to observe that, for any value of concentration C , filopodial length L decreases as the number of filaments N becomes greater. Making $C = C_{fixed}$ (especially for $C \gg C_{crit}$, as defined in Appendix 1), we essentially have that $L(N, C_{fixed}) = L(N)$ can be computed into

$$L(N) = \bar{k} \left(\frac{e^{N_o/N}}{N} \right),$$

with $\bar{k} = \frac{(C_o - C_{fixed})D\eta}{k_{on}C_{fixed}}$ a positive real constant.

It is verified the relation between L and N since $L = L(N)$ is a decreasing function. An example can be seen in Figure A2.2, for $C = 2 \mu M$.

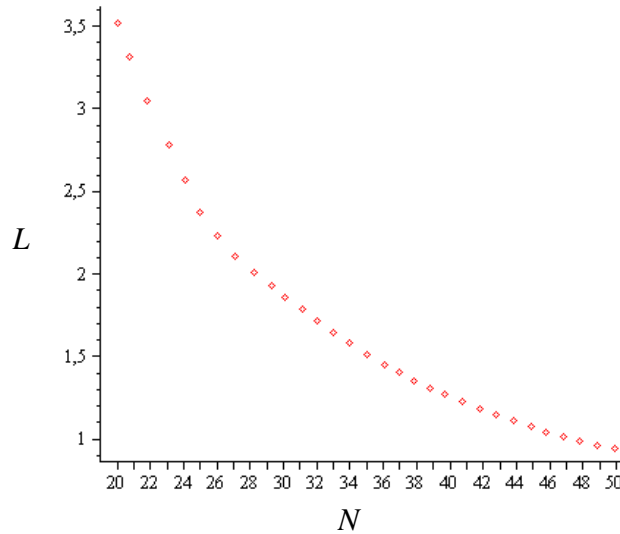


Figure A2.2: Set of points representing function $L = L(N)$, when $C = 2 \mu M$. The y-axis shows L (in micrometers) for each N integer between 20 and 50. Plot created by the author.